REMARKS

Applicants respectfully request reconsideration of the present application in view of the following commentary.

I. Objections to the Specification

The title of the invention is rejected for alleged lack of description. In keeping with the Examiner's suggestion, the title of the invention has been amended to "Polynucleotides encoding signal peptide-containing molecules."

The Examiner alleges that no Tables are found in the specification. Applicants respectfully traverse the objection. A copy of the Return Receipt Postcard is submitted herewith as evidence that 77 pages of the Tables (Tables 1-6) were filed and received by the U.S. PTO on April 7, 2004. Nevertheless, in an effort to expedite the prosecution, a courtesy copy of the Tables is provided accompanying this response.

The Examiner objected to the specification for missing information in the cross-reference. The first paragraph of the specification has been amended accordingly to incorporate the parent application information.

Accordingly, Applicants respectfully request withdrawal of all objections to the specification.

II. Claim Rejection under 35 U.S.C. §101

Claims 56-64 are rejected for alleged lack of utility. Applicants respectfully traverse the rejection.

More specifically, the Examiner acknowledges that the specification discloses that the claimed protein is a signal peptide-containing protein, but asserts that the application "does not disclose a specific and substantial biological role of this protein or its significance."

On the contrary, a BLAST search against NCBI's protein database reveals that the claimed SEQ ID NO: 43 shares 99% identity with human resistin-like molecule (RELM)-beta protein, which is also referred to as "found in inflammatory zone" (FIZZ) and belongs to a cysteine-rich secretory protein family. Hogan *et al.* (*J. Allergy Clin. Immunol.*, 2006, 118: 257-268, EXHIBIT A) reported that RELM-beta protein is a cysteine-rich cytokine that is constitutively expressed in the colon and has a central role in the regulation of colonic inflammation. In addition, Renigunta *et al.* describe that human RELM-beta protein is a mitogenic factor in lung cells and that is may contribute to hypoxic-induced pulmonary vascular remodeling processes or hypoxia related fibrotic lung disease (*FEBS Lett.*, 2006, 580: 900-903, EXHIBIT B).

These later confirmed functions are consistent with the description in the original specification. For example, the paragraph bridging pages 1 and 2 describes that the claimed signal peptide-containing molecules are secretory proteins comprising "receptors, extracellular matrix molecules, cytokines, hormones, growth and differential factors, neuropeptides, vasomediators, phosphokinases, phosphotases, phospholipases, phosphodiesterases, G and Ras-related proteins, ion channels, transporters/pumps, proteases, and transcription factors." The paragraph bridging pages 5 and 6 further provides exemplary functions of the cytokines.

Thus, at least one specific utility for the claimed subject matter is asserted. Accordingly, Applicants respectfully request withdrawal of the rejection under 35 U.S.C. §101 for lack of utility.

III. Claim Rejection under 35 U.S.C. §112, first paragraph

Claims 56-64 are rejected for alleged lack of enablement. In particular, the Examiner contends that the specification is not enabling because it does not provide a credible utility of the claimed subject matter and that the specification does not provide enablement for sequences that are 95% identical to claimed SEQ ID NO: 43 or 177. Applicants respectfully traverse the rejection.

As discussed in the foregoing paragraphs, the claimed SEQ ID NO: 43 or 177 possesses at least one credible and specific utility. Therefore, one skilled in the art would have known how to use the claimed invention.

Applicants thank the Examiner for his acknowledgement that the specification is enabling for SEQ ID NO: 43 and 177. Applicants further submit that the specification is also enabling for polynucleotides encoding proteins which are at least 95% identical to SEQ ID NO: 43 or 177. The specification provides in detail that the sequence of a polynucleotide or a polypeptide can be altered by deletion, insertion, or substitution, such that the altered polynucleotide encodes "a polypeptide with at least one functional characteristic of [the original polypeptide]" or the altered polypeptide has "a silent change and result in a functionally equivalent [polypeptide]." See, for example, at page 17, first full paragraph, and at page 28, first and second full paragraphs.

As disclosed by Patel *et al.* (Science, 2004, 304: 1154-1158, EXHIBIT C), a resistin family protein is cysteine-rich and therefore can form a disulfide-dependent multimeric assembly. The specification discloses that claimed SEQ ID NO: 43 comprises 12 cysteine residues in its length of 111 amino acids, which translates into a cysteine content of 11%. The skilled artisan would have appreciated that cysteine is crucial in protein structures because a disulfide bond can form between two cysteine residues, thereby assembling a 3-D structure of the protein. Thus, the skilled artisan would understand that homologs that are at least 95% identical to SEQ ID NO: 43 or 177 do not comprise alterations at certain positions, such as the cysteine residues, which would have caused a structure change. Accordingly, the specification satisfies the enablement requirement.

Claims 56-64 are also rejected for alleged lack of written description due to recitation of "at least 95% identical to SEQ ID NO: 43 or 177." Applicants respectfully traverse the rejection on the same ground discussed above. Because the skilled artisan would have understood that the homologs do not comprise the sequence alterations that would have caused a structure or

function change, the specification provides sufficient written description of the claimed subject matter. Thus, the rejections under 35 U.S.C. §112, first paragraph should be withdrawn.

IV. Claim Rejection under 35 U.S.C. 102(e)

Claims 56, 59-60 and 63 are rejected under 35 U.S.C. 102(e) for allegedly being anticipated by U.S. Patent Publication No. 2004/0018980 by Gurney *et al.* Applicants respectfully traverse the rejection.

Gurney is a continuation application of U.S. Patent Application No. 09/380,913, which is a national stage application of international application No. PCT/US99/08615, filed on April 20, 1999. Therefore, the 102(e) date of the cited patent publication is its corresponding PCT filing date of April 20, 1999. The present application benefits from the earliest priority date of June 26, 1998, which antedates the 102(e) date of the cited reference. Thus, the Gurney publication is not qualified art against the present application under 35 U.S.C. 102(e). Accordingly, Applicants respectfully request withdrawal of the rejection.

CONCLUSION

Applicants believe that the present application is now in condition for allowance. Favorable reconsideration of the application as amended is respectfully requested.

The Examiner is invited to contact the undersigned by telephone if it is felt that a telephone interview would advance the prosecution of the present application.

The Commissioner is hereby authorized to charge any additional fees which may be required regarding this application under 37 C.F.R. §§ 1.16-1.17, or credit any overpayment, to Deposit Account No. 19-0741. Should no proper payment be enclosed herewith, as by a check or credit card payment form being in the wrong amount, unsigned, post-dated, otherwise improper or informal or even entirely missing, the Commissioner is authorized to charge the unpaid amount to Deposit Account No. 19-0741. If any extensions of time are needed for timely

acceptance of papers submitted herewith, Applicants hereby petition for such extension under 37 C.F.R. §1.136 and authorizes payment of any such extensions fees to Deposit Account No. 19-0741.

Respectfully submitted,

Date April 10, 2007

By _____

FOLEY & LARDNER LLP
Customer Number: 22428
Telephone: (202) 672-5538
Facsimile: (202) 672-5399

Michele M. Simkin
Attorney for Applicant
Registration No. 34,717

Published in final edited form as:
J Allergy Clin Immunol. 2006 July ; 118(1): 257–268.

Resistin-like molecule β regulates innate colonic function: Barrier integrity and inflammation susceptibility

Simon P. Hogan, PhD[a,*], **Luqman Seidu, MD**[a,*], **Carine Blanchard, PhD**[a], **Katherine Groschwitz, BS**[b], **Anil Mishra, PhD**[a], **Margaret L. Karow, PhD**[c], **Richard Ahrens, BS**[a], **David Artis, PhD**[d], **Andrew J. Murphy, PhD**[c], **David M. Valenzuela, PhD**[c], **George D. Yancopoulos, MD, PhD**[c], and **Marc E. Rothenberg, MD, PhD**[a]

a *The Division of Allergy and Immunology, Department of Pediatrics, Cincinnati Children's Hospital Medical Center, University of Cincinnati College of Medicine;*

b *The Department of Immunobiology, University of Cincinnati College of Medicine;*

c *Regeneron Pharmaceuticals, Inc, Tarrytown, NY;*

d *The Department of Pathobiology, University of Pennsylvania School of Veterinary Medicine, Philadelphia.*

Abstract

Background: Resistin-like molecule (RELM) β is a cysteine-rich cytokine expressed in the gastrointestinal tract and implicated in insulin resistance and gastrointestinal nematode immunity; however, its function primarily remains an enigma.

Objective: We sought to elucidate the function of RELM-β in the gastrointestinal tract.

Methods: We generated RELM-β gene-targeted mice and examined colonic epithelial barrier function, gene expression profiles, and susceptibility to acute colonic inflammation.

Results: We show that RELM-β is constitutively expressed in the colon by goblet cells and enterocytes and has a role in homeostasis, as assessed by alterations in colon mRNA transcripts and epithelial barrier function in the absence of RELM-β. Using acute colonic inflammatory models, we demonstrate that RELM-β has a central role in the regulation of susceptibility to colonic inflammation. Mechanistic studies identify that RELM-β regulates expression of type III regenerating gene (REG) (REG3β and γ), molecules known to influence nuclear factor κB signaling.

Conclusions: These data define a critical role for RELM-β in the maintenance of colonic barrier function and gastrointestinal innate immunity.

Clinical implications: These findings identify RELM-β as an important molecule in homeostatic gastrointestinal function and colonic inflammation, and as such, these results have implications for a variety of human inflammatory gastrointestinal conditions, including allergic gastroenteropathies.

---

*These authors contributed equally to this work.

Supported in part by the DDRDC Pilot and Feasibility Grant (NIH R24 DK64403; S.P.H.), R01 AI42242 (M.E.R.), AI45898 (M.E.R.), AI53479 (M.E.R.), and the Burroughs Wellcome Fund (M.E.R.) RO1 AI61570 (D.A.) and the Crohn's and Colitis Foundation of America's William and Shelby Modell Family Foundation Research Award (D.A.), and T32 AI060515 (L.S.).

Disclosure of potential conflict of interest: A. Mishra has received grant support from the National Institutes of Health. A. J. Murphy owns stock in and is employed by Regeneron Pharmaceuticals, Inc. M. E. Rothenberg owns stock in Ception Therapeutics, is the inventor of a patent application filed by CCHMC concerning RELM-β, has received grant support from Cambridge Antibody Technology, and is on the speakers' bureau for Merck. The rest of the authors have declared that they have no conflict of interest.

Marc E. Rothenberg, MD, PhD, Division of Allergy and Immunology, Cincinnati Children's Hospital Medical Center, 3333 Burnet Ave, ML7028, Cincinnati OH 45229. E-mail: Rothenberg@cchmc.org.

Keywords

Allergy; colitis; gastrointestinal; inflammatory; innate; IL-13; mucosal; resistin

As we enter the new millennium, the health of the western world is threatened by an increasing prevalence of immune-mediated diseases. For example, asthma (now affecting 300 million persons), inflammatory bowel disease (IBD; now affecting >1 million persons), and obesity (now affecting nearly 300 million persons) are some of the fastest growing and most pervasive public health problems in developed countries and are recognized to involve inflammatory mechanisms.[1-3] Of even greater concern is the co-occurrence of multiple inflammatory disorders in the same individual (eg, obesity and asthma), leading to increased morbidity.[4] Although the co-occurrence of multiple inflammatory disorders suggests common underlying disease mechanisms, there is a surprising paucity of data concerning the specific mechanisms that might be operational.

Resistin, also called *adipocyte-secreted factor* or *found in inflammatory zone 3* (FIZZ3), is a novel hormone secreted by adipocytes and has been proposed to link obesity with insulin resistance and type II diabetes.[5-9] The resistin family of proteins (resistin, resistin-like molecule [RELM] a, RELM-β, and RELM-β) consists of several approximately 12.5-kd conserved subunits with 10 or 11 cysteine residues that promote the formation of unique disulfide-dependent multimeric assembly units.[8,9] Recent investigations with experimental models have demonstrated that resistin mediates insulin resistance by antagonizing insulin action and modulating one or more steps in the insulin-signaling pathway.[10,11] RELM-α, designated FIZZ1, was originally found in inflammatory zones in a murine model of experimental asthma, yet its role in allergic inflammation has not been elucidated.[8] Subsequent investigations have shown that RELM-α is also expressed in adipose tissue, heart, lung, and tongue, whereas RELM-β (FIZZ2) is expressed in the intestine.[8] Recently, RELM-γ has been identified, and its highest levels of expression have been found in hematopoietic tissues.[12] Preliminary studies have demonstrated that RELMs are secreted proteins that inhibit adipocyte differentiation and neuronal cell survival,[8] suggesting that the primary function of these molecules might not be restricted to regulating insulin resistance. Indeed, recent investigations suggest that at least one member of the resistin family, RELM-β, might have an immunoregulatory function.[13] Using a murine model of T_H2-associated nematode infection, investigators demonstrated that RELM-β is produced by goblet cells in the intestine and possesses antiparasitic activity through an IL-13-dependent mechanism.[13] Despite the growing association of RELM family members with inflammatory conditions, there is a paucity of information concerning the function of this family of cytokines. To determine the definitive role of resistin family members, we generated RELM-β gene-targeted mice. We now report the consequences of RELM-β deficiency on colonic epithelial barrier function and susceptibility to colonic inflammation.

METHODS

Generation of RELM-β gene-targeted mice

RELM-$\beta^{-/-}$ mice were designed and developed by VelociGene technology.[14] In brief, the RELM-β gene was replaced by a reporter-selection cassette, which consists of a β-galactosidase enzyme gene and a neomycin resistance gene. The knockout-reporter construct was created by means of bacterial homologous recombination into a bacterial artificial chromosome encoding RELM-β and was constructed so that the cassette's β-galactosidase gene is placed in frame with the AUG of RELM-β (Fig 1, *A*). The construct deletes amino acids 2 through 82 of RELM-

β contained in exons 1 through 3 of the gene. The knockout-reporter construct was linearized and electroporated into 129S1/Sv-derived embryonic stem (ES) cells, CJ7 clone, and correctly targeted clones were identified by using Taqman screening with 2 probes in the RELM-β gene as loss-of-allele probes.[14] Three correctly targeted clones were identified from 192 colonies. Chimeric mice were generated by microinjecting C57BL/6 embryos with the ES clones. Mice from clone 140B-H3 were backcrossed twice to C57BL/6 mice, and F2 mice were crossed to create homozygous RELM-β gene-targeted mice. Mice were identified as heterozygotes and homozygotes by means of the Taqman assay, with probes for the Neo and LacZ genes and the RELM-β loss-of-allele probes. Mice were genotyped by means of PCR (RELM-β forward primer, cctgagctttctggagagtg; RELM-β reverse primer, cctcctcatcaagaaactttag; and lacZ primer, gtctgtcctagcttcctcactg), producing a wild-type (WT) band of 545 bp and a targeted band of 351 bp. Experiments on RELM-$\beta^{-/-}$ mice were performed on 6- to 8-week-old mice and background-matched WT control animals derived from littermates. All procedures were performed in accordance with the ethical guidelines in the "Guide for care and use of laboratory animals" of the Institutional Animal Care and Use Committee approved by the Veterinary Services Department of the Cincinnati Children's Hospital Medical Center.

Ussing chambers

Four 1-cm segments of mucosa were stripped of muscle and mounted in U2500 Dual Channel Ussing chambers (Warner Instruments, Hamden, Conn) that exposed 0.30 cm^2 of tissue to 10 mL of Krebs buffer. Agar-salt bridges and electrodes were used to measure the potential difference. Every 50 seconds the tissues were short circuited at 1 V (EC 800 Epithelial Cell voltage Clamp; Warner Instruments), and the short-circuit current was monitored continuously. In addition, every 50 seconds the clamp voltage was adjusted to 1 V for 10 seconds to allow calculation of tissue resistance using Ohm's law. After the preparation had stabilized for 10 minutes and baseline potential difference and resistance had been established, fluorescein isothiocyanate (FITC)-dextran (2.2 mg/mL; molecular mass, 4.4 kd; Sigma-Aldrich, St Louis, Mo) was added to the mucosal reservoir. Medium (0.25 mL of 10 mL) was removed from the serosal reservoir and replaced with fresh medium every 20 minutes over a period of 180 minutes for measurement of FITC-dextran.

Solutions and drugs

Krebs buffer contained 4.70 mM KCl, 2.52 mM $CaCl_2$, 118.5 mM NaCl, 1.18 mM NaH_2PO_4, 1.64 mM $MgSO_4$, and 24.88 mM $NaHCO_3$ on each side. The tissues were allowed to equilibrate for 15 minutes in Krebs buffer containing 5.5 mM glucose. All reagents were obtained from Sigma-Aldrich unless stated otherwise.

Microarray analysis

To evaluate the effect of the loss of RELM-β on the colonic mucosa, we used Affymetrix GeneChip (Santa Clara, Calif) micro-arrays (MOE430_2, a whole-genome expression chip encoding 45,101 genes) to obtain gene expression profiles from 5 independent WT and 6 independent gene-targeted animals. GeneChip CEL data were subjected to normalization and quantification by using the Robust MultiArray Analysis algorithm developed by Irizarry et al,[15] as implemented in GeneSpring 7.0 (Sun Microsystems, Santa Clara, Calif). Gene expression levels for each gene were normalized relative to the median value across the 6 microarrays.

Induction of acute colonic inflammation

Dextran sodium sulfate-induced acute colonic inflammation—Dextran sodium sulfate (DSS; ICN Biomedical Inc, Costa Mesa, Calif) used for the induction of acute colonic

inflammation was supplied as the sodium salt with an average molecular weight of 41 kd. It was used as a supplement in the drinking water of the mice for 8 days as 2.5% (wt/vol) solution.

Trinitrobenzene sulfonate-induced acute colonic inflammation—Mice were lightly anesthetized with isoflurane and then administered trinitrobenzene sulfonate (TNBS) (3.75 mg/150 μL dissolved in ethanol [50%]/saline [50%]) or vehicle (ethanol [50%]/saline [50%]) intrarectally through a catheter equipped with a 1-mL syringe. The catheter was advanced into the rectum until the tip was 4 cm proximal to the anal verge, at which time the haptenating agent was administered in a total volume of 150 μL. Mice were held in a vertical position for 30 seconds after the intrarectal injection to ensure distribution of the haptenating agent within the entire colon and cecum.

Disease activity index

The disease activity index (DAI) was derived by scoring 3 major clinical signs (weight loss, diarrhea, and rectal bleeding).[16] The clinical features were scored separately and then correlated with a histologic score. *DAI = (Body weight loss)+ (Diarrhea score) + (Rectal bleeding score).*

Body weight.—A change in body weight was calculated as the difference between the expected and actual weight. The formula for predicted body weight was derived by means of simple regression by using the body weight data for the control group. The following formula was used: $Y = a + kx$, where Y is body weight change (loss or gain), k is daily increase in body weight, x is day, and a is starting body weight.

Diarrhea.—The appearance of diarrhea was defined as mucus-fecal material adherent to anal fur. The presence or absence of diarrhea was scored as either 1 or 0, respectively. The presence or absence of diarrhea was confirmed by means of examination of the colon after completion of the experiment. Mice were killed, and the colon was excised from the animal. Diarrhea was defined by the absence of fecal pellet formation in the colon and the presence of continuous fluid fecal material in the colon.

Rectal bleeding.—The appearance of rectal bleeding was defined as diarrhea containing visible blood, mucus, or both or gross rectal bleeding and scored as described for diarrhea.

Assessment of intestinal inflammation

Assessment of body weight and evaluation of stool consistency (diarrhea) and rectal bleeding were performed on a daily basis. Body weight was expressed as percentage body weight change from baseline. Diarrhea and rectal bleeding were defined as described above. The presence-absence of diarrhea and rectal bleeding was given a score of 0 or 1 and the diarrhea-rectal bleeding score (0-2) is the accumulation of these values.

Intestinal histopathologic examination

Animals were killed on day 7, and the colon was excised. The length of the colon was measured with digmatic calipers (Mitutoyo, Kawasaji, Japan). Tissue specimens were then fixed in 4% paraformaldehyde and stained with hematoxylin and eosin and Masson trichrome by using standard histologic techniques. The percentage colon length with mucosal ulceration was determined by performing morphometric analysis of the colon with the ImageProPlus 4.5 software package (Media Cybernetics, Inc, Silver Spring, Md). In brief, digital images of longitudinal sections (1-2 cm in length) of hematoxylin and eosin-stained colons were produced.

Assessment of inflammation in TNBS colitis

The colons were divided longitudinally into 2 parts, one of which was used for histologic assessment. The longitudinally divided colons were fixed in 4% formalin and embedded in paraffin for routine histology. One investigator, who was blinded for treatment allocation of the mice, scored the following parameters, as previously reported[17,18]: (1) percentage of area involved, (2) edema, (3) erosionulceration, (4) crypt loss, and (5) infiltration of mononuclear and polymorphonuclear cells (neutrophils and eosinophils) into the lamina propria and submucosa. The percentage of area involved and the crypt loss were scored on a scale ranging from 0 to 4 as follows: 0, normal; 1, less than 10%; 2, 10%; 3, 10% to 50%; and 4, greater than 50%. Erosions were defined as 0 if the epithelium was intact, 1 for involvement of the lamina propria, 2 for ulcerations involving the submucosa, and 3 when ulcerations were transmural. The severity of the other parameters was scored on a scale of 0 to 3 as follows: 0, absent; 1, weak; 2, moderate; 3, severe.

Murine colonoscopy

Mice were anesthetized with triple sedative (ketamine, 35 mg/kg; xylazine, 5 mg/kg; and acepromazine, 1 mg/kg), and colonoscopies were performed with a small-animal rigid telescope (30°, 1.9 mm × 10 cm) connected to a Cold light Fountain Xenon nova (Model 20 131520) and an Endovision TRICAM SL (Model 20) PAL/NTSC camera (Karl Storz Veterinary Endoscopy, Goleta, Calif).

Detection of RELM-β[1] cells by means of immunohistochemistry

The colon segment of the gastrointestinal tract was immunostained with antiserum against mouse RELM-β, as previously described.[13] Briefly, 5-μm sections were quenched with H_2O_2, blocked with normal goat serum, and stained with a rabbit anti-murine RELM-β antiserum. The slides were then washed and incubated with biotinylated goat anti-rabbit antibody and avidin-peroxidase complex (Vectastain ABC Peroxidase Elite kit; Vector Laboratories, Burlingame, Calif). The slides were developed by using nickel diaminobenzidine enhanced cobalt chloride to form a black precipitate and counterstained with nuclear fast red.

Northern blot analysis

RNA was extracted from the lung tissue with Trizol reagent (Gibco-BRL, Grand-Island, NY), according to the manufacturer's protocol. Twenty micrograms of total RNA was used for Northern blot analysis, as previously described.[19]

Real-time PCR analysis

The RNA samples (500 ng) were subjected to reverse transcription analysis with Superscript II reverse transcriptase (Invitrogen, Carlsbad, Calif), according to the manufacturer's instructions. Regenerating gene (REG)3β and REG3γ were quantified by means of real-time PCR with the LightCycler instrument and LightCycler FastStart DNA Master SYBR Green I as a ready-to-use reaction mix (Roche Diagnostics Corp, Indianapolis, Ind). Results were then normalized to GAPDH amplified from the same cDNA mix and expressed as fold induction compared with the control values. cDNAs were amplified by using the following primers: murine *REG3β* (151 bp), tcccaggcttatggctccta and gcaggccagttctgcatca; murine *REG3γ* (251 bp), catcaactgggagacgaatcc and cagaaatcctgaggctcttgaca; and *GAPDH* (400 bp), tggaaatcccatcaccatct and gtcttctgggtggcagtgat.

Statistical analysis

Data are expressed as means ± SEM. Statistical significance comparing different sets of mice was determined by using the Student *t* test. In experiments comparing multiple experimental groups, statistical differences between groups were analyzed by using the 1-way ANOVA nonparametric Kruskal-Wallis test. *P* values of less than .05 were considered significant. All analyses were performed with Prism 4.0 software.

RESULTS

RELM-$\beta^{-/-}$ mice were generated by means of homologous recombination with VelociGene technology (Fig 1, *A*).[14] These mice were fully fertile and produced offspring at predicted Mendelian inheritance patterns, with no gross abnormalities observed. The specific ablation of the RELM-β gene was demonstrated by the absence of RELM-β mRNA and protein expression in the colon (Fig 1, *B* and *C*). Notably, RELM-$\beta^{-/-}$ mice still had expression of RELM-β mRNA, as demonstrated by means of Northern blot analysis in the allergen-challenged lung (data not shown). To test the effect of RELM-β deletion on the composition and homeostasis of the peripheral immune system, the development and activation status of B- and T-cell subsets were analyzed by means of flow cytometry. There was no significant difference in the level and phenotype of lymphocytes in the spleen and mesenteric lymph nodes in RELM-$\beta^{-/-}$ mice. Furthermore, there was also no difference in the complete blood counts and differentials (data not shown).

Analysis of RELM-β mRNA expression in various gastrointestinal compartments at baseline revealed a high level of RELM-β expression in the large intestine (Fig 1, *B*, and data not shown). Immunohistologic staining demonstrated that RELM-β expression was predominantly restricted to goblet cells and enterocytes (Fig 1, *C*). Notably, the colons of RELM-$\beta^{-/-}$ mice were morphologically normal and contained similar levels of goblet cells, and their mucin gene products compared with those of WT control mice (data not shown).

We were next interested in examining whether RELM-β deficiency affected epithelial cells in the colon. Initially we examined colonic epithelial cell populations (goblet cells and endocrine cells) in the colons of WT and RELM-$\beta^{-/-}$ mice and found no difference in the numbers of epithelial cell populations between the groups (results not shown). We next examined intestinal epithelial cell resistance in RELM-$\beta^{-/-}$ and WT mice. Resistance, a measure of tissue permeability, was significantly decreased in RELM-$\beta^{-/-}$ mice compared with WT mice (Fig 2, *A*). To confirm altered epithelial cell barrier function in RELM-$\beta^{-/-}$ mice, we examined intestinal permeability by analyzing FITC-dextran transport in colonic segments *ex vivo*. Compared with control mice, RELM-$\beta^{-/-}$ colons had increased intestinal permeability to FITC-dextran (Fig 2, *B*). For example, the FITC-dextran permeability of the colonic layer of RELM-$\beta^{-/-}$ mice was significantly increased by 3 hours compared with colonic layers from WT animals (0.75 ± 0.36 mg/mL vs 2.6 ± 0.4 mg/mL $\times 10^{-12}$ at 180 minutes, $P < .01$). On average, we observed a 266% increase in FITC-dextran permeability of the colonic layer of RELM-$\beta^{-/-}$ mice compared with that seen in WT animals. Collectively, these studies demonstrate a role for RELM-β in epithelial cell barrier function.

The colonic epithelium acts as a selective barrier to luminal antigens and pathogens. Clinical and experimental studies suggest that disruption of epithelial barrier function can predispose to chronic intestinal inflammatory processes. Indeed, disruption of barrier-protective genes (CD73, multidrug resistance gene 1, intestinal trefoil factor, and hypoxia inducible factor 1) alters barrier function and increases susceptibility to chemically induced colitis.[20-23] The localized expression of RELM-β within the colonic epithelium and the demonstration of altered epithelial barrier function in RELM-$\beta^{-/-}$ mice led us to hypothesize that RELM-β might have

a role in colonic inflammatory susceptibility. In particular, we hypothesized that increased permeability would increase susceptibility to colonic inflammation in RELM-$\beta^{-/-}$ mice. We thus used 2 models of acute inflammatory colonic injury, a DSS-induced T cell-independent model that reproduces features of ulcerative colitis[24] and a second model of TNBS-induced colitis that captures features of Crohn's disease,[25-27] and examined the effect of RELM-β deficiency on colonic injury.

WT and RELM-$\beta^{-/-}$ mice were treated with DSS, and we examined colonic RELM-β expression throughout the time course (Fig 3). Notably, although there was some variability between mice, levels of RELM-β mRNA increased after DSS exposure (Fig 3, *A*). Surprisingly, RELM-$\beta^{-/-}$ mice had marked protection from most disease features, including weight loss, colonic shortening, diarrhea-rectal bleeding, and protection from mortality (Fig 3, *B-F*). For example, on day 7, the DAI reached 7.37 ± 2.4 in WT mice compared with 1.53 ± 1.53 in RELM-$\beta^{-/-}$ mice (mean ± SEM; n = 4-5 mice per group; $P < .05$), respectively, after DSS treatment. Histologic assessment of the degree of tissue inflammation revealed that RELM-$\beta^{-/-}$ mice had less epithelial damage and submucosal inflammation compared with WT mice (Fig 4, *A-F*). The protection from experimental disease occurred at all time points in this acute model of colonic inflammation. Additionally, we assessed the degree of mucosal damage by performing colonoscopy in WT and RELM-$\beta^{-/-}$ mice (Fig 4, *G-L*; see this article's Fig E1 and Videos 1-3 in the Online Repository at www. jacionline.org). Colonoscopy of WT control-treated mice revealed a healthy, translucent colonic mucosa with visible vasculature (Fig 4, *G*). In contrast, the colonic mucosa of DSS-treated WT mice appeared friable, with readily detectable erythema, strictures, and mucosal injury, as characterized by ulcerations, rectal bleeding, and mucus (Fig 4, *H-J*). Notably, these lesions were barely detectable in RELM-$\beta^{-/-}$ mice (Fig 4, *K* and *L*). Control-treated RELM-$\beta^{-/-}$ mice exhibit markedly reduced endoscopic, pathologic, and clinical signs (diarrhea, rectal bleeding, or weight loss) and gross morphologic changes to the gastrointestinal tract normally associated with spontaneous intestinal inflammation (Fig 4, *C*, and results not shown). Because a DSS-induced colonic inflammation model has been previously shown to occur independent of an adaptive immune response,[28] our data highlight the involvement of RELM-β in innate immunity.

To identify the RELM-β-expressing cell population in the inflamed colon, we performed immunohistochemistry with anti-murine RELM-β antiserum. In DSS-treated WT mice we identified RELM-β expression in gastrointestinal epithelial cells and also in infiltrating inflammatory cells (Fig 4, *M* and *N*). The RELM-β^{1} staining of the epithelium was predominantly restricted to goblet cells (Fig 4, *M*). Thus the variable expression of RELM-β mRNA in DSS-treated mice (Fig 3, *A*) likely reflects the loss of RELM-β^{+} epithelial cells. The RELM-β^{+} inflammatory cells were localized to the muscularis mucosa and were also present within the ulcerated epithelial mucosa (Fig 4, *N*). We observed no positive staining in the colonic epithelium from RELM-$\beta^{-/-}$ mice (results not shown).

RELM-β expression has previously been associated with T_H2-immune responses, such as experimental asthma and helminthic infestations.[8,13] As such, we were interested in testing the hypothesis that DSS-induced RELM-β expression was dependent on the cytokine IL-13; this cytokine has previously been shown to be important in T_H2-associated immunity.[29] As such, we subjected WT and IL-$13^{-/-}$ mice to DSS-induced experimental colitis. Notably, the expression of RELM-β was markedly decreased in IL-$13^{-/-}$ mice (Fig 3, *A*). Indeed, IL-$13^{-/-}$ mice were protected from pathologic responses associated with DSS-induced colitis (DAI index was measured on day 7: 3.905 ± 0.44 vs 2.55 ± 0.13, DSS-treated WT mice (BALB/c) vs IL-$13^{-/-}$ mice; mean ± SEM [n = 3-4]; $P< .05$).

We next examined the role of RELM-β in the development of TNBS-induced colitis, a rapidly evolving transmural colitis. Administration of TNBS to RELM-$\beta^{-/-}$ mice was associated with

increased disease severity, as assessed on the basis of clinical symptoms (weight loss), survival, and tissue histology (cryptitis and intercryptal inflammation and ulceration), compared with that seen in WT mice (Fig 5). Histologic analysis of colonic tissue from TNBS-treated RELM-$\beta^{-/-}$ mice revealed extensive ulceration and erosion of the colonic epithelium, crypt loss, and a pronounced cellular infiltrate that was primarily comprised of mononuclear and polymorphonuclear (neutrophils and eosinophils) cells (Table I). Histologic scoring of colonic tissue revealed significantly greater pathology than that observed in TNBS-treated WT mice (Table I).

We observed no significant alteration in colonic morphology between control-treated WT and RELM-$\beta^{-/-}$ mice (Table I). The very modest disease induced in WT mice might be due to the relative resistance of the C57Bl/6 strain to this model of colitis.[27] The protection from DSS-induced injury and the enhanced susceptibility to TNBS-induced colitis might be related to different induction patterns of RELM-β in each model. Indeed, in contrast to DSS exposure, TNBS treatment of WT mice did not enhance colonic RELM-β expression compared with that seen in control mice (Fig 5, C).

To elucidate the molecular basis of altered colonic function in RELM-$\beta^{-/-}$ mice, we took an empiric approach involving genome-wide expression profile analysis with Affymetrix oligonucleotide chips and probing colon RNA from WT and RELM-$\beta^{-/-}$ mice. Using criteria of a 2.0-fold change and a Welch *t* test with a *P* value cutoff of .05, we identified 32 genes altered in the RELM-$\beta^{-/-}$ mice (Fig 6, *A*). Of these transcripts, 8 were upregulated, and 24 were downregulated. Importantly, RELM-β was the most decreased gene, validating the approach, and there was no evidence of compensatory increases in RELM-α expression; in fact, expression of the latter gene was modestly reduced. Functional classification of the altered transcripts revealed a significant predominance of the C-type lectin gene superfamily (approximately 15%). Several families of functional molecules emerged. In particular, the most dysregulated gene family members of the type III subclass of the REG gene family (REG3β and REG3γ) were downregulated 2.7- and 2.2-fold in the RELM-$\beta^{-/-}$ mice, respectively (Fig 6, *B*). The type III subclass of the REG gene family (REG3 α, β, γ, and δ) are orthologues of the human pancreatitis-associated protein.[30] These proteins are synthesized by Paneth cells in the small intestine and by crypt epithelium in the colon. Given that our analysis used a whole genome-wide approach and that 2 related immunity genes were similarly downregulated, we prioritized confirming these observations by performing real-time PCR analysis. Indeed, we were able to demonstrate a mean 2-fold decrease in REG3β and REG3γ mRNA in the colons of RELM-$\beta^{-/-}$ mice compared with WT mice (Fig 6, *C* and *D*). These studies demonstrate that RELM-β has a role in the regulation of REG3β and REG3γ expression in the colon.

DISCUSSION

The resistin family of proteins is composed of cysteinerich cytokines implicated in insulin and gastrointestinal nematode resistance. The precise role of these molecules in mucosal inflammation has not yet been fully elucidated. In the current study we have examined the role of RELM-β in the gastrointestinal tract. We demonstrate that RELM-β is predominantly expressed by goblet cells and epithelial cells within the colonic epithelium and is involved in the maintenance of colonic epithelial cell barrier function. Gene array analysis revealed that RELM-β has a role in regulating intestinal homeostasis because a number of transcripts normally expressed in the colon were altered in the absence of RELM-β. Notably, the altered genes were rich in enterocyte products, especially innate immune mediators, such as the type III REG gene family members. Using acute colonic inflammatory models, we show an important role for RELM-β in colonic injury susceptibility. RELM-β deficiency was associated with reduced susceptibility to DSS-induced colitis but increased susceptibility to TNBS-induced colitis. Thus our initial hypothesis that RELM-β deficiency would simply enhance

susceptibility to colonic inflammation was an oversimplification. Although differentially affecting both models, these results underscore the critical participation of RELM-β in regulating colonic inflammation. Prior studies have reported that distinct mechanisms are involved in TNBS-versus DSS-induced colitis.[27,31] We show that the pathogenic role of RELM-β is associated in part with dys-regulation of type III REG gene expression, providing some mechanistic insight that helps explains the RELM-β-mediated effects.

To elucidate whether the increased colonic permeability in RELM-$\beta^{-/-}$ mice could be explained by altered tight junction protein function, we performed electron microscopy on colonic epithelial cells from WT and RELM-$\beta^{-/-}$ mice (results not shown). We observed normal colonic epithelial architecture and desmosome formations between epithelial cells in the RELM-$\beta^{-/-}$ mice, suggesting that altered permeability might not be due to altered tight junction protein function. This is consistent with gene chip analysis because we did not observe any significant change in the expression of tight junction proteins in RELM-$\beta^{-/-}$ mice compared with WT mice (results not shown). Notably, a number of experimental studies have demonstrated altered intestinal permeability (transepithelial resistance and permeability) without any clinical phenotype (diarrhea and epithelial cell ulceration and erosions), suggesting that the increased permeability might be unrelated to the clinical phenotype observed after TNBS treatment. Interestingly, recent investigations have demonstrated a genetic link between mutations in CARD15 with increased intestinal permeability in families with IBD,[32] yet approximately 25% of first-degree relatives of patients with IBD show increased intestinal permeability in the absence of clinical symptoms.[33,34]

RELM-β deficiency was associated with decreased expression of REG3β and REG3γ mRNA in the colon. Although the overall fold change in type III REG proteins (REG3β and REG3γ) was modest, we demonstrated a similar 2.5-fold reduction in levels using 2 independent experimental systems. Notably, we did not observe any change in other REG protein family members, highlighting the specificity to these proteins. Furthermore, the modest change in genome transcripts indicates no major alteration (either directly or indirectly through compensatory mechanisms) as a result of RELM-β deficiency. The increased permeability observed in RELM-$\beta^{-/-}$ mice was associated with decreased expression of REG3β and REG3γ mRNA in the colon. The function of these proteins in the gastrointestinal tract has only preliminarily been elucidated; recent evidence suggests that they might be involved in epithelial cell repair and Schwann cell regeneration.[30] The involvement of REG3β and REG3γ in RELM-β-mediated maintenance of colonic epithelial cell barrier function requires further analysis.

We demonstrate that RELM-β deficiency is associated with decreased susceptibility to DSS-induced colitis and increased susceptibility to TNBS-induced colitis. These 2 models have previously been shown to involve distinct disease mechanisms, such as involving both T cell-dependent and T cell-independent pathways.[27] Collectively, these studies suggest that RELM-β might act a critical checkpoint in the regulation of innate immunity. Notably, REG3β has been shown to downregulate TNF-α-induced nuclear factor κB (NF-κB) activation in monocytic and epithelial cells, reduce proinflammatory cytokine mRNA levels, and regulate innate immune responses.[30,35] Both in human IBD and in murine models of IBD, the inflammation is likely to depend, at least in part, on the activation and nuclear translocation of NF-κB family members.[36] It is tempting to speculate that RELM-β-mediated dysregulation of REG3β and REG3γ expression might regulate susceptibility to NF-κB-dependent inflammation and disease pathology. The analysis of NF-κB activation in RELM-β-deficient mice now deserves future attention.

Notably, we demonstrate that colonic expression of RELM-β was dependent on IL-13. This is consistent with our previous investigations using gastrointestinal nematode models associated with T_H2 immunity.[13] In these investigations we demonstrated that gastrointestinal nematode

infestation associated with T_H2 inflammation upregulates RELM-β expression. Furthermore, we demonstrated that gastrointestinal nematode-induced expression of RELM-β was dependent on the IL-4Rα pathway. To confirm a role for IL-13, we showed that administration of recombinant IL-13 induces RELM-β expression in the intestine.

Structural analysis of RELM family members, resistin, and RELM-β reveals a multimeric structure comprised of protomers consisting of carboxy-terminal, disulfide-rich, β-sandwich "head" domain and an amino-terminal α-helical domain.[9] It is notable that the 3-dimensional structure of RELM-β requires regulated disulfide-dependent assembly similar to that used by IgM.[9] As a secreted product produced by intestinal epithelial cells, RELM-β can function as a regulatory molecule involved in luminal molecule recognition and transportation across the epithelial barrier. This view is supported by our finding that in the absence of RELM-β, there is decreased expression of immunologic effector molecules in the colon. Prior studies have associated RELM-β with innate immunity because expression is induced by bacterial colonization in the gastrointestinal tract through a Cdx2-dependent mechanism.[37] Furthermore, RELM-β has been shown to directly bind to parasitic nematodes and possesses antichemotactic activity against the parasite.[13] The selective decreased expression of type III REG proteins in the absence of RELM-β draws attention to the interaction of RELM-β and REG3, directly or indirectly. These data, taken together with our present findings that RELM-β is critical in acute models of inflammation, draw attention to the central role of RELM-β in innate intestinal immunity.

Although elegant studies in mice have demonstrated a role for resistin and RELM in regulating glucose metabolism, the exact homolog of murine RELM-β is controversial. We have not observed differences in baseline glucose levels in RELM-$\beta^{-/-}$ mice (data not shown). Taken together, murine RELM-β behaves more as a cytokine involved in immune regulation rather than a metabolic hormone. Our results highlight the importance of determining the exact biology of the RELM family members in the human system. Our finding defines a new biology for the RELM family of proteins by identifying a regulatory role for RELM-β in colonic barrier function and colonic inflammatory injury. These results have potential clinical applications because altered intestinal inflammation is seen in a variety of human diseases, including IBD and allergic gastroenteropathy. The finding that RELM-β is downstream from IL-13 signaling after DSS exposure highlights the potential involvement of RELM-β in T_H2-associated inflammatory responses. Notably, the chromosome position of human RELM-β (3q13.1) has recently been linked to allergic inflammation, tempting speculation that perhaps RELM-β is responsible.[38] Although not directly examined in this study, these results imply a similar immunomodulatory role for RELM-β in T_H2-associated human lung disease (eg, asthma), especially in view of the overexpression of RELM-β in experimental asthma models.[39,40]

Acknowledgements

We thank Drs Nives Zimmermann, Fred Finkelman, Gurjit K. Hershey, Thomas Korfhagen, Patricia Fulkerson, Dominique Brandt, Bruce Aronow, and Gary Ross for helpful discussions and review of this manuscript and Andrea Lippelman for editorial assistance.

Abbreviations used

DAI, Disease activity index; DSS, Dextran sodium sulfate; ES, Embryonic stem; FITC, Fluorescein isothiocyanate; FIZZ, Found in inflammatory zone; IBD, Inflammatory bowel disease; NF-κB, Nuclear factor κB; RELM, Resistin-like molecule; REG, Regenerating gene; TNBS, Trinitrobenzene sulfonate; WT, Wild-type.

REFERENCES

1. Macdonald TT, Monteleone G. Immunity, inflammation, and allergy in the gut. Science 2005;307:1920–5. [PubMed: 15790845]
2. Umetsu DT, McIntire JJ, Akbari O, Macaubas C, DeKruyff RH. Asthma: an epidemic of dysregulated immunity. Nat Immunol 2002;3:715–20. [PubMed: 12145657]
3. Abelson P, Kennedy D. The obesity epidemic. Science 2004;304:1413. [PubMed: 15178768]
4. Weiss ST, Shore S. Obesity and asthma: directions for research. Am J Respir Crit Care Med 2004;169:963–8. [PubMed: 14742299]
5. Steppan CM, Bailey ST, Bhat S, Brown EJ, Banerjee RR, Wright CM, et al. The hormone resistin links obesity to diabetes. Nature 2001;409:307–12. [PubMed: 11201732]
6. Steppan CM, Brown EJ, Wright CM, Bhat S, Banerjee RR, Dai CY, et al. A family of tissue-specific resistin-like molecules. Proc Natl Acad Sci U S A 2001;98:502–6. [PubMed: 11209052]
7. Flier JS. The missing link with obesity? Nature 2001;409:292–3. [PubMed: 11201721]
8. Holcomb IN, Kabakoff RC, Chan B, Baker TW, Gurney A, Henzel W, et al. FIZZ1, a novel cysteine-rich secreted protein associated with pulmonary inflammation, defines a new gene family. EMBO J 2000;19:4046–55. [PubMed: 10921885]
9. Patel SD, Rajala MW, Rossetti L, Scherer PE, Shapiro L. Disulfide-dependent multimeric assembly of resistin family hormones. Science 2004;304:1154–8. [PubMed: 15155948]
10. Banerjee RR, Rangwala SM, Shapiro JS, Rich AS, Rhoades B, Qi Y, et al. Regulation of fasted blood glucose by resistin. Science 2004;303:1195–8. [PubMed: 14976316]
11. Rajala MW, Obici S, Scherer PE, Rossetti L. Adipose-derived resistin and gut-derived resistin-like molecule-beta selectively impair insulin action on glucose production. J Clin Invest 2003;111:225–30. [PubMed: 12531878]
12. Schinke T, Haberland M, Jamshidi A, Nollau P, Rueger JM, Amling M. Cloning and functional characterization of resistin-like molecule gamma. Biochem Biophys Res Commun 2004;314:356–62. [PubMed: 14733912]
13. Artis D, Wang ML, Keilbaugh SA, He W, Brenes M, Swain GP, et al. RELMbeta/FIZZ2 is a goblet cell-specific immune-effector molecule in the gastrointestinal tract. Proc Natl Acad Sci U S A 2004;101:13596–600. [PubMed: 15340149]
14. Marcus RC, Matthews GA, Gale NW, Yancopoulos GD, Mason CA. Axon guidance in the mouse optic chiasm: retinal neurite inhibition by ephrin "A"-expressing hypothalamic cells in vitro. Dev Biol 2000;221:132–47. [PubMed: 10772797]
15. Irizarry RA, Hobbs B, Collin F, Beazer-Barclay YD, Antonellis KJ, Scherf U, et al. Exploration, normalization, and summaries of high density oligonucleotide array probe level data. Biostatistics 2003;4:249–64. [PubMed: 12925520]
16. Stevceva L, Pavli P, Husband A, Matthaei KI, Young IG, Doe WF. Eosinophilia is attentuated in experimental colitis induced in IL-5 deficient mice. Genes Immun 2000;1:213–8. [PubMed: 11196714]
17. Ten Hove T, Drillenburg P, Wijnholds J, te Velde AA, van Deventer SJ. Differential susceptibility of multidrug resistance protein-1 deficient mice to DSS and TNBS-induced colitis. Dig Dis Sci 2002;47:2056–63. [PubMed: 12353855]
18. Camoglio L, te Velde AA, de Boer A, ten Kate FJ, Kopf M, van Deventer SJ. Hapten-induced colitis associated with maintained Th1 and inflammatory responses in IFN-gamma receptor-deficient mice. Eur J Immunol 2000;30:1486–95. [PubMed: 10820397]
19. Rothenberg ME, Luster AD, Lilly CM, Drazen JM, Leder P. Constitutive and allergen-induced expression of eotaxin mRNA in the guinea pig lung. J Exp Med 1995;181:1211–6. [PubMed: 7869037]
20. Karhausen J, Furuta GT, Tomaszewski JE, Johnson RS, Colgan SP, Haase VH. Epithelial hypoxia-inducible factor-1 is protective in murine experimental colitis. J Clin Invest 2004;114:1098–106. [PubMed: 15489957]

21. Synnestvedt K, Furuta GT, Comerford KM, Louis N, Karhausen J, Eltzschig HK, et al. Ecto-5'-nucleotidase (CD73) regulation by hypoxia-inducible factor-1 mediates permeability changes in intestinal epithelia. J Clin Invest 2002;110:993–1002. [PubMed: 12370277]
22. Panwala CM, Jones JC, Viney JL. A novel model of inflammatory bowel disease: mice deficient for the multiple drug resistance gene, mdr1a, spontaneously develop colitis. J Immunol 1998;161:5733–44. [PubMed: 9820555]
23. Mashimo H, Wu DC, Podolsky DK, Fishman MC. Impaired defense of intestinal mucosa in mice lacking intestinal trefoil factor. Science 1996;274:262–5. [PubMed: 8824194]
24. Forbes E, Murase T, Yang M, Matthaei KI, Lee JJ, Lee NA, et al. Immunopathogenesis of experimental ulcerative colitis is mediated by eosinophil peroxidase. J Immunol 2004;172:5664–75. [PubMed: 15100311]
25. Hendrickson BA, Gokhale R, Cho JH. Clinical aspects and pathophysiology of inflammatory bowel disease. Clin Microbiol Rev 2002;15:79–94. [PubMed: 11781268]
26. Bouma G, Strober W. The immunological and genetic basis of inflammatory bowel disease. Nat Rev 2003;3:521–33.
27. Strober W, Fuss IJ, Blumberg RS. The immunology of mucosal models of inflammation. Annu Rev Immunol 2002;20:495–549. [PubMed: 11861611]
28. Dieleman LA, Ridwan BU, Tennyson GS, Beagley KW, Bucy RP, Elson CO. Dextran sulfate sodium-induced colitis occurs in severe combined immunodeficient mice. Gastroenterol 1994;107:1643–52.
29. Elias JA, Lee CG, Zheng T, Ma B, Homer RJ, Zhu Z. New insights into the pathogenesis of asthma. J Clin Invest 2003;111:291–7. [PubMed: 12569150]
30. Okamoto H. The REG gene family and REG proteins: with special attention to the regeneration of pancreatic B-cells. J Hepatobiliary Pancreat Surg 1999;6:254–62. [PubMed: 10526060]
31. Blumberg RS, Saubermann LJ, Strober W. Animal models of mucosal inflammation and their relation to human inflammatory bowel disease. Curr Opin Immunol 1999;11:648–56. [PubMed: 10631550]
32. Buhner S, Buning C, Genschel J, Kling K, Herrmann D, Dignass A, et al. Genetic basis for increased intestinal permeability in families with Crohn's disease: role of CARD15 3020insC mutation? Gut 2006;55:342–7. [PubMed: 16000642]
33. Peeters M, Geypens B, Claus D, Nevens H, Ghoos Y, Verbeke G, et al. Clustering of increased small intestinal permeability in families with Crohn's disease. Gastroenterol 1997;113:802–7.
34. Wyatt J, Vogelsang H, Hubl W, Waldhoer T, Lochs H. Intestinal permeability and the prediction of relapse in Crohn's disease. Lancet 1993;341:1437–9. [PubMed: 8099141]
35. Gironella M, Iovanna JL, Sans M, Gil F, Penalva M, Closa D, et al. Antiinflammatory effects of pancreatitis associated protein in inflammatory bowel disease. Gut 2005;54:1244–53. [PubMed: 15870231]
36. Fichtner-Feigl S, Fuss IJ, Preiss JC, Strober W, Kitani A. Treatment of murine Th1- and Th2-mediated inflammatory bowel disease with NF-kappa B decoy oligonucleotides. J Clin Invest 2005;115:3057–71. [PubMed: 16239967]
37. Wang ML, Shin ME, Knight PA, Artis D, Silberg DG, Suh E, et al. Regulation of RELM/FIZZ isoform expression by Cdx2 in response to innate and adaptive immune stimulation in the intestine. Am J Physiol Gastrointest Liver Physiol 2005;288:G1074–83. [PubMed: 15576623]
38. Brasch-Andersen C, Haagerup A, Borglum AD, Vestbo J, Kruse TA. Highly significant linkage to chromosome 3q13.31 for rhinitis and related allergic diseases. J Med Gen 2006;43:10–7.
39. Zimmermann N, King NE, Laporte J, Yang M, Mishra A, Pope SM, et al. Dissection of experimental asthma with DNA microarray analysis identifies arginase in asthma pathogenesis. J Clin Invest 2003;111:1863–74. [PubMed: 12813022]
40. Zimmermann N, Hershey GK, Foster PS, Rothenberg ME. Chemokines in asthma: cooperative interaction between chemokines and IL-13. J Allergy Clin Immunol 2003;111:227–42. [PubMed: 12589338]

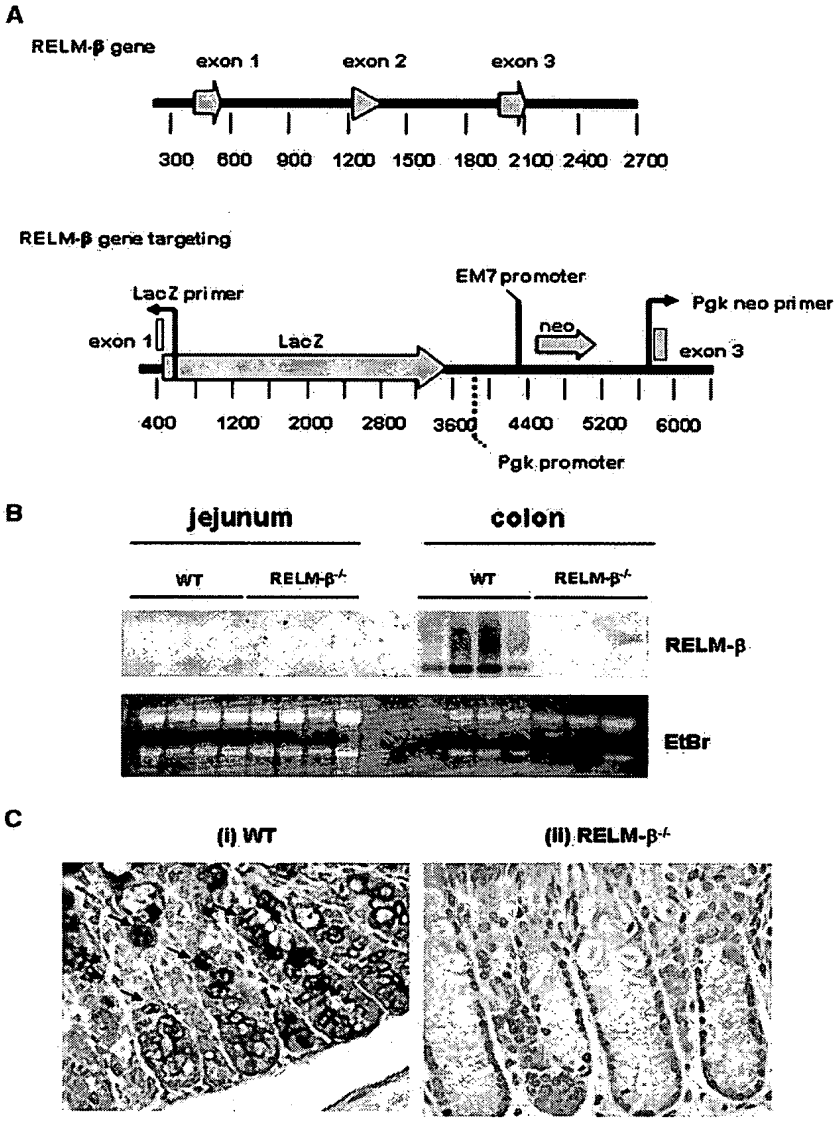

FIG 1.

Generation of RELM-$\beta^{-/-}$ mice. RELM-$\beta^{-/-}$ mice were developed by using VelociGene technology.[14] A, Diagram shows the WT murine RELM-β gene locus and the gene-targeted locus. The RELM-β gene was replaced by a reporter-selection cassette, which consists of a b-galactosidase enzyme gene (LacZ) and a neomycin resistance gene (Neo). B, Northern blot analysis of total jejunum and colon RNA (20 mg) was used to examine RELM-β mRNA expression in WT and RELM-$\beta^{-/-}$ mice. As an RNA loading control, the position of the 18S and 28S RNA band in the ethidium bromide (EtBr)-stained gels is also shown. Each lane represents a separate animal. C, Immunohistochemically stained sections of colon from WT and RELM-$\beta^{-/-}$ mice using the RELM-β-specific polyclonal antiserum. Filled arrows depict RELM-β^{1} cells. Original magnification: C, 3200.

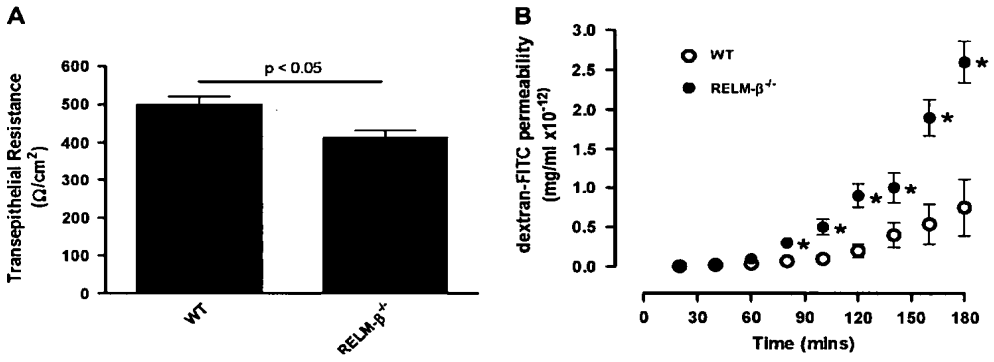

FIG 2.

RELM-β deficiency alters transepithelial barrier permeability. A, Transepithelial resistance of colonic segments of muscle-free intestinal mucosa from WT and RELM-$\beta^{-/-}$ mice. B, FITC-dextran (molecular weight 4400) permeability in muscle-free intestinal mucosal specimens from the colon from WT and RELM-$\beta^{-/-}$ mice. Values are presented as means 6 SEM (n 5 3-8 mice per group). Statistical significance of differences was determined by using an unpaired Student t test. $^{*}P < .05$ compared with WT mice.

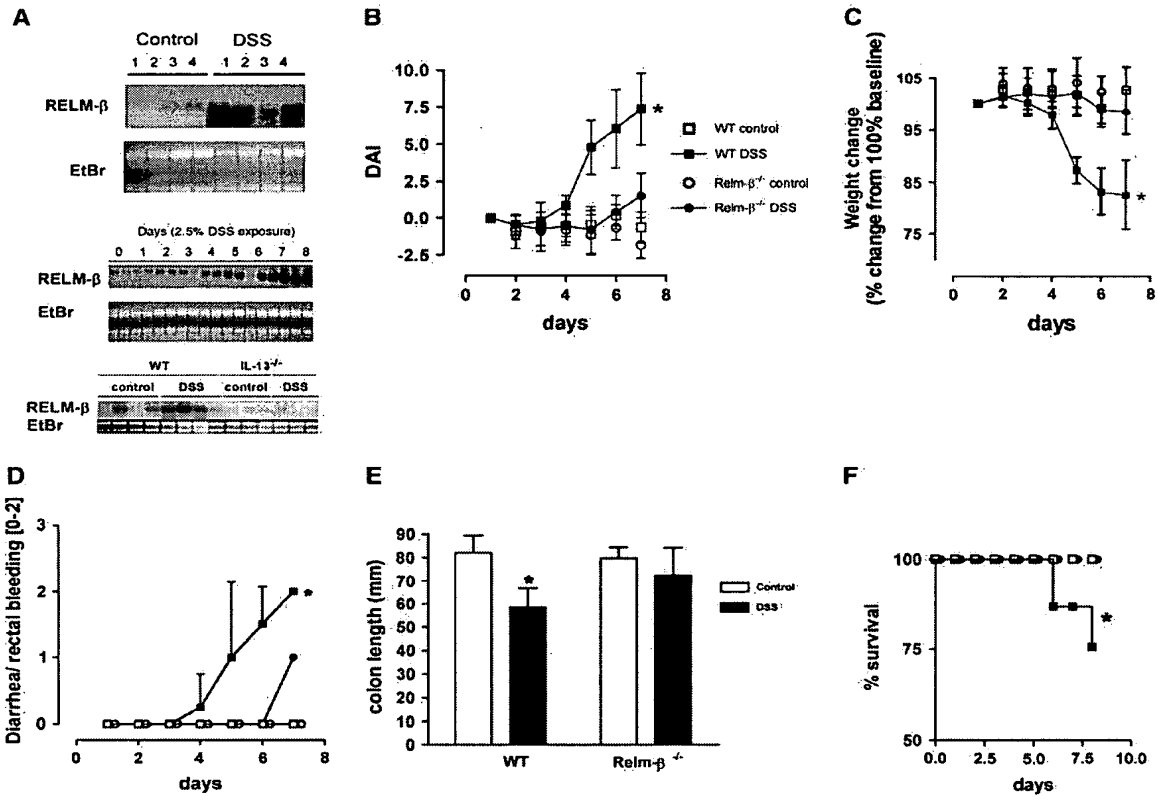

FIG 3.

DSS treatment induces experimental colitis in WT and RELM-$\beta^{-/-}$ mice. A, Northern blot analysis of RELM-β mRNA expression in the colons of control (top panel) and DSS-treated (middle panel) WT mice and kinetics (days 0-8) of RELM-β mRNA expression in the colons of WT mice and IL-$13^{-/-}$ mice (bottom panel) on day 7. Total RNA is shown by ethidium bromide (EtBr) staining. DAI (B), weight change (C), diarrhea-rectal bleeding score (D), and colon length (E; day 7) of control- and DSS-treated WT and RELM-$\beta^{-/-}$ mice. F, The percentage survival during the course of DSS treatment in WT and RELM-$\beta^{-/-}$ mice. Data in Fig 3, B through F, represent the mean 6 SEM of 4 to 5 mice per group from triplicate experiments. Statistical significance of differences was determined by using the Kruskal-Wallis test ($^{*}P < .05$).

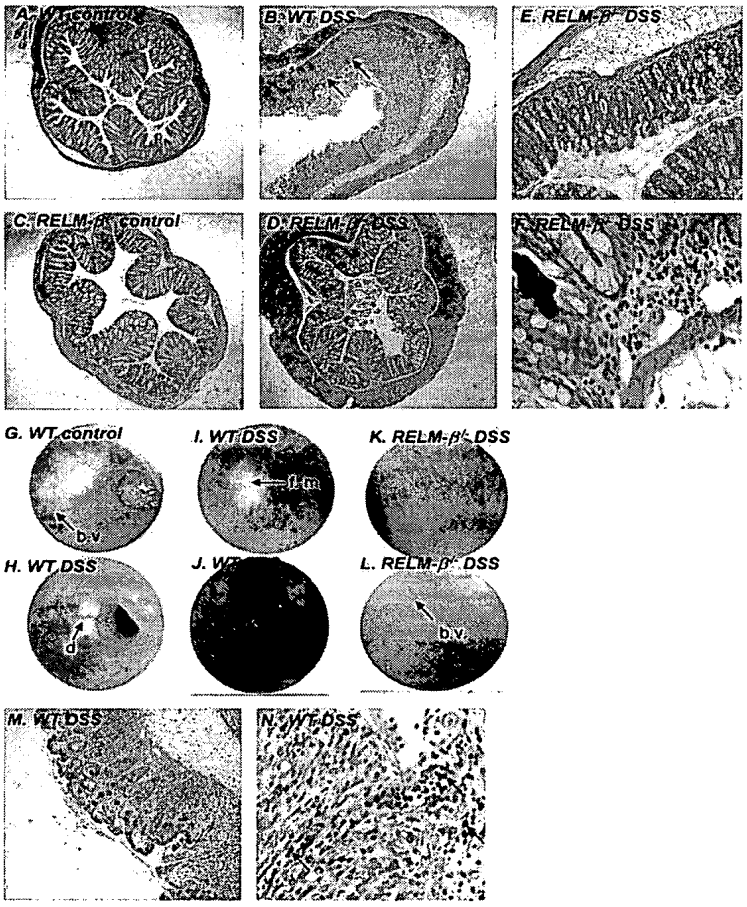

FIG 4.

Histopathology and colonoscopy in the colons of DSS-treated WT and RELM-$\beta^{-/-}$ mice. A-F, Representative photomicrographs of colons from control and DSS-treated WT and RELM-$\beta^{-/-}$ mice. G-L, Representative colonoscopy photographs of colons of control and DSS-treated WT and RELM-$\beta^{-/-}$ mice. M and N, Representative photomicrographs of immunohistochemically stained colon sections from DSS-treated WT mice using the RELM-β-specific polyclonal antiserum. Black arrows depict RELM-^{1} inflammatory cells. Black arrows in Fig 4, B, depict ulceration of the epithelial cell layer: black arrows in Fig 4, G and L, depict normal colonic vasculature (b.v., blood vessel); black arrows in Fig 4, I, H, and J, depict mucus and diarrhea (d), friable mucosa (f. m.), and rectal bleeding (b). Fig 4, H, Narrowing of colon, with evidence of a stricture. Original magnification: A-D, 350; E and M, 3100; F and N, 3200.

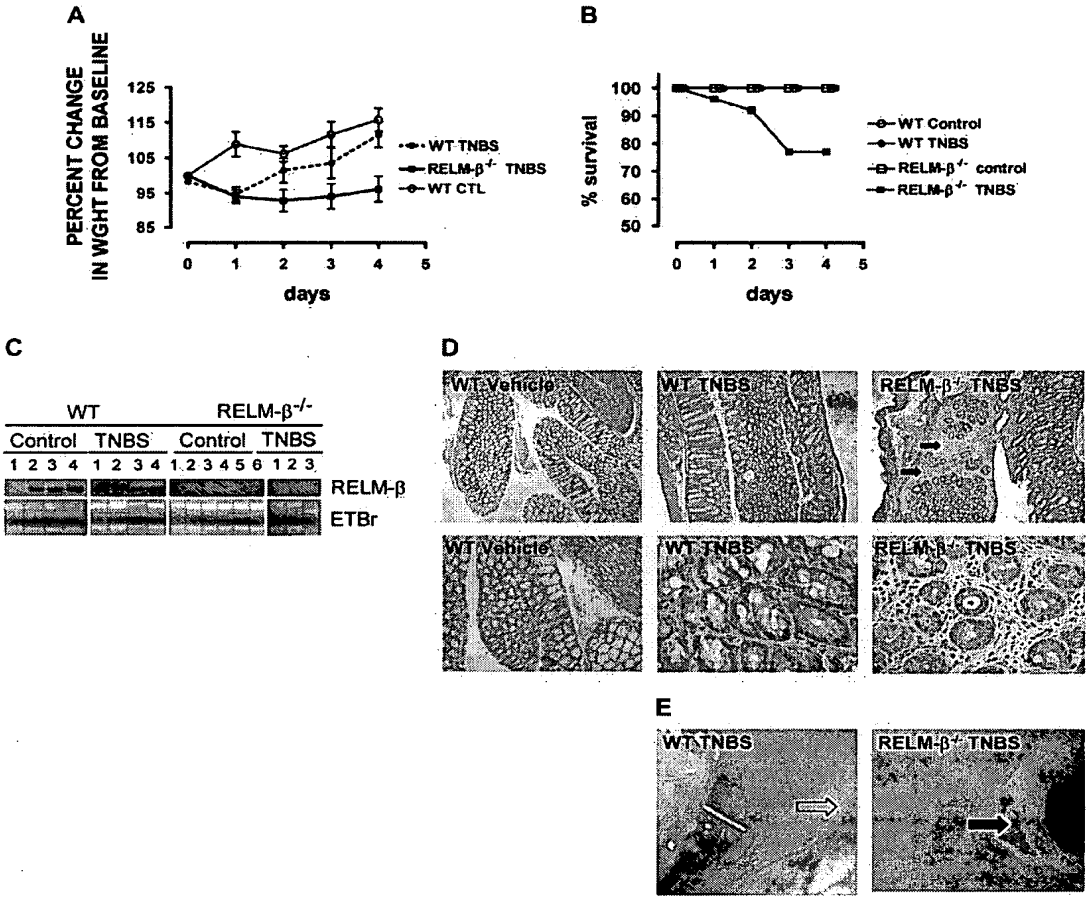

FIG 5.

Colon histopathology and colonoscopy in TNBS-treated WT and RELM-$\beta^{-/-}$ mice. A, Percentage weight change of control-treated and TNBS-treated WT and RELM-$\beta^{-/-}$ mice. B, Percentage survival during the course of DSS treatment in WT and RELM-$\beta^{-/-}$ mice. C, Northern blot analysis of RELM-β mRNA expression in the colons of control-treated and TNBS-treated WT and RELM-$\beta^{-/-}$ mice on day 5. Total RNA is shown by means of ethidium bromide (EtBr) staining. D, Hematoxylin and eosin staining of representative colon transverse sections on day 5 after TNBS administration. E, Representative colonoscopy from TNBS-treated WT and RELM-$\beta^{-/-}$ mice. The black arrows in Fig 5, D, depict cellular infiltrate. The open arrow in Fig 5, E, depicts normal colonic vasculature, and the black arrow depicts a colonic ulcer. Data in Fig 5, A and B, represent the mean 6 SEM of 4 to 5 mice per group from triplicate experiments. Statistical significance of differences was determined by using the Kruskal-Wallis test. $^{*}P < .05$.

A

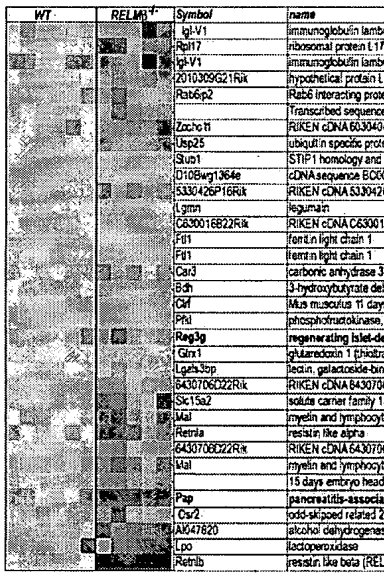

Symbol	name	Fold change	genbank	probe
Igl-V1	immunoglobulin lambda chain, variable 1	3.304	M94350	1424931_a_at
Rpl17	ribosomal protein L17	2.68	BF453359	1453763_at
Igl-V1	immunoglobulin lambda chain, variable 1	2.551	AK008145	1436523_a_at
2010309G21Rik	hypothetical protein LOC207685	2.449	AK008551	1428720_a_at
Rsb6p2	Rsb6 interacting protein 2	2.204	BB199103	1441493_at
	Transcribed sequences	2.093	BB283625	1444399_at
Zoch ti	RIKEN cDNA 6030404K05 gene	2.079	BG060248	1439631_at
Usp25	ubiquitin specific protease 25	2.04	NM_012918	1448939_at
Stub1	STIP1 homology and U-Box containing protein 1	0.5	NM_019719	1416580_a_at
D10Bwg1364e	cDNA sequence BC005632	0.499	BC005632	1415753_at
5330426P16Rik	RIKEN cDNA 5330426P16 gene	0.487	AK019912	1430030_at
Lgmn	legumain	0.484	NM_011175	1448883_at
C630016B22Rik	RIKEN cDNA C630016B22 gene	0.477	BB711990	1434253_s_at
Fth1	ferritin light chain 1	0.474	NM_008049	1422302_a_at
Fth1	ferritin light chain 1	0.471	NM_010240	1418364_a_at
Car3	carbonic anhydrase 3	0.451	NM_007606	1460256_at
Bdh	3-hydroxybutyrate dehydrogenase (heart, mitochondrial)	0.446	BF322712	1426659_at
Clrl	Mus musculus 11 days pregnant adult female ovary and uterus cDNA,C-type lectin related f, full insert sequence.	0.444	AK017207	1431240_at
Pfkl	phosphofructokinase, liver, B-type	0.443	BE914497	1439148_a_at
Reg3g	**regenerating islet-derived 3 gamma (REG3γ)**	**0.44**	**NM_011260**	**1448872_at**
Glrx1	glutaredoxin 1 (thioltransferase)	0.43	AF276917	1416593_at
Lgals3bp	lectin, galactoside-binding, soluble, 3 binding protein	0.428	NM_011150	1448380_at
6430706D22Rik	RIKEN cDNA 6430706D22 gene	0.409	BM248225	1454688_at
Slc15a2	solute carrier family 15 (H+/peptide transporter), member 2	0.407	NM_021301	1417600_at
Mal	myelin and lymphocyte protein, T-cell differentiation protein	0.403	AK019046	1432558_a_at
Retnla	resistin like alpha	0.403	NM_020509	1449015_at
6430706D22Rik	RIKEN cDNA 6430706D22 gene	0.394	BM248225	1433685_a_at
Mal	myelin and lymphocyte protein, T-cell differentiation protein	0.382	NM_010762	1417275_at
	15 days embryo head cDNA, clone D930035F11	0.375	BQ176176	1435467_at
Pap	**pancreatitis-associated protein (REG3β)**	**0.364**	**NM_011035**	**1416297_s_at**
Osr2	odd-skipped related 2 (Drosophila)	0.306	AY036074	1425155_a_at
AI647820	alcohol dehydrogenase PAN18-like	0.301	AI650442	1460606_at
Lpo	lactoperoxidase	0.236	NM_080420	1448998_at
Retnlb	resistin like beta (RELMβ)	0.0118	NM_023381	1418368_at

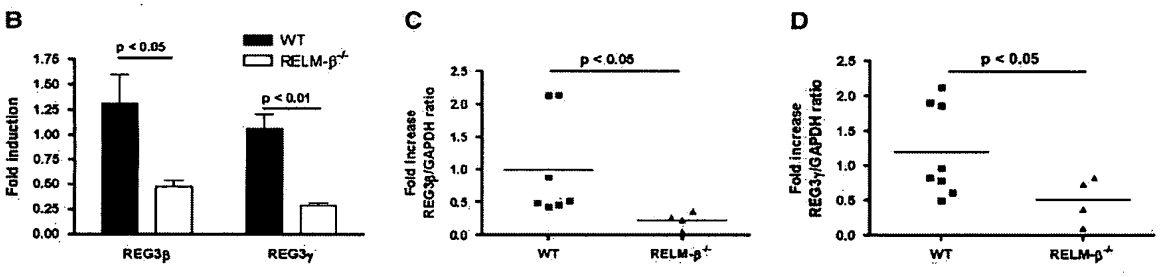

FIG 6.

Gene profile analysis of the colon in the absence of RELM-β. A, Microarray analysis of the transcripts expressed in colonic samples. RNA from each mouse was subjected to chip analysis with Affymetrix mouse Genome MOE430_2 GeneChips. The RELM-$\beta^{-/-}$ group is composed of 5 mice, and the WT group is composed of 6 mice. The 32 genes differentially expressed (2-fold cut off and $P < .05$) in the RELM-$\beta^{-/-}$ mice compared with the WT mice have been ordered (fold change); upregulated genes are shown in red, and downregulated genes are shown in blue. The magnitude of the gene changes is proportional to the darkness of the color. Each column represents an individual mouse, and each line represents a separate gene. B, Quantitative analysis of REG3β and REG3γ expression levels in the colons of WT and RELM-$\beta^{-/-}$ mice using Affymetrix mouse Genome U430 Plus 2.0 GeneChips. C and D, Quantitative analysis of REG3β (Fig 6, C) and REG3γ (Fig 6, D) mRNA levels in the colons of WT and RELM-$\beta^{-/-}$ mice by using real-time PCR analysis. REG3 expression was normalized to GADPH expression in each individual sample. Results are expressed as fold change over WT mice. The black line represents the mean value in each group.

TABLE I

Histologic colitis score of colons of TNBS-treated WT and RELM-$\beta^{-/-}$mice

	WT mice		RELM-$\beta^{-/-}$mice	
	Control	TNBS	Control	TNBS
Area involved (%)	0 ± 0	0.3 ± 0.7	0.1 ± 0.4	2.3 ± 2.1*
Crypt loss (%)	0 ± 0	0.2 ± 0.4	0.1 ± 0.4	1.8 ± 1.5*
Erosion-ulceration	0 ± 0	0.2 ± 0.4	0.1 ± 0.4	3.3 ± 3.2*
Cellular infiltration				
Lamina propria	0 ± 0	0.2 ± 0.4	0.0 ± 0.0	1.5 ± 1.3*
Submucosa	0 ± 0	0.1 ± 0.3	0.0 ± 0.0	1.8 ± 1.5*
Edema	0 ± 0	0.2 ± 0.4	0.1 ± 0.4	1.8 ± 1.5*

Data are presented as mean histologic colitis scores (points) ± SD (n = 4-8 mice per group). The Kruskal-Wallis test was performed to analyze differences between treatment groups (*$P < .05$).

FEBS Letters 580 (2006) 900–903

Human RELMβ is a mitogenic factor in lung cells and induced in hypoxia

Aparna Renigunta[a], Christiane Hild[a], Frank Rose[a], Walter Klepetko[b], Friedrich Grimminger[a], Werner Seeger[a], Jörg Hänze[a,*]

[a] *University of Giessen Lung Center (UGLC), Medical Clinic II, Biochemistry, Friedrichstr. 24, Justus-Liebig University, D-35392 Giessen, Germany*
[b] *Cardiothoracic Surgery, University Hospital, Währinger Grütel 18-20, 1220 Vienna, Austria*

Received 18 November 2005; revised 20 December 2005; accepted 3 January 2006

Available online 18 January 2006

Edited by Lukas Huber

Abstract RELMβ (resistin-like molecule) represents the most related human homologue of mouse RELMα, also known as hypoxic-induced mitogenic factor (HIMF). In this study, we isolated RELMβ cDNA from human lung tissue and performed regulatory and functional expression studies. RELMβ mRNA was upregulated in hypoxia in human lung A549 cell line as well as primary cultured adventitial fibroblasts and smooth muscle cells (SMC) of pulmonary arteries. Upon transfection of a RELMβ encoding expression plasmid into these cells, we observed significant induction of proliferation particularly in SMC and A549 cells, which could be blocked by phosphatidyl-inositol 3-kinase (PI3K) inhibitors LY294002 and wortmannin. The results suggest that human RELMβ may contribute to hypoxic-induced pulmonary vascular remodeling processes or hypoxia related fibrotic lung disease.

Keywords: Resistin like moleculeβ; Hypoxic-induced mitogenic factor; Pulmonary artery; Smooth muscle cells; Fibroblast; Hypoxia; Proliferation

1. Introduction

RELMβ (resistin-like molecule) and resistin are the two human members of the resistin gene family also named FIZZ2 and FIZZ3 (found in inflammatory zone) encoding small cysteine-rich secreted proteins [1,2]. In mouse, a third member RELMα (FIZZ1) has been identified not present in human [3,4]. Mouse RELMα is also described as hypoxia-inducible mitogenic factor (HIMF) and strongly contributes to hypoxic-induced pulmonary vascular remodeling by triggering proliferation of smooth muscle cells (SMC) and exerting strong vasoconstrictive effects on pulmonary vasculature. Additionally, angiogenic properties have been described for HIMF [3]. Since RELMβ is the closest human homologue of mouse HIMF, we were interested in RELMβ gene expression especially in human lung. We isolated its cDNA from human lung homogenate, and studied its hypoxic dependent regulation in pulmonary vascular cells and human lung epithelial A549 cell line. We observed significant induction of RELMβ in hypoxia and found proliferative effects particularly in A549 cells and SMC from pulmonary artery. Induction of proliferation appeared to be mediated by phosphatidyl-inositol-kinase (PI3K) pathway, since LY294002 and wortmannin inhibited proliferation strongly in RELMβ transfected cells.

2. Materials and methods

2.1. Cell culture and human lung tissue

Culturing of human epithelial lung cell line A549 was performed according to the protocol given by the American type culture collection. Human cell preparations were established from excess lung tissue originating from human donor lungs employed for transplantation. This protocol was approved by the Justus-Liebig University Ethics committee. Cells were isolated by careful dissection of parenchymal connective tissue as described. Primary adventitial fibroblasts (FB) and SMC from the pulmonary artery were isolated and cultured as described [5]. In brief, primary FB were isolated from human pulmonary artery by careful dissection of parenchymal connective tissue. The adventitia of <1 mm^3 tissue pieces was removed and placed into 12-well cell culture plates with 500 μl culture medium. Primary SMC were isolated from human pulmonary artery by carefully preparing <1 mm^3 pieces of media, devoid of adventitial tissue as assessed by microscopic control. Experiments were performed with cells in passage 3 or 4.

2.2. Transfection

For transfection, cells were grown to ~80% confluence. 0.2 μg Plasmid-DNA was mixed with synthetic peptide Tat-RGD (GML GIS YGR KKR RQR RRP PQT GGC RGD MFG C) which was employed as an enhancer of transfection. 2.5 μg of Tat-RGD was used per well for A549 cells and 0.8 μg/well for FB and SMC. The volume was made up to 25 μl with Hank's buffered saline. This mixture was incubated at room temperature for 15 min. Then 0.5 μl/well Lipofectamin 2000® (Invitrogen, Carlsbad, CA, USA) was added and incubated at room temperature for further 15 min. This mixture was added to the cells. Followed by incubation at 37 °C for 4 h, the medium was replaced and cells cultured under standard conditions for 24 h.

2.3. Isolation and construction of expression plasmid for RELMβ cDNA

For cloning of the full length RELMβ cDNA we performed RT-PCR using RNA extracts from human lung tissue with primers derived from human RELMβ cDNA sequence (Accession No.: AF323084): PHIMF-f: ccc cag gac act gac tct gta and M-HIMF-f: aaa ctg agt tct cag cct cct c. The purified PCR product was ligated into pGEM-T-easy plasmid (Promega) and positive clones were sequenced. Inserts from pGEM-T-easy plasmid were amplified by PCR for subcloning into pCMV expression plasmid (Clontech, Paolo Alto, USA) using the following primers: HIMF-kozak-kpn1: ctt ggt acc gcc gcc acc ATG GGG CCG TCC TCT TGC CTC C; HIMF-HA-TGA-xho1: gaa ctc gag tca gcc gcc acc agc gta atc tgg aac atc gta tgg gta gcc acc ggt cag gtg gca gca gcg ggc agt ggt cc. The forward primer contained a *Kozak* sequence as an optimized translation start and the reverse primer carried a hemeagglutinin A (HA) tag in frame at the C-terminus.

*Corresponding author. Fax: +49 641 99 42429.
E-mail address: joerg.haenze@uglc.de (J. Hänze).

Abbreviations: RELM, resistin like molecule; HIMF, hypoxic-induced mitogenic factor; FIZZ, protein found in inflammatory zone; SMC, smooth muscle cells; FB, fibroblast

0014-5793/$32.00
doi:10.1016/j.febslet.2006.01.012

2.4. RELMβ-mRNA analysis by RT-PCR

RNA was extracted from human lung tissue or cells incubated for 24 h in normoxic or hypoxic (1% oxygen concentration) conditions using guanidine thiocyanate-acid phenol (RNAzol B, WAK-Chemie, Germany). Total RNA for human tissues screening were purchased (Premium RNA; Clontech, Paolo Alto, USA). 1 μg of RNA per sample was copied to cDNA using reverse transcriptase (MMLV-RT, Invitrogen, Carlsbad, CA, USA) with 100 ng 15-mers of oligo-dT primer. As a negative control, MMLV-RT was omitted (data not shown). The following primers were used: hRELMβ+: 5′ CCC TTC TCC AGC TGA TCA AC 3′, hRELMβ−: 5′ CCA CGA ACC ACA GCC ATA G 3′, HPRT+: 5′ TCG AGA TGT GAT GAA GGA GAT GGG A 3′, HPRT−: 5′ TCA AAT CCA ACA AAG TCT GGC CTG T 3′. The cycling conditions were 95 °C for 15 m, followed by 40 cycles of 94 °C for 10 s, 52 °C for 30 s, 72 °C for 30 s and a final extension with 72 °C for 10 m. Real-time PCR was performed using the ABI Prism 7700 detection system (Applied Biosystems, Foster City, CA, USA) with SYBR-Green as fluorescent dye, enabling real-time detection of PCR products according to the manufacturer's protocol. HPRT mRNA was used as internal control for calculation of ΔCT (Threshold cycle) values and relative quantification.

2.5. Western-blot

Cells were lysed using Laemmli buffer and denatured for 5 m at 95 °C and run on a sodium dodecyl sulfate–polyacrylamide gel. After electroblot of the gel to a nylon membrane (PVDF, Pal), HA specific bands were visualized by a monoclonal mouse antibody against HA added at a dilution of 1:10000 (Sigma–Aldrich) and chemiluminescence (ECL, Amersham, Freiburg, Germany) by using a second biotin-coupled anti-mouse antibody and a complex of biotin and streptavidin coupled with horseradish peroxidase. As a loading control, samples were also analyzed by Western-blot analysis for cytoplasmic β-actin with a mouse monoclonal anti β-actin antibody (Abcam, 1:10000 dilution).

2.6. MTT assay

The MTT (3-(4,5-dimethylthiazol-2-yl)-2,5-diphenyltetrazolium bromide) assay was performed as a measurement of number of viable cells. Cells were seeded in 96-wellplates and transfected by expression plasmid. After 24 h, MTT (0.2 mg/ml) was added to each well, and incubation continued for 1–2 h at 37 °C. The extent ofMTT reduction to formazan within cells was quantified by spectrophotometric measurement at 490 nm.

2.7. BrdU incorporation

Cellular DNA synthesis (cell cycle S-phase) was assessed by incorporation of the thymidine analogue 5-bromo-20-deoxyuridine (BrdU) into the DNA of replicating cells using a commercially available colorimetric immunoassay according to the recommended protocol of the company (Roche, Mannheim, Germany). After addition of BrdU to cells they were fixed and incorporated BrdU was measured by ELISA using a specific BrdU antibody. The values given in the figures represent the raw data obtained by photometric measurement at 450 nm.

3. Results

For analysis of human RELMβ gene expression, we initially isolated a full-length cDNA of RELMβ from human lung tissue RNA by RT-PCR strategy. The nucleic acid sequence (Submitted to EMBL Accession No.: AM050721) differed at positions 59 and 97 after start of translation from a published sequence (Accession No.: AF323084), resulting in two amino-acid exchanges (proline to leucine and lysine to glutamine). The alignment of cDNAs of human RELMβ and mouse HIMF (NCBI Accession No.: BC029248) reveals sequence identity of 69%. Comparison of the amino acid sequences yields a sequence similarity of 58.6% and a sequence identity of 49.6%.

Tissue screening of RELMβ expression revealed expression in lung, heart, kidney and adrenal gland, highest expression in intestine, whereas in brain and liver no signal was detectable (Fig. 1A). Since HIMF plays an important role in hypoxic adaptive processes in lung physiology in mouse, we analyzed hypoxic gene regulation of RELMβ, a HIMF homologue, in human lung cells. To this end, we employed the lung epithelial A549 cell line, as well as primary cultured SMC and adventitial FB from human pulmonary arteries (Fig. 1B). RELMβ mRNA was analyzed in extracts of these cells by realtime-RT-PCR. When related to the house keeping gene hypoxanthin-phospho-ribosyl-transferase (HPRT) mRNA, we found highest basal RELMβ mRNA levels in SMC followed by A549 and FB cells. Strongest RELMβ mRNA hypoxic induction was observed in A549 cells followed by SMC and FB. For further functional analysis, we transfected these cells by an expression plasmid recombinant with RELMβ cDNA and tagged with hemeaglutinin A (HA) for protein analysis by anti-HA antibody. Control cells were transfected with the corresponding empty plasmid. Transfected cells were studied with regard to proliferation by measuring the overall cellular mitochondrial respiratory chain activity with MTT assay and cellular DNA synthesis by BrdU incorpration (Fig. 2A and B). Induction of proliferation by RELMβ was observed in all investigated cell types, being stronger in A549 and SMC than

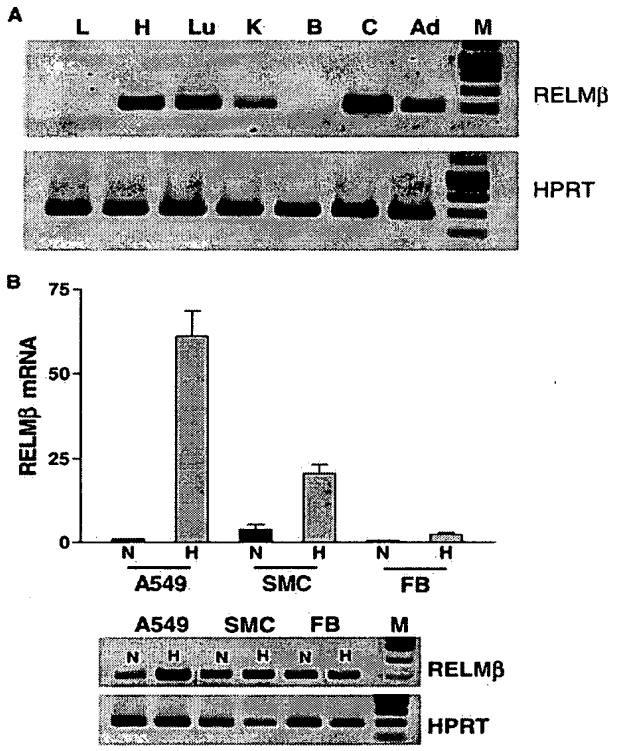

Fig. 1. (A) RELMβ mRNA expression as analyzed by RT-PCR in various human tissues (L: liver; H: heart; Lu: Lung; K: kidney; B: brain; C: colon intestine; Ad: adrenal gland). As a control, house keeping RT-PCR product of HPRT mRNA is shown. (B) Quantification of RELMβ mRNA in A549 cells, SMC and FB cultured in normoxia (N) or hypoxia (H) for 24 h by real-time RT-PCR in comparison to HPRT mRNA (mean ± S.E.M., $n = 3$). A representative gel electrophoretic analysis of the integrity and specificity of the PCR products from the realtime RT-PCRs is shown below the bar graph.

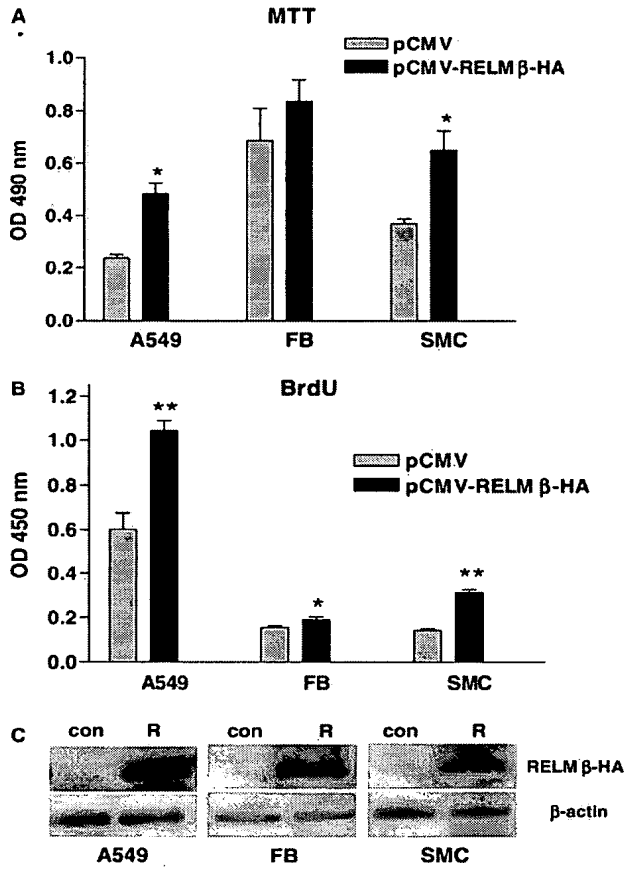

Fig. 2. Analysis of proliferation by MTT test or BrdU incorporation of A549 cells, SMC and FB cells transfected with RELMβ-HA tagged expression plasmid (pCMV-RELMβ-HA) or empty plasmid (pCMV). Significant induction of proliferation in cells overexpressing hRELMβ is observed. (A) MTT results (mean ± S.D., $n = 4$ $^{*} < 0.05$ Mann–Whitney-test). (B) BrdU results (mean ± S.D., $n = 8$ for A549, $n = 6$ for FB, $n = 8$ for SMC, $^{*} < 0.05$, $^{**} < 0.01$ Mann–Whitney-test). (C) As a control for RELMβ overexpression, cellular extracts were analyzed by HA-Western-blot showing signals only in case of pCMV-RELMβ-HA transfected cells (R) but not in empty plasmid transfected cells (pCMV). Shown is a representative blot of $n > 3$ experiments.

FB cells. Transfection and expression of HA-tagged RELMβ cDNA was confirmed by HA Western-blot analysis (Fig. 2C) showing immunoreactivity in RELMβ transfected cells but not in empty plasmid transfected cells. Since the mitogenic effect of HIMF in mouse cells could be blocked by inhibitors of PI3K/Akt signal transduction, we performed experiments employing wortmannin or LY294002 for inhibition of PI3K. In A549 cells which were transfected by RELMβ expression plasmid, we observed significant reduction of proliferation (>50%) when treated with wortmannin or LY294002. In cells transfected with empty vector, we observed no effect on proliferation using these inhibitors. As a further control, we included non-transfected cells in the experiments. These cells revealed higher S-phase activity when compared to the transfected cells and demonstrated a significant but slight decrease (~15%) of proliferation upon PI3K inhibitor treatments (Fig. 3).

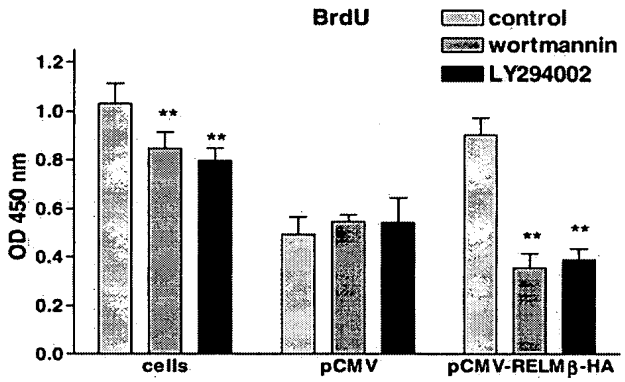

Fig. 3. Analysis of proliferation as measured by BrdU incorporation in A549 cells. Cells were either non-transfected (cells) or transfected by pCMV-HA, or by pCMV-RELMβ-HA and then incubated with LY29004 (40 μM) or wortmannin (100 nM) added to the medium (mean ± S.D., $n = 5$, $^{**} < 0.01$ Mann–Whitney-test).

4. Discussion

In this study, we have analyzed the gene expression, hypoxic regulation and proliferative effects of RELMβ in human lung cells. Our study was inspired by investigations on the related HIMF gene in mouse, also described in other context as RELMα or FIZZ1 [3]. Human RELMβ represents the gene with the highest homology with mouse HIMF, however, it is not considered as the human ortholog gene of mouse HIMF, which appears not to exist [4]. In this report, we have analyzed the expression, hypoxic regulation and pro-proliferative potency of RELMβ on human lung cells. We analyzed the expression pattern of human RELMβ on mRNA level by RT-PCR in several human tissues and found highest expression in lung, heart, colon, and adrenal gland, followed by kidney. Two studies examined HIMF expression in mouse. At protein level HIMF was only detectable by Western-blot in lung from hypoxic treated mice [3]. At mRNA level as analyzed by Northern-blot [6], HIMF was abundantly expressed in lung and less but significantly expressed in heart and skeletal muscle, whereas no signal was observed in brain and liver in accordance with our study. In conclusion, so far described differences and common grounds exist for expression of RELMβ in human, and of HIMF in mouse.

We found hypoxic induction of RELMβ in A549 cell line and primary vascular cells from human pulmonary arteries. The hypoxic induction was strongest in A549 cells followed by SMC and FB. Probably, this observation reflects that the expression of a given gene is regulated by specific factors which differ between cells. Hypoxic gene induction may be HIF-dependent via hypoxia-responsive-elements (HRE) [7]. Bioinformatic analysis of the human RELMβ gene revealed five putative HRE (RCGTG) binding sites. One site was located in the intervening intron sequence 2, and four at the 3′ flanking region (Table 1A). These putative regulatory DNA sequences need further experimental proof for their functional relevance. As comparison, putative HREs of the corresponding mouse HIMF gene are shown (Table 1B). Two HRE sites in the 5′ flanking region were detected which also require experimental investigation.

Table 1A
Putative HRE sequences of human RELMβ gene (EMBL Accession No.: AF352731)

HRE sequence	Location
gacgt **ACGTG** cagggaga	IVS2 4033/4016
cacta **ACGTG** gcatctag	3′FS +314/+331
tgtcc **ACGTG** atctcatt	3′FS +417/+434
aacat **ACGTG** tgcatgtg	3′FS +674/+691
catag **GCGTG** ggcaagga	3′FS +1303/+1286

Table 1B
Putative HRE sequences of mouse RELMα (HIMF) gene (EMBL Accession No.: mm_ensembl11:CHR16_11_1177_04)

HRE sequence	Location
tacag **ACGTG** gatgctct	5′FS −3805/−3788
tgtgt **GCGTG** tgtgtgtg	5′FS −624/−610

HRE core sequence: RCGTG (R is A or G), IVS: Intervening sequence (intron), FS: flanking sequence (numbering: 3′FS: + is downstream from end of transcription; 5′FS: − is upstream from start of transcription; IVS2: numbering with regard to complete gene sequence).

In transfected cells overexpressing RELMβ, significant proliferative effects were observed. Thus, this study suggests that RELMβ in the human system is similarly regulated as described for HIMF in mouse, and acts as a hypoxia-driven pro-proliferative factor. Moreover, the pro-proliferative effect of RELMβ could be suppressed by two PI3K inhibitors, a characteristic also observed for HIMF in mouse cells. PI3K has been demonstrated to mediate proliferation in human pulmonary SMC via serine/threonine kinase Akt which directly affects cell cycle regulation [8]. Thus, the signalling mechanisms by so far unknown receptors appear to be similar between RELMβ and HIMF. Consequently, RELMβ in human may play a role in hypoxic-induced pulmonary remodelling leading to pulmonary hypertension, and in fibrotic lung diseases associated with hypoxia.

Further features of HIMF were explored in mice experiments. Beside proliferative effects, HIMF was demonstrated to have angiogenic (subcutaneous mouse in vivo matrigel plug model) and vasoconstrictive properties in pulmonary artery [3]. In addition, HIMF was shown to play a role in lung development, by regulation of apoptosis and participation in alveolarization and lung maturation [9] and compensatory lung growth after pneumectomy [10]. Also, HIMF (FIZZ1) was shown to be strongly increased during allergic pulmonary inflammation [6]. The exploration of these characteristics regarding RELMβ in the human system remains open. So far, functional aspects of RELMβ and resistin have been mainly described in mice with respect to resistence to insulin [2,11,12]. Resistin, mainly expressed in adipocytes, and RELMβ, expressed particularly expressed in epithelial cells from intestine, were demonstrated to mediate resistance to insulin leading to increased glucose production.

In sum, our study revealed new findings for human RELMβ as a factor which is induced in hypoxia and which exerts pro-proliferative effects. These effects were observed in human primary vascular cells originating from pulmonary arteries, and in lung A549 cell line. Thus, features of human lung RELMβ resemble those of HIMF in mouse lungs.

Acknowledgments: This work was supported by the Deutsche Forschungsgemeinschaft: Sonderforschungs-bereich SFB 547, project B9, and the Graduate Seminar (GK534) "Biological Fundamentals of Vascular Medicine" sponsoring A. Renigunta.

References

[1] Patel, S.D., Rajala, M.W., Rossetti, L., Scherer, P.E. and Shapiro, L. (2004) Disulfide-dependent multimeric assembly of resistin family hormones. Science 304, 1154–1158.
[2] Steppan, C.M. et al. (2001) A family of tissue-specific resistin-like molecules. Proc. Natl. Acad. Sci. USA 98, 502–506.
[3] Teng, X., Li, D., Champion, H.C. and Johns, R.A. (2003) FIZZ1/RELMalpha, a novel hypoxia-induced mitogenic factor in lung with vasoconstrictive and angiogenic properties. Circ. Res. 92, 1065–1067.
[4] Yang, R.Z., Huang, Q., Xu, A., McLenithan, J.C., Eisen, J.A., Shuldiner, A.R., Alkan, S. and Gong, D.W. (2003) Comparative studies of resistin expression and phylogenomics in human and mouse. Biochem. Biophys. Res. Commun. 310, 927–935.
[5] Rose, F. et al. (2002) Hypoxic pulmonary artery fibroblasts trigger proliferation of vascular smooth muscle cells: role of hypoxia-inducible transcription factors. FASEB J. 16, 1660–1661.
[6] Holcomb, I.N. et al. (2000) FIZZ1, a novel cysteine-rich secreted protein associated with pulmonary inflammation, defines a new gene family. EMBO J. 19, 4046–4055.
[7] Wenger, R.H., Stiehl, D.P. and Camenisch, G. (2005) Integration of oxygen signaling at the consensus HRE. Sci STKE 2005, re12.
[8] Goncharova, E.A., Ammit, A.J., Irani, C., Carroll, R.G., Eszterhas, A.J., Panettieri, R.A. and Krymskaya, V.P. (2002) PI3K is required for proliferation and migration of human pulmonary vascular smooth muscle cells. Am. J. Physiol. Lung. Cell Mol. Physiol. 283, L354–L363.
[9] Wagner, K.F., Hellberg, A.K., Balenger, S., Depping, R., Dodd, O.J., Johns, R.A. and Li, D. (2004) Hypoxia-induced mitogenic factor has antiapoptotic action and is upregulated in the developing lung: coexpression with hypoxia-inducible factor-2alpha. Am. J. Respir. Cell Mol. Biol. 31, 276–282.
[10] Li, D., Fernandez, L.G., Dodd-o, J., Langer, J., Wang, D. and Laubach, V.E. (2005) Upregulation of hypoxia-induced mitogenic factor in compensatory lung growth after pneumonectomy. Am. J. Respir. Cell Mol. Biol. 32, 185–191.
[11] Rajala, M.W., Obici, S., Scherer, P.E. and Rossetti, L. (2003) Adipose-derived resistin and gut-derived resistin-like molecule-beta selectively impair insulin action on glucose production. J. Clin. Invest. 111, 225–230.
[12] Steppan, C.M. et al. (2001) The hormone resistin links obesity to diabetes. Nature 409, 307–312.

Science
AAAS

Disulfide-Dependent Multimeric Assembly of Resistin Family Hormones

Saurabh D. Patel, *et al.*

Science **304**, 1154 (2004);
DOI: 10.1126/science.1093466

Science (print ISSN 0036-8075; online ISSN 1095-9203) is published weekly, except the last week in December, by the American Association for the Advancement of Science, 1200 New York Avenue NW, Washington, DC 20005.

teins were present in the cytosol. The specificity for glyphosate is high. Other common agrichemicals such as phosphinothricin, atrazine, and sulfonylureas are not acetylated by GAT (*11*).

Improved *gat* variants from the fifth iteration enabled the regeneration of glyphosate-tolerant transgenic tobacco plants. The plants were morphologically normal and fertile. To evaluate the tolerance profile of the tobacco plants, we selected T_1 plants that contained a segregating *gat* gene, using a glyphosate spray of 1 lb. acid equivalents per acre (ae/ac) and followed that with a dose-response regime using sprays of 2 to 24 lb. ae/ac. Untransformed plants showed severe symptoms or were killed by 1 lb. ae/ac (fig. S3A), whereas several transgenic GAT lines tolerated the highest dose sprayed (fig. S3B).

Fifth-iteration *gat* genes also allowed production of glyphosate-tolerant maize plants. T_0 plants were sprayed at the four-leaf stage with 104 oz./ac Roundup UltraMAX (4× field rate, equivalent to 3 lb. ae/ac glyphosate). The regenerants survived the treatment, but exhibited chlorotic banding and growth inhibition (Fig. 4B). Glyphosate tolerance improved with increases in the catalytic efficiency of GAT. With expression of seventh-iteration genes, nearly 50% of the maize regenerants showed no chlorotic banding and no growth inhibition (Fig. 4C). Most transformed plants expressing the best 10th and 11th round *gat* genes were tolerant to 6× glyphosate spray and showed no adverse symptoms (Fig. 4D). Efficacy trials of lines containing genes from several shuffling iterations are under way in the field to evaluate the commercial potential of this glyphosate tolerance trait.

Our approach shows that enzymes with useful yet insufficient activities can subsequently be improved by applying directed evolution until the desired activity is gained. DNA shuffling allowed us to develop crop plants exhibiting tolerance to the herbicide glyphosate, an important transgenic phenotype in global agriculture.

References and Notes

1. C. James, *Global Review of Commercialized Transgenic Crops: 2002 Feature Bt Maize*, International Service for the Acquisition of Agri-biotech Applications, *ISAAA Briefs*, no. 29 (ISAAA, Ithaca, NY, 2003).
2. J. E. Franz, M. K. Mao, J. A. Sikorski, *Glyphosate: A Unique Global Herbicide* (American Chemical Society, Washington, DC, 1997).
3. S. R. Padgette *et al.*, in *Herbicide-Resistant Crops: Agricultural, Environmental, Economic, Regulatory, and Technical Aspects*, S. O. Duke, Ed. (CRC Press, Boca Raton, FL, 1996), pp. 53-84.
4. J. A. Gougler, D. R. Geiger, *Plant Physiol.* **68**, 668 (1981).
5. W. A. Pline, J. W. Wilcut, S. O. Duke, K. L. Edmisten, R. Wells, *J. Agric. Food Chem.* **50**, 506 (2002).
6. D. M. Stalker, K. E. McBride, L. D. Malyj, *Science* **242**, 419 (1988).
7. C. J. Thompson *et al.*, *EMBO J.* **6**, 2519 (1987).
8. M. De Block *et al.*, *EMBO J.* **6**, 2513 (1987).
9. G. Barry *et al.*, in *Biosynthesis and Molecular Regulation of Amino Acids in Plants*, vol. 7, B. K. Singh, H. E. Flores, J. C. Shannon, Eds. (Current Topics in Plant Physiology series, American Society Plant Physiology, Rockville, MD, 1992), pp. 139–145.
10. See (*2*), p. 497.
11. Materials and methods are available as supporting material on *Science* Online.
12. S. C. Kinsky, *J. Biol. Chem.* **235**, 94 (1960).
13. E. M. Khalil, J. De Angelis, P. A. Cole, *J. Biol. Chem.* **273**, 30321 (1998).
14. The following genes were cloned by PCR on the basis of GenBank or *Bacillus* genome sequences, then expressed and assayed as described for *gat* genes in *E. coli* (*11*): M22827, *Streptomyces viridochromogenes pat*; X05822, *S. hygroscopicus bar*; M62753, *S. coelicolor bar*; D90785 ORF_ID:o273#3, *E. coli pat*; Y08559, *B. subtilis ywnH*; X06118, *E. coli rimJ*; X06117, *E. coli rimI*; U50399, *Arabidopsis thaliana HLS1*; M16183, *S. lavendulae sta*; M95912 *Saccharomyces cerevisiae mak3*; X15852, R plasmid *aacC1*; BG12054, *ydaF*; BG13164, *yjcK*; BG11421, *ykkB*; BG14128, *yvoF*.
15. Isolates B6 and DS3 were isolated by Maxygen, Inc., from local soil samples. They were identified as *B. licheniformis* on the basis of 16*S* ribosomal sequencing.
16. S. F. Altschul *et al.*, *Nucleic Acids Res.* **25**, 3389 (1997).
17. F. Dyda, D. C. Klein, A. B. Hickman, *Annu. Rev. Biophys. Biomol. Struct.* **29**, 81 (2000).
18. A. F. Neuwald, D. Landsman, *Trends Biochem. Sci.* **22**, 154 (1997).
19. L. A. Castle, S. Bertain, H.-J. Cho, unpublished observations.
20. W. P. C. Stemmer, *Proc. Natl. Acad. Sci. U.S.A.* **91**, 10747 (1994).
21. A. Crameri, S.-A. Raillard, E. Bermudez, W. P. C. Stemmer, *Nature* **391**, 288 (1998).
22. J. E. Ness *et al.*, *Nature Biotechnol.* **20**, 1251 (2002).
23. K. Draker, G. D. Wright, *Biochemistry* **43**, 446 (2004).
24. K. A. Scheibner, J. De Angelis, S. K. Burley, P. A. Cole, *J. Biol. Chem.* **277**, 18118 (2002).
25. Z.-Y. Zhao, W. Gu, T. Cai, D. A. Pierce, U.S. Patent 5,981,840 (2004).
26. Single-letter abbreviations for the amino acid residues are as follows: A, Ala; C, Cys; D, Asp; E, Glu; F, Phe; G, Gly; H, His; I, Ile; K, Lys; L, Leu; M, Met; N, Asn; P, Pro; Q, Gln; R, Arg; S, Ser; T, Thr; V, Val; W, Trp; and Y, Tyr.

27. We thank Y. Chen, T. Chen, L. Giver, C. Ivy, C. Krebber, G. Wu, J. Wilkinson, A. Wong, N. Trinh, A. Madrigal, A. Umthun, P. Olsen, and W. Mehre for excellent technical assistance; J. Minshull, S. Govindarajan, R. Emig, and the Maxygen bioinformatics team; D. Dagarin and A. Wadley at Byotix for the glyphosate tolerance tests with *gat* tobacco.

Supporting Online Material

www.sciencemag.org/cgi/content/full/304/5674/1151/DC1
Materials and Methods
Figs. S1 to S3
References

13 February 2004; accepted 15 April 2004

Disulfide-Dependent Multimeric Assembly of Resistin Family Hormones

Saurabh D. Patel,[1] Michael W. Rajala,[2] Luciano Rossetti,[3,4] Philipp E. Scherer,[2,3,4] Lawrence Shapiro[1,5,6*]

Resistin, founding member of the resistin-like molecule (RELM) hormone family, is secreted selectively from adipocytes and induces liver-specific antagonism of insulin action, thus providing a potential molecular link between obesity and diabetes. Crystal structures of resistin and RELMβ reveal an unusual multimeric structure. Each protomer comprises a carboxy-terminal disulfide-rich β-sandwich "head" domain and an amino-terminal α-helical "tail" segment. The α-helical segments associate to form three-stranded coiled coils, and surface-exposed interchain disulfide linkages mediate the formation of tail-to-tail hexamers. Analysis of serum samples shows that resistin circulates in two distinct assembly states, likely corresponding to hexamers and trimers. Infusion of a resistin mutant, lacking the intertrimer disulfide bonds, in pancreatic-insulin clamp studies reveals substantially more potent effects on hepatic insulin sensitivity than those observed with wild-type resistin. This result suggests that processing of the intertrimer disulfide bonds may reflect an obligatory step toward activation.

The increasing prevalence of obesity in Western societies is a cause of great medical concern (*1*, *2*). Elevated body mass index correlates with susceptibility to disease states including type II diabetes, coronary artery disease, hypertension, and dyslipidemias (*3*). Type II diabetes currently affects 17 million Americans (*4*) and has become a major public health problem. Nonetheless, the molecular basis for the link between obesity and insulin resistance—the hallmark of type II diabetes—remains unclear (*5*).

Insulin resistance in type II diabetes, and in several animal models of obesity-associated insulin resistance, can often be improved systemically by treatment with agonists for

[1]Department of Biochemistry and Molecular Biophysics, Columbia University, New York, NY 10032, USA. [2]Department of Cell Biology and [3]Department of Medicine, Division of Endocrinology and [4]Diabetes Research and Training Center, Albert Einstein College of Medicine, Bronx, NY 10461, USA. [5]Naomi Berrie Diabetes Center and [6]Edward S. Harkness Eye Institute, Columbia University, New York, NY 10032, USA.

*To whom correspondence should be addressed. E-mail: lss8@columbia.edu

the nuclear receptor peroxisome proliferator-activated receptor γ (PPARγ) (*6–8*). A prominent class of therapeutic PPARγ agonists is the thiazolidinediones (TZDs), which trigger improvements in insulin sensitivity in a number of different tissues, including liver, muscle, and adipose tissue (*9*, *10*). This raises the question of how functional modulation of a transcription factor, active primarily in adipocytes, can alter insulin responsiveness in diverse organs. Circulating factors secreted from adipocytes have been shown to affect insulin sensitivity in a number of different tissues [recently reviewed in (*11*)]. Thiazolidinediones and other non-TZD PPARγ agonists regulate the circulating levels of several adipokines (*12–14*). Resistin was identified in a number of studies (*15–17*), including a screen for adipocyte-specific transcripts down-regulated by treatment with TZDs (*13*).

Resistin expression levels are altered in genetic and diet-induced animal models of obesity by insulin treatment, nutritional status, and treatment with TZDs (*13*). Resistin shows no significant sequence identity to previously characterized proteins and exhibits similarity only to the other family members, RELMα, RELMβ, and the recently discovered RELMγ (*15*, *18*, *19*). All family members are characterized by ten conserved cysteine residues. Resistin and RELMβ contain an additional cysteine near their amino termini, which is conserved among species. Each resistin family member studied has a unique differential tissue distribution (*15*, *18*, *19*). Notably, whereas resistin expression in the mouse is restricted to adipocytes, RELMβ is secreted by cells in the intestinal tract. Both resistin (*13*, *20*) and RELMβ can readily be detected in plasma (*20*). Insulin- and glucose-clamp studies have shown that both resistin and RELMβ specifically blunt insulin action in the liver, resulting in reduced insulin-mediated suppression of gluconeogenesis and increased glycogenolysis (*20*). Consistent with these reports, mice lacking resistin exhibit low fasted blood glucose levels because of reduced hepatic glucose production (*21*). Notably, the effects on gluconeogenesis are opposite to those reported for the adipocyte-secreted hormone adiponectin (also called Acrp30), which increases insulin sensitivity of the same liver-specific functions (*22*).

Adiponectin has a novel structure, composed of a tumor necrosis factor (TNF)–like head domain linked to a collagenous tail (*23*, *24*). Three adiponectin protomers associate to form trimers featuring an amino terminal collagen-like domain. Two subunits of the adiponectin trimer are linked by a disulfide bond mediated by Cys22 in the collagen-like domain, and the third subunit is disulfide bonded to another trimer, forming a hexamer (*25*). Mutation of Cys22 results in trimeric structures that fail to assemble into higher order forms (*25*). Hexamers, which correspond to the low-molecular-weight (LMW) form of circulating adiponectin, provide the building blocks for the high-molecular-weight (HMW) form, which adopts a "bouquet" structure comprising 12 to 18 protomers (*25*), similar in overall structure to the complement protein C1q (*24*). Once secreted, the LMW and HMW forms of adiponectin do not interchange, and the relative amounts secreted from adipocytes are subject to regulation by insulin and other factors (*25*). TZD treatment specifically increases the proportion of HMW form secreted (*26*).

Here we show that resistin, a physiological antagonist of hepatic insulin action, adopts a complex multimeric structure strikingly similar to adiponectin: Both have forms characterized by coiled-coil trimers that form tail-to-tail hexamers through disulfide bonds near their amino termini. Furthermore, we show that, like adiponectin, resistin circulates in serum in two distinct assembly states. The disulfide-linked hexamer of resistin is the major species, but a smaller complex, lacking the amino terminal disulfide bonds is also detected. Physiological clamp studies reported here show that a cysteine mutant unable to form intertrimer disulfide bonds (Cys6Ser), and likely corresponding to the smaller complex, shows substantially higher bioactivity.

Mouse resistin and RELMβ were expressed in mammalian HEK-293T cells and purified by standard chromatographic procedures (*27*). We obtained two different crystal forms of resistin in space groups C2 and $C222_1$, and one form for RELMβ in space group I222 (table S1). Initial low-resolution phases for the $C222_1$ crystal form were obtained by a single-wavelength anomalous diffraction (SAD) experiment of a crystal derivatized with a mercury compound, mersalyl acid. These phases were augmented by phases obtained with a quick-soak bromide SAD experiment (*28*). Bijvoet difference Fourier maps derived from the native sulfur anomalous scattering were used to help in density interpretation (fig. S1). The refined structure from the $C222_1$ crystal form was used to determine the structure of the resistin C2 crystal form by molecular replacement, and the refined C2 structure was used in molecular replacement phasing of the RELMβ crystal.

Resistin and RELMβ, as expected from their high sequence identity (43% in the mature proteins), adopt similar overall structures (Fig. 1). Each protomer is composed of a disulfide-rich β-sandwich "head" domain at the C terminus linked to a helical "tail" region at the N terminus (Fig. 1A; Fig. 2, A and B). The head domain adopts a six-stranded jelly-roll topology and contains two three-stranded all-antiparallel β sheets. A DALI search (*29*) revealed no similar domains in the Protein Data Bank (PDB). However, the overall folding topology is similar to that of the C-terminal domain from octopus hemocyanin (PDB code 1js8), the only other currently known six-stranded jelly roll. The globular domain from resistin contains five disulfide bonds (Cys35-Cys88, Cys47-Cys87, Cys56-Cys73, Cys58-Cys75, and Cys62-Cys77) that are topologically conserved in the RELMβ structure. Sequence comparisons reveal complete conservation of these cysteine residues throughout the resistin family (Fig. 2A), suggesting that the disulfide pattern will be broadly conserved.

Identical multimer structures are observed in all three crystal forms (Fig. 1B). Three

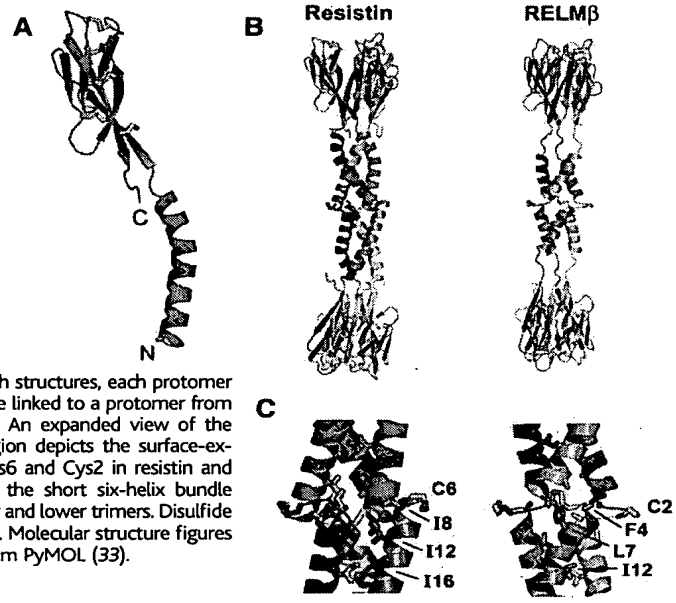

Fig. 1. Ribbon diagram representations of resistin and RELMβ. (**A**) A single resistin protomer, molecule A from the $C222_1$ crystal form, depicts the architecture of resistin family proteins, which are composed of a carboxy-terminal disulfide-rich globular domain and an amino-terminal α-helical region. (**B**) These protomers assemble to form trimer-dimer hexamers, shown for both resistin and RELMβ. In both structures, each protomer from one trimer is disulfide linked to a protomer from the associated trimer. (**C**) An expanded view of the trimer-dimer interface region depicts the surface-exposed disulfide bonds (Cys6 and Cys2 in resistin and RELMβ, respectively) and the short six-helix bundle formed between the upper and lower trimers. Disulfide bonds are drawn in yellow. Molecular structure figures are drawn with the program PyMOL (*33*).

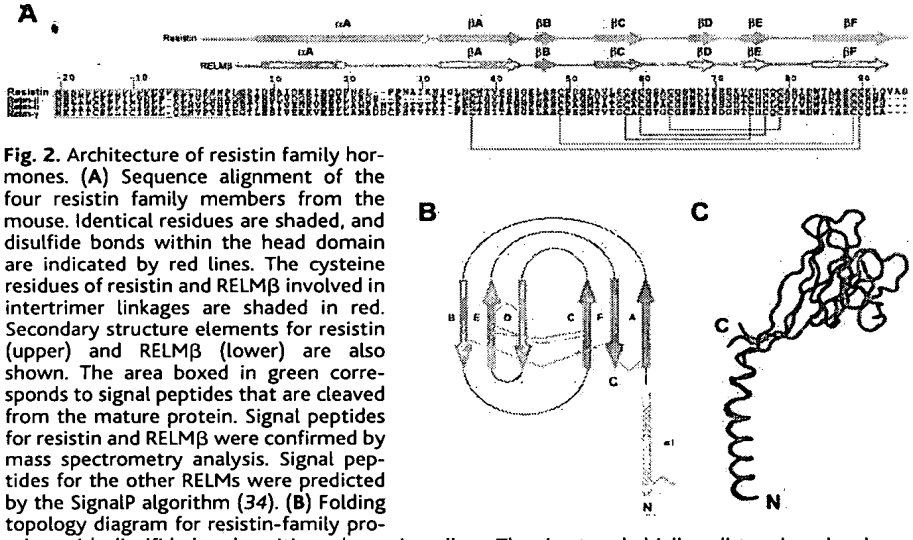

Fig. 2. Architecture of resistin family hormones. (A) Sequence alignment of the four resistin family members from the mouse. Identical residues are shaded, and disulfide bonds within the head domain are indicated by red lines. The cysteine residues of resistin and RELMβ involved in intertrimer linkages are shaded in red. Secondary structure elements for resistin (upper) and RELMβ (lower) are also shown. The area boxed in green corresponds to signal peptides that are cleaved from the mature protein. Signal peptides for resistin and RELMβ were confirmed by mass spectrometry analysis. Signal peptides for the other RELMs were predicted by the SignalP algorithm (*34*). (B) Folding topology diagram for resistin-family proteins, with disulfide bond positions drawn in yellow. The six-stranded jelly-roll topology has been found in one other structure, the C-terminal domain from octopus hemocyanin (PDB code 1js8). (C) The globular head domain is linked to the coil region through a flexible neck region. Superposition of two protomers from the resistin $C222_1$ crystal form, shown as α-carbon worms, depict the extent of variability in the orientation of this domain relative to the coiled coil, which varies up to 21.7° in the structures presented here.

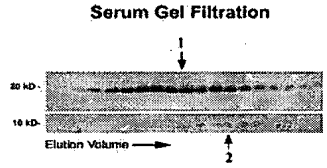

Fig. 3. Two distinct assembly states of resistin secreted from adipocytes and circulating in serum. Nonreducing Western blots of serum from wild-type mice fractionated by size-exclusion chromatography. Two overlapping elution peaks are observed. One corresponds to the major hexamer species, which runs on nonreducing gels as a covalent dimer. The less abundant peak elutes later, indicating an assembly smaller than the hexamer, and runs on nonreducing gels as a monomer, showing the lack of interchain disulfide bonds.

protomers associate through the formation of a parallel coiled coil by the amino-terminal helical regions. The β-sandwich domains do not share a large common hydrophobic core interface, as TNF family trimers do (*24*). In the $C222_1$ structure of resistin, the head domains appear to hang loosely from the helical stalk (Fig. 2C). These trimers are further interlinked to form tail-tail hexamers. To achieve this linkage, the amino-terminal coiled-coil tips from each of two trimers splay apart to enable tail-to-tail interdigitation, forming a short antiparallel six-helix bundle (Fig. 1C). Each helix from a trimer coiled coil is disulfide bonded through Cys6 (Cys2 in RELMβ) to a Cys6 (Cys2) from the opposing trimer.

For resistin, two leucine side chains from each protomer interdigitate to form the core of the short three-up/three-down six-helix bundle (Fig. 1C). The diminutive nature of this interface suggests that, but for the trimer-trimer disulfide bonds, the hexamer association would likely be unstable. For RELMβ, although electron density for the disulfide bonds is clear, nearby side chains in the six-helix bundle core are largely disordered, suggesting that they are unlikely to play a major role in stabilizing the trimer-trimer interface. Cys6 (Cys 2 in RELMβ) is conserved among resistin and RELMβ from all species, but is notably absent from RELMα. This agrees with prior observations showing that the covalent structure of RELMα is monomeric, whereas resistin and RELMβ are each covalently linked as disulfide-dependent homodimers. Furthermore, mutagenesis studies have shown that Cys6 is indeed the critical cysteine that mediates disulfide-dependent dimerization of resistin (*30*).

The interchain disulfide bonds of resistin and RELMβ are novel in that they are highly solvent when exposed, ranging from 84.6% to 89.5% solvent accessibility for RELMβ and 59.8% to 61% for the $C222_1$ crystal form of resistin (*27*). Analysis of the 24,666 disulfide bonds contained in protein structures in the PDB reveals an average solvent exposure for all disulfide bonds of 9.9%, and of 16.7% for 1,209 interchain disulfide bonds. Furthermore, the only interchain protein disulfide bonds (63 total) with solvent accessibilities >50% involve cysteine residues near the carboxy termini of artificially truncated antibody fragments. Thus, the resistin and RELMβ disulfides represent the most highly exposed disulfide bonds yet found in high-resolution structures for an intact protein.

Overall, the resistin and RELMβ structures are very similar (Fig. 1). The "head" domains have no sequence insertions or deletions relative to one another. Structure superpositions of the protomer head domains yield root mean square deviations (RMSDs) for α carbons of ~0.98 Å between resistin (residues 32 to 91) and RELMβ (residues 23 to 82). RELMβ has a shorter coiled-coil region, comprising only four turns of helix from each protomer, compared with six turns in resistin. However, the overall length of the RELMβ and resistin hexamers (each ~140 Å) is similar, as a result of an extended nonhelical "neck" region in RELMβ (Fig. 1B). The Cys6- or Cys2-mediated disulfide bonds in each complex are highly solvent exposed, but their orientations differ: In resistin, the disulfide bond from one trimer to another is made to the clockwise-adjacent protomer, as opposed to the counterclockwise-adjacent protomer in RELMβ (Fig. 1C). The threefold relationship among protomers from a single trimer is noncrystallographic in all cases. In the resistin structures, the side chains of Phe20 and Phe24 adopt similar conformations in two protomers and a substantially different orientation in the third, thus breaking the threefold symmetry of the coiled coil. This symmetry break is not seen in the RELMβ coiled coil. Mapping sequence identity of the resistin family onto the resistin or RELMβ structures shows the highest sequence variation in the coil region. Both the resistin and RELMβ complexes exhibit positive electrostatic surfaces in their "head" regions and negative electrostatic potential in their coiled-coil domains (fig. S3).

To assess the biological relevance of the novel multimeric assembly reported here, and the hexamer-forming disulfide bonds in particular, we analyzed mouse serum for the presence of hexamer and other forms of resistin. Nonreducing SDS gel analysis of medium conditioned by differentiated 3T3-L1 adipocytes (*31*) reveals a disulfide-bonded resistin dimer representing 80 to 90% of total protein, and a monomeric form lacking interchain disulfide bonds representing 10 to 20% of total resistin. Fractionation of either conditioned medium or serum by size-exclusion chromatography (Fig. 3) also revealed two distinct populations of resistin. The predominant form of resistin elutes from calibrated gel filtration columns with a calculated mass of ~54 kD and migrates as a covalent dimer on nonreducing gels (Fig. 3). The chromatographic and electrophoretic behavior of this fraction (the HMW form) is identical to that of the purified hexamer for which structures

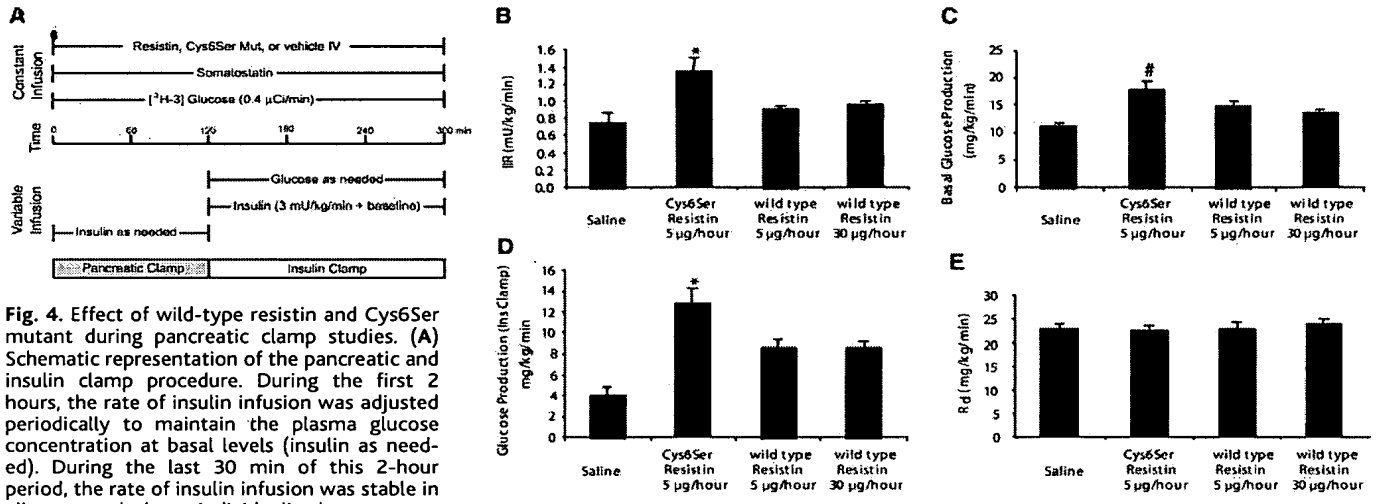

Fig. 4. Effect of wild-type resistin and Cys6Ser mutant during pancreatic clamp studies. **(A)** Schematic representation of the pancreatic and insulin clamp procedure. During the first 2 hours, the rate of insulin infusion was adjusted periodically to maintain the plasma glucose concentration at basal levels (insulin as needed). During the last 30 min of this 2-hour period, the rate of insulin infusion was stable in all rats, and these individualized rates were continued throughout the study. At the completion of the pancreatic clamp (at t = 120 min), an additional infusion of insulin (3 mU/kg/min) was administered to similarly raise the plasma insulin levels in all groups, and a variable infusion of a 25% glucose solution was started and periodically adjusted (glucose as needed) to maintain the plasma glucose concentration at approximately 7 mM for the rest of the study. **(B)** Rates of insulin infusion (IIR) required to maintain the plasma glucose concentrations at the basal levels. **(C)** Effects of wild-type resistin and Cys6Ser on the rate of glucose production. **(D)** Effects of wild-type resistin and Cys6Ser on the rate of glucose production under hyperinsulinemic conditions. **(E)** Effects of wild-type resistin and Cys6Ser on peripheral insulin sensitivity. Some measurements for wild-type resistin were drawn from a previous study (*20*). *, $P < 0.05$ Cys6Ser versus vehicle or wild-type resistin 5 μg/hour and 30 μg/hour; #, $P < 0.05$ versus vehicle. Sample size was at least n = 5 for all conditions.

were determined. 3T3-L1–conditioned media and serum also contain a second and overlapping resistin peak eluting later with a calculated mass of ~46 kD. Western blot analysis shows that this smaller species (the LMW form) migrates as a monomer on nonreducing gels, indicating that the disulfide bonds involved in hexamer stabilization are not present.

The combined observations of a smaller assembly as judged by gel filtration, the trimeric nature of noncovalent resistin assembly through coiled-coil interactions, and the absence of the critical disulfide bonds, suggest that this LMW fraction likely corresponds to a complex lacking the critical intertrimer disulfide. We note that the calculated mass for the LMW peak is greater than half that of the hexamer. However, the shapes of the resistin protein and its assemblies are highly asymmetric, and thus size-exclusion chromatography cannot be expected to yield accurate mass determinations.

To determine whether the presence of the LMW form of resistin is of biological relevance, we prepared a mutant version of resistin that lacks the critical Cys6 and has a serine residue instead, Cys6Ser. As expected, after purification from 293T cells overexpressing this mutant protein, it fails to form covalently bound dimers upon analysis with nonreducing SDS–polyacrylamide gel electrophoresis (SDS-PAGE) (*30*). We have previously used the pancreatic-insulin clamp technique to address the metabolic effects of recombinant resistin (*20*) as well as to determine the effects of the genomic ablation of the resistin gene on glucose homeostasis (*21*). A schematic representation of the experimental design is shown in Fig. 4A. Infusion of low concentrations of Cys6Ser mutant required considerably higher insulin infusion rates to sustain euglycemic conditions compared with even the high dose of wild-type resistin, indicating a higher degree of insulin resistance in the presence of Cys6Ser mutant (Fig. 4B). In line with these observations, hepatic glucose production was considerably increased (Fig. 4C), again more potently in Cys6Ser-infused animals as compared with those infused with wild-type resistin. Thus, despite elevated rates of insulin infusion, the rate of glucose production was increased by Cys6Ser infusion. At the completion of the pancreatic clamp period (at t = 120 min), an additional regular infusion of insulin (3 mU/kg/min) was administered to similarly raise the plasma insulin levels in all groups, and a variable infusion of a 25% glucose solution was started and periodically adjusted to maintain the plasma glucose concentration at ~7 mM for the rest of the study. Under these conditions, both wild-type and Cys6Ser-mutant resistin significantly decreased hepatic insulin sensitivity as judged by the increased hepatic glucose output. Similar to the basal conditions, the Cys6Ser mutant was substantially more potent at the low concentration than was wild-type resistin at the high concentration (Fig. 4D). Whole-body glucose disposal, however, was similar under all conditions (Fig. 4E), suggesting that both the Cys6Ser-mutant and wild-type resistin target primarily the liver.

These results are consistent with a model that LMW resistin (mimicked by the Cys6Ser mutant) is the bioactive ligand. Resistin may have to be processed to the LMW form before it can exert its bioactivity. We have proposed a similar mechanism for adiponectin based on the observation that a mutant version of adiponectin lacking a critical coiled-coil region cysteine residue (Cys22) that fails to assemble into higher order structures beyond the trimer is considerably more bioactive (*25*).

Mechanisms for regulation of assembly for adiponectin and resistin are not yet understood. However, the regulated disulfide-dependent assembly of another serum-borne protein, immunoglobulin M, is now known to involve thioredoxin-like proteins of the endoplasmic reticulum (*32*). For both adiponectin and resistin, the mutant forms lacking critical disulfide bonds in their coiled-coil domains are most active. This suggests a possible receptor-binding geometry in which the coiled-coil tails, occluded in the HMW forms and free in the mutant or processed forms, might be involved in receptor interactions.

In summary, crystal structures for resistin and RELMβ reveal hexameric assemblies consisting of trimers linked to form hexamers through highly exposed disulfide bonds at the amino termini of their coiled-coil domains. This unusual structure is suggestive of possible regulation through disulfide cleavage or by regulation during assembly. Consistent

with this is the observation of two distinct forms of resistin—the HMW hexamer and the LMW form—in serum and adipocyte-conditioned medium. The LMW form displays significantly increased bioactivity. The overall multimeric assembly of the resistin family is similar to that of adiponectin. The comparable domain architecture of these two adipocyte-specific hormones, despite diametrically opposed physiological effects, suggests a common regulatory mechanism and points to new avenues of research focusing on modulation of adipokine secretion and activity by cysteine-mediated complex formation or processing.

References and Notes

1. C. L. Ogden, K. M. Flegal, M. D. Carroll, C. L. Johnson, *JAMA* **288**, 1728 (2002).
2. K. M. Flegal, M. D. Carroll, C. L. Ogden, C. L. Johnson, *JAMA* **288**, 1723 (2002).
3. J. J. Reilly *et al.*, *Arch. Dis. Child.* **88**, 748 (2003).
4. U. S. Census, *Bureau of the Census, 2000 Census Estimates;* www.cdc.gov/diabetes/pubs/estimates.htm.
5. I. M. Jazet, H. Pijl, A. E. Meinders, *Neth. J. Med.* **61**, 194 (2003).
6. T. Fujita *et al.*, *Diabetes* **32**, 804 (1983).
7. T. Fujiwara, S. Yoshioka, T. Yoshioka, I. Ushiyama, H. Horikoshi, *Diabetes* **37**, 1549 (1988).
8. P. E. Beales, P. Pozzilli, *Diabetes Metab. Res. Rev.* **18**, 114 (2002).
9. H. Hauner, *Diabetes Metab. Res. Rev.* **18** (suppl. 2), S10 (2002).
10. R. R. Henry, *Endocrinol. Metab. Clin. North Am.* **26**, 553 (1997).
11. M. W. Rajala, P. E. Scherer, *Endocrinology* **144**, 3765 (2003).
12. A. H. Berg, T. P. Combs, X. Du, M. Brownlee, P. E. Scherer, *Nature Med.* **7**, 947 (2001).
13. C. M. Steppan *et al.*, *Nature* **409**, 307 (2001).
14. T. P. Combs *et al.*, *Endocrinology* **143**, 998 (2002).
15. I. N. Holcomb *et al.*, *EMBO J.* **19**, 4046 (2000).
16. K. H. Kim, K. Lee, Y. S. Moon, H. S. Sul, *J. Biol. Chem.* **276**, 11252 (2001).
17. M. W. Rajala *et al.*, *Mol. Endocrinol.* **16**, 1920 (2002).
18. C. M. Steppan *et al.*, *Proc. Natl. Acad. Sci. U.S.A.* **98**, 502 (2001).
19. B. Gerstmayer *et al.*, *Genomics* **81**, 588 (2003).
20. M. W. Rajala, S. Obici, P. E. Scherer, L. Rossetti, *J. Clin. Invest.* **111**, 225 (2003).
21. R. R. Banerjee *et al.*, *Science* **303**, 1195 (2004).
22. T. P. Combs, A. H. Berg, S. Obici, P. E. Scherer, L. Rossetti, *J. Clin. Invest.* **108**, 1875 (2001).
23. P. E. Scherer, S. Williams, M. Fogliano, G. Baldini, H. F. Lodish, *J. Biol. Chem.* **270**, 26746 (1995).
24. L. Shapiro, P. E. Scherer, *Curr. Biol.* **8**, 335 (1998).
25. U. B. Pajvani *et al.*, *J. Biol. Chem.* **278**, 9073 (2003).
26. U. B. Pajvani *et al.*, *J. Biol. Chem.* **279**, 12152 (2004).
27. Materials and methods are available as supporting material on *Science* Online.
28. Z. Dauter, M. Dauter, K. R. Rajashankar, *Acta Crystallogr. D Biol. Crystallogr.* **56**, 232 (2000).
29. L. Holm, C. Sander, *Nucleic Acids Res.* **26**, 316 (1998).
30. R. R. Banerjee, M. A. Lazar, *J. Biol. Chem.* **276**, 25970 (2001).
31. D. L. Brasaemle *et al.*, *J. Lipid Res.* **38**, 2249 (1997).
32. T. Anelli *et al.*, *EMBO J.* **22**, 5015 (2003).
33. W. L. DeLano (2002), http://pymol.sourceforge.net
34. H. Nielsen, J. Engelbrecht, S. Brunak, G. von Heijne, *Protein Eng.* **10**, 1 (1997).

35. We thank the personnel of Advanced Photon Source (APS) beamlines 31-ID and 32-ID; National Synchrotron Light Source beamlines X4, X9, and X25; and A. Gogos and T. Boggon for help with data collection; M. Collins, A. Gogos, and D. Brasaemle for help with biochemical experiments; and F. P. Davis and A. Sali for help with solvent accessibility calculations. We also thank Z. Wang, J.-Y. Kim, and A. Narwocki for help at various stages of this project. We are grateful to W. A. Hendrickson and P. D. Kwong for critical comments. The structures reported in this paper have been deposited in the PDB as 1RFX, 1RGX, and 1RH7. This work was supported in part by grants from NIH and the Research to Prevent Blindness Foundation. Part of this work was performed as part of the National Institute of General Medical Sciences' New York Structural Genomics Research Consortium (NYSGXRC). Use of the APS was supported by the U.S. Department of Energy, Office of Science, Office of Basic Energy Science, under Contract No. W-31-109-Eng-38. Use of the SGX Collaborative Access Team (SGX-CAT) beamline facilities at sector 31 of the APS was provided by Structural GenomiX, Inc., which constructed and operates the facility.

Supporting Online Material

www.sciencemag.org/cgi/content/full/304/5674/1154/DC1
Materials and Methods
Figs. S1 to S3
Table S1
References

10 November 2003; accepted 19 April 2004

Hereditary Early-Onset Parkinson's Disease Caused by Mutations in *PINK1*

Enza Maria Valente,[1*‡] Patrick M. Abou-Sleiman,[2*] Viviana Caputo,[1,3†] Miratul M. K. Muqit,[2,4†] Kirsten Harvey,[5] Suzana Gispert,[6] Zeeshan Ali,[6] Domenico Del Turco,[7] Anna Rita Bentivoglio,[9] Daniel G Healy,[2] Alberto Albanese,[10] Robert Nussbaum,[11] Rafael González-Maldonado,[12] Thomas Deller,[7] Sergio Salvi,[1] Pietro Cortelli,[13] William P. Gilks,[2] David S. Latchman,[4,14] Robert J. Harvey,[5] Bruno Dallapiccola,[1,3] Georg Auburger,[8‡] Nicholas W. Wood[2‡]

Parkinson's disease (PD) is a neurodegenerative disorder characterized by degeneration of dopaminergic neurons in the substantia nigra. We previously mapped a locus for a rare familial form of PD to chromosome 1p36 (PARK6). Here we show that mutations in *PINK1* (PTEN-induced kinase 1) are associated with PARK6. We have identified two homozygous mutations affecting the PINK1 kinase domain in three consanguineous PARK6 families: a truncating nonsense mutation and a missense mutation at a highly conserved amino acid. Cell culture studies suggest that PINK1 is mitochondrially located and may exert a protective effect on the cell that is abrogated by the mutations, resulting in increased susceptibility to cellular stress. These data provide a direct molecular link between mitochondria and the pathogenesis of PD.

Parkinson's disease (PD) is a common neurodegenerative disorder that is characterized by the loss of dopaminergic neurons in the substantia nigra and the presence of cytoplasmic protein inclusions known as Lewy bodies. The majority of PD cases are sporadic; however, the identification of a number of genes responsible for rare familial forms of PD has provided important insights into the underlying mechanisms of the disease. These genes, encoding α-synuclein, parkin, UCH-L1, and DJ-1, have implicated protein misfolding, impairment of the ubiquitin-proteasome system, and oxidative stress in the pathogenesis of the disease (*1*, *2*).

We previously mapped PARK6, a locus linked to autosomal recessive, early-onset PD, to a 12.5-centimorgan (cM) region on chromosome 1p35-p36 by autozygosity mapping in a large consanguineous family from Sicily (*3*). Subsequent identification of two additional consanguineous families [one from central Italy (family IT-GR) (*4*) and one from Spain] provided additional evidence of linkage to PARK6. A critical recombination event in the Spanish family refined the candidate region to a 3.7-cM interval between flanking markers D1S2647 and D1S1539. Fine mapping of single-nucleotide polymorphisms and newly generated short tandem repeat markers in the three families defined a 2.8-megabase region of homozygosity within contig NT_004610, containing approximately 40 genes.

Candidate genes were prioritized on the basis of their putative function and expression in the central nervous system, as assessed by bioinformatic analysis and by exon amplification from a human substantia nigra cDNA library. Sequence analysis of candidate genes in affected members from each family led to the identification of two homozygous mutations in the *PTEN- induced putative kinase 1* (*PINK1*) gene. The mutations segregated with the disease phenotype in the three consanguineous families, were confirmed in the cDNA, and were absent from 400 control chromosomes, including 200 chromosomes from Sicilian individuals. The Spanish family carried a G→A

Express Mail No.: EV 332 008 975 US
Mail Stop: Patent Application
Commissioner for Patents
P.O. Box 1450
Alexandria, VA 22313-1450

Mailed: April 7, 2004
Docket No.: PF-0541-1 DIV

Inventors: Lal et al.
Title: **SIGNAL PEPTIDE-CONTAINING MOLECULES**
Filing Date: Herewith

Enclosed:

1. Return Receipt Postcard;
2. Transmittal for **Divisional** Application (3 pp., in duplicate);
3. Application Data Sheet (ADS) (9 pp.);
4. Blanket Exemption from Requirements Under § 42 U.S.C. 2182 Letter (1 pg.);
5. Specification corresponding to prior application, consisting of:
   72 pages of Specification 77 pages of Tables (Tables 1-6);
   9 pages of Claims
   1 page of Abstract
6. Copy of originally executed Declaration & Power of Attorney (7 pp.);
7. Revocation and Power of Attorney (2 pp.);
8. Preliminary Amendment (7 pp.);
9. Information Disclosure Statement (2 pp.); and
10. List of References Cited PTO-1449 (1 pg.).

DS/jl

Method of Payment: Deposit Account

Express Mail No.: EV 332 008 975 US
Mail Stop: Patent Application
Commissioner for Patents
P.O. Box 1450
Alexandria, VA 22313-1450

Mailed: April 7, 2004
Docket No.: PF-0541-1 DIV

Inventors: Lal et al.
Title: **SIGNAL PEPTIDE-CONTAINING MOLECULES**
Filing Date: Herewith

Enclosed:

1. Return Receipt Postcard;
2. Transmittal for **Divisional** Application (3 pp., in duplicate);
3. Application Data Sheet (ADS) (9 pp.);
4. Blanket Exemption from Requirements Under § 42 U.S.C. 2182 Letter (1 pg.);
5. Specification corresponding to prior application, consisting of:
   72 pages of Specification 77 pages of Tables (Tables 1-6);
   9 pages of Claims
   1 page of Abstract
6. Copy of originally executed Declaration & Power of Attorney (7 pp.);
7. Revocation and Power of Attorney (2 pp.);
8. Preliminary Amendment (7 pp.);
9. Information Disclosure Statement (2 pp.); and
10. List of References Cited PTO-1449 (1 pg.).

DS/jl

Method of Payment: Deposit Account

TABLE 1

Protein SEQ ID NO:	Nucleotide SEQ ID NO:	Clone ID	Library	Fragments
1	135	443531	MPHGNOT03	443531H1 (MPHGNOT03), 1406807F6 (LATRTUT02), 443531T6 (MPHGNOT03), SBBA00451F1, SBBA00676F1
2	136	632860	NEUTGMT01	632860H1 (NEUTGMT01), 784715R3 (PROSNOT05), 509590H1 (MPHGNOT03)
3	137	670010	CRBLNOT01	670010H1 (CRBLNOT01), 669971R1 (CRBLNOT01), 1553045F1 (BLADTUT04)
4	138	726498	SYNOOAT01	726498H1 (SYNOOAT01), 726498R6 (SYNOOAT01), 866599R3 (BRAITUT03)
5	139	795064	OVARNOT03	795064H1 (OVARNOT03), 4339458H1 (BRAUNOT02), 937605R3 (CERVNOT01), 2381151F6 (ISLTNOT01), 1466346F6 (PANCTUT02)
6	140	924925	BRAINOT04	924925H1 (BRAINOT04), 3268330H1 (BRAINOT20), 759120R3 (BRAITUT02)
7	141	962390	BRSTTUT03	962390H1 (BRSTTUT03), 1907958F6 (CONNTUT01), 023569F1 (ADENINB01), 167282F1 (LIVRNOT01), 1309211F1 (COLNFET02), SAUA00696F1, SAUA02860F1
8	142	1259405	MENITUT03	1259405H1 (MENITUT03), 2472425H1 (THP1NOT03), 774303R1 (COLNNOT05), 1520779F1 (BLADTUT04), 1693833F6 (COLNNOT23), 1831858T6.comp (THP1AZT01), 1527737T6.comp (UCMCL5T01)
9	143	1297384	BRSTNOT07	1297384H1 (BRSTNOT07), 1269310F6 (BRAINOT09), 1457367F1 (COLNFET02), 415587R1 (BRSTNOT01), SANA02967F1
10	144	1299627	BRSTNOT07	1299627H1 (BRSTNOT07), 1359140F6 (LUNGNOT09), 1349224F1 (LATRTUT02), SBAA01431F1, SBAA02909F1, SBAA01156F1
11	145	1306026	PLACNOT02	1306026H1 (PLACNOT02), 1464088R6 (PANCNOT04), SBAA02496F1, SBAA04305F1
12	146	1316219	BLADTUT02	1316219H1 (BLADTUT02), 2458603F6 (ENDANOT01), 2504756T6 (CONUTUT01)
13	147	1329031	PANCNOT07	1329031H1 (PANCNOT07), 1329031T6 (PANCNOT07), 1329031F6 (PANCNOT07)

TABLE 1 (cont.)

Protein SEQ ID NO:	Nucleotide SEQ ID NO:	Clone ID	Library	Fragments
14	148	1483050	CORPNOT02	1483050H1 (CORPNOT02), 855049H1 (NGANNOT01), 077017F1 (SYNORAB01), 1483050F6 (CORPNOT02), 1480024T6 (CORPNOT02), 1483050T6 (CORPNOT02), 759486R1 (BRAITUT02)
15	149	1514160	PANCTUT01	1514160H1 (PANCTUT01), 1866765T7 (SKINBIT01), 782676R1 (MYOMNOT01), 008055X4 (HMC1NOT01), 008055X5 (HMC1NOT01), 1866765F6 (SKINBIT01), SAOA03127F1
16	150	1603403	LUNGNOT15	1603403H1 (LUNGNOT15), 372910F1 (LUNGNOT02), 733299R7 (LUNGNOT03)
17	151	1652303	PROSTUT08	1652303H1 (PROSTUT08), 1671806H1 (BLADNOT05), 1341743T1 (COLNTUT03), 3803812H1 (BLADTUT03), 1878546F6 (LEUKNOT03), 1428640F1 (SINTBST01), 2058609R6 (OVARNOT03), 1331621F1 (PANCNOT07), 1306331T1 (PLACNOT02)
18	152	1693358	COLNNOT23	1693358H1 (COLNNOT23), 2498265H1 (ADRETUT05), 1867125F6 (SKINBIT01), 1693358T6 (COLNNOT23), 2245848R6 (HIPONON02)
19	153	1707711	DUODNOT02	1707711H1 (DUODNOT02), 1484609T1 (CORPNOT02), 1707711F6 (DUODNOT02), 1267959F1 (BRAINOT09), 1484609F1 (CORPNOT02), SAJA00930F1, SAJA01300R1, SAJA00999R1
20	154	1738735	COLNNOT22	1738735H1 (COLNNOT22), SAJA00944R1, SAJA00137F1, SAJA03629F1
21	155	1749147	STOMTUT02	1749147H1 (STOMTUT02), 1749147F6 (STOMTUT02), 1749147T6 (STOMTUT02)
22	156	1817722	PROSNOT20	1817722H1 (PROSNOT20), 2011085H1 (TESTNOT03)
23	157	1831290	THP1AZT01	1831290H1 (THP1AZT01), 3473958H1 (LUNGNOT27), 1972268F6 (UCMCL5T01), 1301277F1 (BRSTNOT07), 1521574F1 (BLADTUT04), 1561690T6 (SPLNNOT04), 891461R1 (STOMTUT01)

TABLE 1 (cont.)

Protein SEQ ID NO:	Nucleotide SEQ ID NO:	Clone ID	Library	Fragments
24	158	1831477	THP1AZT01	1831477H1 (THP1AZT01), 1582867H1 (DUODNOT01), 1336769T1 (COLNNOT13), 1933092H1 (COLNNOT16), 1519909F1 (BLADTUT04), 1220946H1 (NEUTGMT01), 809556T1 (LUNGNOT04), 1217559T1 (NEUTGMT01), 1309225F1 (COLNFET02)
25	159	1841607	COLNNOT07	1841607H1 (COLNNOT07), SBHA03588F1
26	160	1852391	LUNGFET03	1852391H1 (LUNGFET03), 734140H1 (TONSNOT01), 1852391F6 (LUNGFET03)
27	161	1854555	HNT3AZT01	1854555H1 (HNT3AZT01), 2511711H1 (CONUTUT01), 782453R1 (MYOMNOT01), 1854555F6 (HNT3AZT01), 1840675T6 (COLNNOT07), 2109736H1 (BRAITUT03)
28	162	1855755	PROSNOT18	1855755H1 (PROSNOT18), 3040236H1 (BRSTNOT16), 1283207F1 (COLNNOT16), 833763T1 (PROSNOT07), 1920926R6 (BRSTTUT01)
29	163	1861434	PROSNOT19	1861434H1 (PROSNOT19), 980291R1 (TONGTUT01), 1861434T6 (PROSNOT19), SARA01525F1, SARA02548F1
30	164	1872334	LEUKNOT02	1872334H1 (LEUKNOT02), 1872334F6 (LEUKNOT02), SBGA03684F1
31	165	1877230	LEUKNOT03	1877230H1 (LEUKNOT03), 2519841H1 (BRAITUT21), 1877230T6 (LEUKNOT03), 1254693F1 (LUNGFET03), 077020R1 (SYNORAB01), 1232336F1 (LUNGFET03), 1004952R6 (BRSTNOT03), SARA01879F1, SARA02654F1
32	166	1877885	LEUKNOT03	1877885H1 (LEUKNOT03), 508020F1 (TMLR3DT01), 2751126R6 (THP1AZS08), SARA02571F1
33	167	1889269	BLADTUT07	1889269H1 (BLADTUT07), 1915551H1 (PROSTUT04), 629493X12 (KIDNNOT05), 1441289F1 (THYRNOT03), 1215274X34F1 (BRSTTUT01), 1818447F6 (PROSNOT20), 1208463R1 (BRSTNOT02)
34	168	1890243	BLADTUT07	1890243H1 (BLADTUT07), SARA01884F1, SATA00046F1, SARA03294F1, SARA02790F1

TABLE 1 (cont.)

Protein SEQ ID NO:	Nucleotide SEQ ID NO:	Clone ID	Library	Fragments
35	169	1900433	BLADTUT06	1900433H1 (BLADTUT06), SATA00396F1, SATA02742F1
36	170	1909441	CONNTUT01	1909441H1 (CONNTUT01), 1398811F1 (BRAITUT08), 3039939H1 (BRSTNOT16), 3324740H1 (PTHYNOT03), 1442131F6 (THYRNOT03), 2254056H1 (OVARTUT01), 2199453T6 (SPLNFET02), 1692610F6 (COLNNOT23), 1698531H1 (BLADTUT05)
37	171	1932226	COLNNOT16	1932226H1 (COLNNOT16), 2320569H1 (OVARNOT02), 1932226F6 (COLNNOT16), 2469455T6 (THP1NOT03), 2469455F6 (THP1NOT03), 1907140F6 (OVARNOT07), SATA02592F1
38	172	1932647	COLNNOT16	1932647H1 (COLNNOT16), 1492745T1 (PROSNON01), 1492745H1 (PROSNON01), SASA02355F1, SASA00117F1, SASA00192F1
39	173	2124245	BRSTNOT07	2124245H1 (BRSTNOT07), 1235393F1 (LUNGFET03), 1402264F6 (LATRTUT02), 1303990F1 (PLACNOT02), 1402264T6 (LATRTUT02)
40	174	2132626	OVARNOT03	2132626H1 (OVARNOT03), 1723432T6 (BLADNOT06), 2132626R6 (OVARNOT03), 1736723T6 (COLNNOT22), 1504738F1 (BRAITUT07)
41	175	2280639	PROSNON01	2280639H1 (PROSNON01), 1435330H1 (PANCNOT08), 1377560F6 (LUNGNOT10)
42	176	2292356	BRAINON01	2292356H1 (BRAINON01), 4086827H1 (LIVRNOT06), 1754442F6 (LIVRTUT01), 3571126H1 (HEAPNOT01), 1601305F6 (BLADNOT03)
43	177	2349310	COLSUCT01	2349310H1 (COLSUCT01), 2349310T6 (COLSUCT01)
44	178	2373227	ADRENOT07	2373227H1 (ADRENOT07), 3316444H1 (PROSBPT03), 302685R6 (TESTNOT04), SASA02181F1, SASA01923F1, SASA03516F1
45	179	2457682	ENDANOT01	2457682H1 (ENDANOT01), 2457682F6 (ENDANOT01)
46	180	2480426	SMCANOT01	2480426H1 (SMCANOT01), 2480426F6 (SMCANOT01)

TABLE 1 (cont.)

Protein SEQ ID NO:	Nucleotide SEQ ID NO:	Clone ID	Library	Fragments
47	181	2503743	CONUTUT01	2503743H1 (CONUTUT01), 1853909H1 (HNT3AZT01), 1517619F1 (PANCTUT01), 1467896F6 (PANCTUT02), 490031F1 (HNT2AGT01), 1208654R1 (BRSTNOT02), 880544R1 (THYRNOT02)
48	182	2537684	BONRTUT01	2537684H1 (BONRTUT01), 2005493H1 (TESTNOT03), 730969H1 (LUNGNOT03), 2537601F6 (BONRTUT01), 916487H1 (BRSTNOT04), 996135R1 (KIDNTUT01), 1920738R6 (BRSTTUT01), 1957710F6 (CONNNOT01)
49	183	2593853	OVARTUT02	2593853H1 (OVARTUT02), 807497H1 (STOMNOT02), 914020R6 (STOMNOT02), 889992R1 (STOMTUT01)
50	184	2622354	KERANOT02	2622354H1 (KERANOT02), 2623992H1 (KERANOT02), 1556510F6 (BLADTUT04)
51	185	2641377	LUNGTUT08	2641377H1 (LUNGTUT08), 4341415H2 (BRAUNOT02), SBCA07049F3
52	186	2674857	KIDNNOT19	2674857H1 (KIDNNOT19), 1872373H1 (LEUKNOT02), 470512R6 (MMLR1DT01), 1728547H1 (PROSNOT14), 3013651F6 (MUSCNOT07), SBCA01366F1, SBCA00694F1
53	187	2758485	THP1AZS08	2758485H1 (THP1AZS08), 3097533H1 (CERVNOT03), 1578959F6 (DUODNOT01)
54	188	2763296	BRSTNOT12	2763296H1 (BRSTNOT12), 3486025F6 (KIDNNOT31), SBDA07002F3
55	189	2779436	OVARTUT03	2779436H1 (OVARTUT03), 2779436F6 (OVARTUT03), SBDA07009F3
56	190	2808528	BLADTUT08	2808528H1 (BLADTUT08), 2611513F6 (THYMNOT04), SBDA07021T3
57	191	2809230	BLADTUT08	2809230H1 (BLADTUT08), 2213849H1 (SINTFET03), 711706R6 (SYNORAT04), 958323R1 (KIDNNOT05), 030732F1 (THP1NOB01)
58	192	2816821	BRSTNOT14	2816821H1 (BRSTNOT14), 3746964H1 (THYMNOT08), 2816821F6 (BRSTNOT14), 948722T6 (PANCNOT05), 807947R6 (STOMNOT02)

TABLE 1 (cont.)

Protein SEQ ID NO:	Nucleotide SEQ ID NO:	Clone ID	Library	Fragments
59	193	2817268	BRSTNOT14	2817268H1 (BRSTNOT14), 3591308H1 (293TF5T01), 419522R1 (BRSTNOT01), 2073028F6 (ISLTNOT01), 1308781F6 (COLNFET02)
60	194	2923165	SININOT04	2923165H1 (SININOT04), 2011630H1 (TESTNOT03), 1457250F1 (COLNFET02), 754668R1 (BRAITUT02), 1406510F6 (LATRTUT02)
61	195	2949822	KIDNFET01	2949822H1 (KIDNFET01), SBDA07078F3
62	196	2992192	KIDNFET02	2992192H1 (KIDNFET02), 2534324H2 (BRAINOT18), 2815255T6 (OVARNOT10), 1551107T6 (PROSNOT06), 1551107R6 (PROSNOT06)
63	197	2992458	KIDNFET02	2992458H1 (KIDNFET02), 2618951H1 (GBLANOT01), 1479252F1 (CORPNOT02), 1879054H1 (LEUKNOT03), 1879054F6 (LEUKNOT03), 2215240H1 (SINTFET03), 1535968T1 (SPLNNOT04)
64	198	3044710	HEAANOT01	3044710H1 (HEAANOT01), 3741773H1 (MENTNOT01), 859906X42C1 (BRAITUT03), 1534347F1 (SPLNNOT04), 1421122F1 (KIDNNOT09), 1303865F1 (PLACNOT02), 1704452F6 (DUODNOT02), 1251642F1 (LUNGFET03), 1781694R6 (PGANNON02)
65	199	3120415	LUNGTUT13	3120415H1 (LUNGTUT13), 1360123T1 (LUNGNOT12), 1375015H1 (LUNGNOT10)
66	200	126758	LUNGNOT01	126758H1 (LUNGNOT01), 126758X11 (LUNGNOT01), 811864T1 (LUNGNOT04)
67	201	674760	CRBLNOT01	674760H1 (CRBLNOT01), 3253976H1 (OVARTUN01), SAUA03387F1
68	202	1229438	BRAITUT01	1229438H1 (BRAITUT01), 1230616H1 (BRAITUT01), 1461187R1 (PANCNOT04), 2493039H1 (ADRETUT05), 2891628H1 (LUNGFET04)
69	203	1236935	LUNGFET03	1236935H1 (LUNGFET03), SBAA00983F1, SBAA02057F1, SBAA00170F1
70	204	1359283	LUNGNOT12	1359283H1 (LUNGNOT12), SBAA01213F1, SBAA03934F1
71	205	1450703	PENITUT01	551298F1 (BEPINOT01), 551298R1 (BEPINOT01), 1450703H1 (PENITUT01), 2748715H1 (LUNGTUT11)

TABLE 1 (cont.)

Protein SEQ ID NO:	Nucleotide SEQ ID NO:	Clone ID	Library	Fragments
72	206	1910668	CONNTUT01	1269346H1 (BRAINOT09), 1380872F1 (BRAITUT08), 1910668F6 (CONNTUT01), 1910668H1 (CONNTUT01), SATA02800F1, SATA03799F1, SARA02035F1
73	207	1955143	CONNNOT01	1955143F6 (CONNNOT01), 1955143H1 (CONNNOT01)
74	208	1961637	BRSTNOT04	867025H1 (BRAITUT03), 1961637H1 (BRSTNOT04), 2809064T6 (BLADTUT08), 2938714H1 (THYMFET02), 2956402H1 (KIDNFET01), 3808735T6 (CONTTUT01)
75	209	1990762	CORPNOT02	1990762H1 (CORPNOT02), 1990762T3 (CORPNOT02), SBGA04911F1, SBGA01201F1, SBGA02205F1
76	210	1994131	CORPNOT02	1994131H1 (CORPNOT02), 2645984F6 (OVARTUT04)
77	211	1997745	BRSTTUT03	1752307F6 (LIVRTUT01), 1853730H1 (HNT3AZT01), 1997745H1 (BRSTTUT03), SAZA00953F1
78	212	2009035	TESTNOT03	2009035H1 (TESTNOT03), 2009035R6 (TESTNOT03)
79	213	2009152	TESTNOT03	2009152H1 (TESTNOT03), 2009152R6 (TESTNOT03), 2783263H1 (BRSTNOT13)
80	214	2061752	OVARNOT03	2061752H1 (OVARNOT03), 2061752T6 (OVARNOT03), 2732805H1 (OVARTUT04), SAZA01310F1, SAZA00830F1
81	215	2061933	OVARNOT03	046580R1 (CORNNOT01), 746061R1 (BRAITUT01), 826996R1 (PROSNOT06), 2061933H1 (OVARNOT03)
82	216	2081422	UTRSNOT08	2081422F6 (UTRSNOT08), 2081422H1 (UTRSNOT08), SBCA04793F1, SBCA05657F1, SBDA00065F1
83	217	2101278	BRAITUT02	2101278H1 (BRAITUT02), SAXA00399F1, SAXA01284F1, SAXA01227F1
84	218	2121353	BRSTNOT07	341437H1 (NEUTFMT01), 687136H1 (UTRSNOT02), 2121353H1 (BRSTNOT07), SASA01311F1

TABLE 1 (cont.)

Protein SEQ ID NO:	Nucleotide SEQ ID NO:	Clone ID	Library	Fragments
85	219	2241736	PANCTUT02	833263H1 (PROSTUT04), 2241736H1 (PANCTUT02), SAZA01148F1, SASA03299F1, SASA01349F1
86	220	2271935	PROSNON01	2271935H1 (PROSNON01), 2276774H1 (PROSNON01), 2760171T6 (THP1AZS08)
87	221	2295344	BRSTNOT05	2295344H1 (BRSTNOT05), 3288561F6 (BONRFET01), SBGA01801F1
88	222	2303994	BRSTNOT05	905482T1 (COLNNOT08), 1858636F6 (PROSNOT18), 2303994H1 (BRSTNOT05)
89	223	2497805	ADRETUT05	2497805F6 (ADRETUT05), 2497805H1 (ADRETUT05)
90	224	2646362	LUNGTUT11	1754702H1 (LIVRTUT01), 2640776T6 (LUNGTUT08), 2646362H1 (LUNGTUT11), 3356773H1 (PROSTUT16)
91	225	2657146	LUNGTUT09	2657146F6 (LUNGTUT09), 2657146H1 (LUNGTUT09)
92	226	2755786	THP1AZS08	288436R1 (EOSIHET02), 1252824F6 (LUNGFET03), 1305549H1 (PLACNOT02), 1364975R1 (SCORNON02), 2018293H1 (THP1NOT01), 2047320H1 (THP1T7T01), 2184537F6 (SININOT01), 2755786H1 (THP1AZS08), 4111022H1 (PROSBPT07)
93	227	2831245	TLYMNOT03	2831245H1 (TLYMNOT03), SBMA01396F1
94	228	3116250	LUNGTUT13	126263F1 (LUNGNOT01), 2729942H1 (OVARTUT04), 3116250H1 (LUNGTUT13)
95	229	3129630	LUNGTUT12	3129630F6 (LUNGTUT12), 3129630H1 (LUNGTUT12), SBDA06436F1
96	230	007632	HMC1NOT01	007632H1 (HMC1NOT01), 007632R6 (HMC1NOT01), 007632T6 (HMC1NOT01)
97	231	1236968	LUNGFET03	1236968H1 (LUNGFET03), SBAA02713F1, SBAA03203F1, SBAA04196F1
98	232	1334153	COLNNOT13	776410R1 (COLNNOT05), 1334153H1 (COLNNOT13), 1334153T1 (COLNNOT13), 1800085F6 (COLNNOT27), 2701948H1 (OVARTUT10)

TABLE 1 (cont.)

Protein SEQ ID NO:	Nucleotide SEQ ID NO:	Clone ID	Library	Fragments
99	233	1396975	BRAITUT08	864113H1 (BRAITUT03), 876139R1 (LUNGAST01), 1268313F1 (BRAINOT09), 1351348T1 (LATRTUT02), 1396975H1 (BRAITUT08), 1485768F6 (CORPNOT02), 1815364F6 (PROSNOT20)
100	234	1501749	SINTBST01	079080R1 (SYNORAB01), 1501749H1 (SINTBST01), 1724970H1 (PROSNOT14)
101	235	1575240	LNODNOT03	081858R1 (SYNORAB01), 1575240H1 (LNODNOT03), 3451462R6 (UTRSNON03)
102	236	1647884	PROSTUT09	1647884H1 (PROSTUT09), 1647884T6 (PROSTUT09), 3998922R6 (HNT2AZS07)
103	237	1661144	BRSTNOT09	720941X17 (SYNOOAT01), 1661144H1 (BRSTNOT09), 2181782H1 (SININOT01)
104	238	1685409	PROSNOT15	755203R1 (BRAITUT02), 1226185T1 (COLNNOT01), 1300837F1 (BRSTNOT07), 1685409H1 (PROSNOT15), 1705256H1 (DUODNOT02)
105	239	1731419	BRSTTUT08	1731419H1 (BRSTTUT08), 1731419X319T3 (BRSTTUT08), 1731419X322F1 (BRSTTUT08), 1731419X326F1 (BRSTTUT08), 1731419X329F1 (BRSTTUT08), 1733786F6 (BRSTTUT08), SZAH01494F1
106	240	2650265	BRSTNOT14	1680316T6 (STOMFET01), 2650265H1 (BRSTNOT14), 2650265T6 (BRSTNOT14), 2760588R6 (BRAINOS12)
107	241	2677129	KIDNNOT19	1592129H1 (CARGNOT01), 2645962H1 (OVARTUT04), 2677129F6 (KIDNNOT19), 2677129H1 (KIDNNOT19), 2910973H1 (KIDNTUT15), 4571722H1 (PROSTMT02), 4906791H2 (TLYMNOT08)
108	242	3151073	ADRENON04	3150857T6 (ADRENON04), 3151073H1 (ADRENON04), 3151073R6 (ADRENON04)
109	243	3170095	BRSTNOT18	3170095F6 (BRSTNOT18), 3170095H1 (BRSTNOT18)

TABLE 1 (cont.)

Protein SEQ ID NO:	Nucleotide SEQ ID NO:	Clone ID	Library	Fragments
110	244	3475168	LUNGNOT27	079680F1 (SYNORAB01), 443811T6 (MPHGNOT03), 1509356T6 (LUNGNOT14), 1873596F6 (LEUKNOT02), 2440867H1 (EOSITXT01), 3475168H1 (LUNGNOT27)
111	245	3836893	DENDTNT01	446637H1 (MPHGNOT03), 1219376R6 (NEUTGMT01), 3735467F6 (SMCCNOS01), 3735467T6 (SMCCNOS01), 3836893H1 (DENDTNT01)
112	246	4072159	KIDNNOT26	2129415T6 (KIDNNOT05), 4072159F6 (KIDNNOT26), 4072159H1 (KIDNNOT26)
113	247	1003916	BRSTNOT03	620937R6 (PGANNOT01), 1003916H1 and 1003916R6 (BRSTNOT03), 1413623H1 (BRAINOT12), 1435945F1 (PANCNOT08), 1479127F1 (CORPNOT02), 1969146R6 (BRSTNOT04), 2517587F6 (BRAITUT21), 2967848H1 (SCORNOT04)
114	248	2093492	PANCNOT04	489651H1 (HNT2AGT01), 1265353T1 (SYNORAT05), 1431505R6 (BEPINON01), 1605237F6 (LUNGNOT15), 2093492H1 and 2093492T6 (PANCNOT04), 4195560H1 (COLITUT02)
115	249	2108789	BRAITUT03	2108789H1 and 2108789R6 (BRAITUT03), 2182008T6 (SININOT01), 3255751R6 and 3255751T6 (OVARTUN01)
116	250	2171401	ENDCNOT03	037241F1 (HUVENOB01), 1821492F6 (GBLATUT01), 2055814T6 (BEPINOT01), 2171401F6 and 2171401H1 (ENDCNOT03), 2668952F6 (ESOGTUT02), 3140313H1 and 3140313T6 (SMCCNOT02), 5031775H1 (EPIBTXT01)
117	251	2212530	SINTFET03	187596R6 and 187596T6 (CARDNOT01), 919634R6 (RATRNOT02), 1992331H1 (CORPNOT02), 2062034H1 (OVARNOT03), 2212530F6 and 2212530H1 (SINTFET03), 2520479H1 (BRAITUT21), 2878284F6 (THYRNOT10), 2992354H1 (KIDNFET02), 4020719F6 (BRAXNOT02)
118	252	2253036	OVARTUT01	2253036H1 and 2253036R6 (OVARTUT01)

TABLE 1 (cont.)

Protein SEQ ID NO:	Nucleotide SEQ ID NO:	Clone ID	Library	Fragments
119	253	2280161	PROSNON01	482326H1 (HNT2RAT01), 934345H1 (CERVNOT01), 1379358F1 and 1379358T1 (LUNGNOT10), 1438562T1 (PANCNOT08), 1467511F6 (PANCTUT02), 1568138F1 (UTRSNOT05), 1636106T6 (UTRSNOT06), 2134534F6 (ENDCNOT01), 2280161H1 and 2280161X19F1 (PROSNON01), 2789845F6 (COLNTUT16), 3096938H1 (CERVNOT03), 3774621F6 (BRSTNOT25), 4222971H1 (PANCNOT07), 5111983H1 (ENDITXT01), 5324177H1 (FIBPFEN06)
120	254	2287485	BRAINON01	1454588F1 (PENITUT01), 1593332F6 (BRAINOT14), 2287485H1 and 2287485R6 (BRAINON01), 3765992H1 (BRSTNOT24), 4374293H1 (CONFNOT03), 4937931H1 (PROSTUS18), SBCA01722F1
121	255	2380344	ISLTNOT01	2380344F6 and 2380344H1 (ISLTNOT01), 2888536T3 (LUNGFET04), SASA03644F1, SASA03689F1
122	256	2383171	ISLTNOT01	956296R1 (KIDNNOT05), 1342250F1 (COLNTUT03), 1468046F1 and 1468046T1 (PANCTUT02), 2383171H1 (ISLTNOT01), SBYA05452U1, SBYA01369U1
123	257	2396046	THP1AZT01	2396046F6, 2396046H1 and 2396118T6 (THP1AZT01)
124	258	2456587	ENDANOT01	2456587H1 and 2456587T6 (ENDANOT01), 2872569H1 (THYRNOT10), SBCA03778F1, SBDA00115F1, SBCA02401F1, SBCA03351F1, SBCA05164F1, SBCA04783F1, SBCA00155F1, SBCA04141F1
125	259	2484813	BONRTUT01	1234970T1 (LUNGFET03), 1338090F6 (COLNNOT13), 2484813H1 (BONRTUT01), SBCA00053F1, SBCA02064F1, SBCA02151F1, SBCA03770F1, SBCA04866F1, SBCA03406F1
126	260	2493851	ADRETUT05	2493851H1 (ADRETUT05), 3805916F6 (BLADTUT03), 4500439H1 and 4500748H1 (BRAVTXT02), 5120601H1 (SMCBUNT01)
127	261	2495719	ADRETUT05	603447R1 (BRSTTUT01), 2495719H1 (ADRETUT05), 2917493F6 (THYMFET03), 4647103H1 (PROSTUT20), SBRA04984D1

TABLE 1 (cont.)

Protein SEQ ID NO:	Nucleotide SEQ ID NO:	Clone ID	Library	Fragments
128	262	2614153	GBLANOT01	1833135R6 (BRAINON01), 1966515R6 (BRSTNOT04), 2331103R6 (COLNNOT11), 2614153H1 (GBLANOT01), 2656691F6 (LUNGTUT09), 3951176H1 (DRGCNOT01)
129	263	2655184	THYMNOT04	2655184H1 (THYMNOT04), SBDA05215F1, SBDA05213F1, SBDA01516F1
130	264	2848362	BRSTTUT13	1297974F1 and 1297974T6 (BRSTNOT07), 2630138F6 (COLNTUT15), 2848362H1 (BRSTTUT13)
131	265	2849906	BRSTTUT13	1541617R1 and 1541617T1 (SINTTUT01), 2684504F6 and 2684504T6 (LUNGNOT23), 2796805H1 (NPOLNOT01), 2849906H1 (BRSTTUT13)
132	266	2899137	DRGCNOT01	2899137H1 (DRGCNOT01), 3026490F6 and 3026490T6 (HEARFET02), 3483359H1 (KIDNNOT31)
133	267	2986229	CARGDIT01	1740227T6 (HIPONON01), 2986229H1 (CARGDIT01)
134	268	3222081	COLNNON03	1754079F6 (LIVRTUT01), 3222081H1 (COLNNON03), 4053813T6 (SPLNNOT13), 4230282H1 (BRAMDIT01), SBDA07029F3

TABLE 2

Protein SEQ ID NO:	Amino Acid Residues	Potential Phosphorylation Sites	Potential Glycosylation Sites	Signature Sequences	Identification	Analytical Methods
1	88	T83 S38 T76		M1 - A21		Signal Peptide HMM
2	128	S30 S40 T47 T119 W125		M1 - F28		Signal Peptide HMM
3	111	T70		M1 - T18		Signal Peptide HMM
4	110	S32 T64	N58	M1 - A29		Signal Peptide HMM
5	78	T27 S39 S39 S44 S22 T27 S28 S57		M1 - R24		Signal Peptide HMM
6	88	T55 S30 S40 T55	N34	M1 - N21		Signal Peptide HMM
7	227	S220 S70 S83 T131 S134 S141 T158 Y123	N100	M1 - Q20		Signal Peptide HMM
8	198	S62 T123 S142 S189 S62 T100 Y85	N60	M1 - A28		Signal Peptide HMM
9	65	T48		M1 - A29		Signal Peptide HMM
10	154			M1 - A29		Signal Peptide HMM

TABLE 2 (cont.)

Protein SEQ ID NO:	Amino Acid Residues	Potential Phosphorylation Sites	Potential Glycosylation Sites	Signature Sequences	Identification	Analytical Methods
11	237	T116 T26 T79 T85 T182 T188 T194 T206 S60 S123 S176 S213	N128	M1 - A19		Signal Peptide HMM
12	225	T158 S128	N166	M1 - G27		Signal Peptide HMM
13	117	S41		M1 - A23		Signal Peptide HMM
14	253	S49 T63 S92 T110 S127 T239	N42 N47 N72 N207	M1 - T20		Signal Peptide HMM
15	171	S43 S94 T114		M88 - R112		Signal Peptide HMM
16	78	S38 S43	N37	M1 - G19		Signal Peptide HMM
17	71	T64 T67		M1 - C19		Signal Peptide HMM
18	188	S36 T58 T133 Y31	N121 N171	M1 - A21		Signal Peptide HMM
19	80	S76		M1 - C19		Signal Peptide HMM
20	80			M1 - G25		Signal Peptide HMM
21	84	S39 S53 S60		M1 - G21		Signal Peptide HMM

TABLE 2 (cont.)

Protein SEQ ID NO:	Amino Acid Residues	Potential Phosphorylation Sites	Potential Glycosylation Sites	Signature Sequences	Identification	Analytical Methods
22	171	S41 T150		M3 - A21		Signal Peptide HMM
23	243	S3 S44 T75 S86 S183 S223 S36 S92 S205 Y40 Y110	N97	M1 - C25		Signal Peptide HMM
24	311	T5 S76 T82 T93 T109 S121 T137 T170 S184 S11 T53 S75 S84 T132 S223 S274 Y69	N49 N91 N108 N128 N135 N190	M1 - A32		Signal Peptide HMM
25	57			M1 - L29		Signal Peptide HMM
26	82	S46 Y26		M1 - S18		Signal Peptide HMM
27	115			M1 - G34		Signal Peptide HMM
28	327	S93 S50 S167 S233 S89 T105 T214 S302 T318	N138 N206	M1 - E25		Signal Peptide HMM
29	133	S63	N105	M1 - E29		Signal Peptide HMM
30	129	S21 S65 T93		M1 - G20		Signal Peptide HMM

TABLE 2 (cont.)

Protein SEQ ID NO:	Amino Acid Residues	Potential Phosphorylation Sites	Potential Glycosylation Sites	Signature Sequences	Identification	Analytical Methods
31	472	S164 T32 S42 T141 T154 S155 T235 T262 T271 T334 T376 S402 S421 S435 T441 S19 S29 T327 S378	N61 N179 N353 N356 N396	M1 - G20	hematopoietic lineage switch 2 (g3169729)	Signal Peptide HMM BLAST - GenBank
32	93	T21		M1 - A18		Signal Peptide HMM
33	92	S57 S5		M1 - G47		SPScan
34	143	T6 T14 T135		M9 - G40		Signal Peptide HMM
35	89	T15 S58 S66		M1 - A19		Signal Peptide HMM
36	560	T7 T76 S150 T224 S228 S257 S358 S474 S529 S539 T186 S219 S368 Y523	N163 N184 N379	M1 - E34		SPScan
37	197	T80 S163		M1 - G28		Signal Peptide HMM
38	437	T47 T146 S233 S391 S403 T43 S130 S273 S339 S364	N46 N189 N382	M1 - A21		Signal Peptide HMM

TABLE 2 (cont.)

Protein SEQ ID NO:	Amino Acid Residues	Potential Phosphorylation Sites	Potential Glycosylation Sites	Signature Sequences	Identification	Analytical Methods
39	330	S197 T49 T150 S193 T214 T215 T49 S111 S237	N46 N64 N166 N191	M1 - G28		Signal Peptide HMM
40	148	T73 S141	N29 N58 N71 N103	M1 - R24	receptor-activity-modifying protein (RAMP; g4165368)	Signal Peptide HMM BLAST - GenBank
41	188	S49		M1 - V25		Signal Peptide HMM
42	222	S89 S165 T174 T182 T83 S155		M1 - S24		Signal Peptide HMM
43	111	S54 S29 S98 S50 S57 T104		M1 - T23		Signal Peptide HMM
44	341	T29 S106 T120 S161 S195 S37 S47 T51 S136 S223 S230 S281		M1 - G22		Signal Peptide HMM
45	148	S21 T63 T63 A146	N40	M1 - G23		Signal Peptide HMM
46	87	S65		M1 - P18		Signal Peptide HMM

TABLE 2 (cont.)

Protein SEQ ID NO:	Amino Acid Residues	Potential Phosphorylation Sites	Potential Glycosylation Sites	Signature Sequences	Identification	Analytical Methods
47	383	T77 S95 S108 S280 S351 S121 S124 S153 T187	N93 N207	M1 - P23		Signal Peptide HMM
48	109	S25 S22		M1 - L18		Signal Peptide HMM
49	185	S62		M1 - A20		Signal Peptide HMM
50	110	T100 T73 S97 Y48	N71	M1 - C21		Signal Peptide HMM
51	126	S17 S110		M1 - G18		Signal Peptide HMM
52	488	S205 T31 S86 T236 S7 T447	N250 N321 N463	M1 - L25	putative involvement in cell wall structure or biosynthesis (g3738170)	Signal Peptide HMM BLAST - GenBank
53	197	T55 S34 S46 S69 T98 S108 T119 T167 S194 S2 S34 T153		M1 - A26		Signal Peptide HMM
54	84	S65 S36 T41 S51 S69 S81	N39	M1 - G25		Signal Peptide HMM
55	97	S56		M1 - A22		Signal Peptide HMM
56	140	S29		M1 - P23		Signal Peptide HMM

TABLE 2 (cont.)

Protein SEQ ID NO:	Amino Acid Residues	Potential Phosphorylation Sites	Potential Glycosylation Sites	Signature Sequences	Identification	Analytical Methods
57	285	S53 S108 T216 S253 S277	N153	M1 - A25		Signal Peptide HMM
58	262	S62 T166 S62 S71 Y246	N190	M1 - G28	3-acylating enzyme (Q44449)	Signal Peptide HMM BLAST - GENESEQ
59	189	S120 T154 T34 T37 S174		M1 - C22		Signal Peptide HMM
60	257	S98 T136 T67 S112 S234 S237		M55 - E84ß		SPScan
61	82	T68	N67	M1 - G18		Signal Peptide HMM
62	202	T21 S117 S120		M1 - G27		Signal Peptide HMM
63	450	S107 S97 S146 S339 S440 S245 T303 S304 S399		M1 - G18		Signal Peptide HMM
64	322	T145 T214 T16 S24 S35 S45 T145 T269 S297 T300 T314 Y87	N53 N130 N289	M1 - G23		Signal Peptide HMM
65	104	S38 S25 S75		M1 - A18		Signal Peptide HMM

TABLE 2 (cont.)

Protein SEQ ID NO:	Amino Acid Residues	Potential Phosphorylation Sites	Potential Glycosylation Sites	Signature Sequences	Identification	Analytical Methods
66	93			M1 through about S18 Transmembrane: M1 through about Y17		SPscan HMM
67	71	S23 S64		M1 through about A24		SPscan HMM MOTIFS
68	394	S392 S393 S31 S127 S179 S334 T338 S358 T383 Y323	N53	M1 through about S31 Transmembrane: about M159 through about F178 about F109 through about S127 about F225 through about V243		SPScan HMM MOTIFS
69	72	S59	N69	M1 through about S23 Transmembrane: M1 through about L16		SPscan HMM MOTIFS
70	71	S11 T26		M1 through about Q18		SPscan HMM MOTIFS
71	247	S41 T79		M1 through about S25		SPscan HMM MOTIFS
72	73	S56		M1 through about G27		SPscan HMM MOTIFS

TABLE 2 (cont.)

Protein SEQ ID NO:	Amino Acid Residues	Potential Phosphorylation Sites	Potential Glycosylation Sites	Signature Sequences	Identification	Analytical Methods
73	70			M1 through about G20		SPscan HMM
74	67			M1 through about G30		SPscan HMM
75	91			M1 through about G26		SPScan
76	56	T29 S46 T51		M1 through about S19		SPscan HMM MOTIFS
77	112	S62 S65		M1 through about G27 Transmembrane: about W79 through about H97		SPscan HMM MOTIFS
78	54		N48	M1 through about N34		SPscan HMM MOTIFS
79	57	T33 R55		M1 through about C18		SPscan HMM MOTIFS
80	52	S34		M1 through about S30		SPscan HMM MOTIFS

TABLE 2 (cont.)

Protein SEQ ID NO:	Amino Acid Residues	Potential Phosphorylation Sites	Potential Glycosylation Sites	Signature Sequences	Identification	Analytical Methods
81	64	T43 Y27		M1 through about S41		SPscan HMM MOTIFS
82	65	S45		M1 through about A31 Transmembrane: about L38 through about F55		SPscan HMM MOTIFS
83	56			M1 through about E23		SPscan HMM
84	120	S69 S109	N89 N95	M1 through about A38 Transmembrane: about L23 through about T41		SPscan HMM MOTIFS
85	67	S28		M1 through about K30 Microbodies C-terminal targetting signal: A65KV		SPscan HMM MOTIFS
86	62	S29 S42 S46	N40	M1 through about S29		SPscan HMM MOTIFS
87	75	S25 S46		M1 through about L19 Transmembrane: about I3 through about G20		SPscan HMM MOTIFS

TABLE 2 (cont.)

Protein SEQ ID NO:	Amino Acid Residues	Potential Phosphorylation Sites	Potential Glycosylation Sites	Signature Sequences	Identification	Analytical Methods
88	80	T28		M1 through about A20		SPscan HMM MOTIFS
89	50	S11		M1 through about C48		SPscan HMM MOTIFS
90	116	S38		M1 through about G22		SPscan HMM MOTIFS
91	67	S43		M1 through about P21		SPscan HMM MOTIFS
92	538	S415 S52 T77 S97 T178 T228 S282 S320 S332 S384 T401 T424 S483 S207 S230 S357 T410 Y263 Y365	N226	M1 through about S18 Tyrosine specific protein phosphatases signature: about V328 through about F340		SPScan BLOCKS PRINTS MOTIFS
93	58			M1 through about S25		SPscan HMM
94	119	S39		M1 through about S22 Transmembrane: about V3 through about S21		SPscan HMM MOTIFS

TABLE 2 (cont.)

Protein SEQ ID NO:	Amino Acid Residues	Potential Phosphorylation Sites	Potential Glycosylation Sites	Signature Sequences	Identification	Analytical Methods
95	128	S91		M1 through about G31 Transmembrane: about F108 through about L126		SPscan HMM MOTIFS
96	124	T115 T43 S91		M1-S20 P116-V124 (urotensin II signature)		SPScan HMM Motifs BLOCKS BLAST
97	182	S28 T70 S172 S25 S32 S48 S108 S131		M1-S23, M1-S25		SPScan HMM Motifs
98	237	S55 S88 S121 S135	N45 N73 N107 N118 N132 N172 N175 N185	M1-A16, M1-S21 C40-C198 (cysteine spacing pattern similar to that of RoBo-1)		SPScan HMM Motifs BLAST
99	160	S36 S59 T143		M1-A27		SPScan HMM Motifs
100	148	T76 S64 Y103		M1-S30, M1-G31		SPScan HMM Motifs
101	170	S78 T4 T30 S130 S25 S29 T122		M1-A23, M1-L28		SPScan HMM Motifs

TABLE 2 (cont.)

Protein SEQ ID NO:	Amino Acid Residues	Potential Phosphorylation Sites	Potential Glycosylation Sites	Signature Sequences	Identification	Analytical Methods
102	150	S50 S78 S91		M1-A26, M1-S28		SPScan HMM Motifs
103	142	T57 T80		M1-A25, M1-G26		SPScan HMM Motifs
104	110	T3		M1-G18, M1-T25		SPScan HMM Motifs
105	120	T29 S40 S72		M1-G22, M1-A20		SPScan HMM Motifs
106	135	T115 S38 T41	N32 N101	M1-G26, M1-C25		SPScan HMM Motifs
107	301	S53 S217 S240 S283 T224		M1-A22		SPScan HMM Motifs
108	103	S88 T73 S84		M1-P19, M1-L22		SPScan HMM, Motifs
109	95	T82 S52 S77	N50	M1-T15, M1-P19		SPScan HMM Motifs

TABLE 2 (cont.)

Protein SEQ ID NO:	Amino Acid Residues	Potential Phosphorylation Sites	Potential Glycosylation Sites	Signature Sequences	Identification	Analytical Methods
110	113	T84 S4		M1-P19, M1-A24		SPScan HMM Motifs
111	234	S179 S184 S51 T70 T158 S168 T228 Y29	N146 N191 N194	M1-A20	NK cell activating receptor (g4493702)	SPScan HMM Motifs BLAST - GenBank
112	119	S39 T61		M1-G30, M1-G27		SPScan HMM Motifs
113	200	S51 T46 S191		M1-G26 Signal Peptide	Signal Peptide Containing Protein, Homology with KIAA0206	SPScan Motifs BLAST
114	225			M1-Q29 Signal Peptide	Signal Peptide Containing Protein	SPScan
115	155	S29		M1-A20 Signal Peptide	Signal Peptide Containing Protein	HMM Motifs
116	468	S143 T156 T227 S235 T271 T293 T436 S453 S117 T148 T213 S263 S417 Y73	N280 N384	M1-G23 Signal Peptide	Signal Peptide Containing Protein	SPScan Motifs
117	403	S19 S320 S69 S151 T171 T97 S393 Y193 Y378	N87	M1-A24 Signal Peptide	Signal Peptide Containing Protein	HMM Motifs

TABLE 2 (cont.)

Protein SEQ ID NO:	Amino Acid Residues	Potential Phosphorylation Sites	Potential Glycosylation Sites	Signature Sequences	Identification	Analytical Methods
118	131	T131 S24 T79 T118 T123 T127	N116	M1-G25 Signal Peptide	Signal Peptide Containing Protein	SPScan Motifs
119	556	T176 S192 S196 T220 S344 S369 S476 T501 S529 S541 T548 T553 S48 S115 S121 T386 T424 S500 Y104	N62 N79 N127 N157 N160	M1-P21 Signal Peptide L226-W244, Y402-W422, V375-L392 and Y355-I376 Transmembrane Domains	Signal Peptide Containing Protein, Weakly similar to Putative Transmembrane Protein (PTM1) Precursor	SPScan Motifs HMM BLAST
120	514	T457 T80 S86 T141 T372 T420 S447 S94 T102 S112 T240 S297 S353 S470	N100 N168 N319	M1-G24 Signal Peptide	Signal Peptide Containing Protein,	SPScan Motifs
121	109	T46 S78 T12		M1-S15 Signal Peptide	Signal Peptide Containing Protein	SPScan MotifS
122	431	S57 T320 S339 S396 S100 S239		M1-L25 Signal Peptide	Signal Peptide Containing Protein, Weakly similar to OXA1L	SPScan Motifs BLAST
123	142			M1-W16 Signal Peptide	Signal Peptide Containing Protein	SPScan

TABLE 2 (cont.)

Protein SEQ ID NO:	Amino Acid Residues	Potential Phosphorylation Sites	Potential Glycosylation Sites	Signature Sequences	Identification	Analytical Methods
124	643	T8 S28 S77 T169 T199 T235 S252 T320 S402 T413 S414 S558 S22 T25 S56 S62 S120 T184 S329 T423 S475 S574 Y226	N251	M1-S28 Signal Peptide, D37-C81, W380-C437, W440-C492 and F526-C583 Thrombospondin Type 1 Domains	Signal Peptide Containing Protein, Thrombospondin Type 1 Protein	SPScan Motifs Pfam BLAST
125	568	S510 T24 T80 S91 T153 T165 S232 S248 S262 T300 T334 S380 S446 S16 T19 T60 S127 S273 T436 T531 S554 T564 Y135 Y489	N322	M1-T19 Signal Peptide	Signal Peptide Containing Protein	SPScan Motifs
126	125	T62 S27 T36		M1-R32 Signal Peptide, V4-L53 Glycosyl Hydrolase Family 9 Active Site Signature	Signal Peptide Containing Protein, Glycosyl Hydrolase Protein	SPScan Motifs PROFILE-SCAN
127	196	T105 T47 T56 S158		M1-S26 Signal Peptide, H79-H123 Ribosomal Protein S18 Signature	Signal Peptide Containing Protein, Ribosomal Protein S18	SPScan Motifs BLAST Pfam PROFILE-SCAN
128	214	S112 S131	N37 N92	M1-S35 Signal Peptide	Signal Peptide Containing Protein, Homology with GTP Binding Protein	SPScan Motifs BLAST

TABLE 2 (cont.)

Protein SEQ ID NO:	Amino Acid Residues	Potential Phosphorylation Sites	Potential Glycosylation Sites	Signature Sequences	Identification	Analytical Methods
129	88			M1-S24 Signal Peptide	Signal Peptide Containing Protein	HMM
130	260	S146 S179 S192 S239 S70 T126 T150	N50 N109	M1-A48 Signal Peptide, G59-S142 Immunoglobulin Domain	Signal Peptide Containing Protein, Immunoglobulin Superfamily Protein	SPScan Motifs Pfam
131	295	T176 T56 S72 S179 S256 S87		M1-A30 Signal Peptide	Signal Peptide Containing Protein	SPScan Motifs
132	183	S11 T41 T42 S83		M1-W24 Signal Peptide, E131-K168 and C105-H115 Adrenodoxin Iron-Sulfur Binding Signature, C111-V116 Cytochrome C Heme Binding Signature, N69-A162 Iron-Sulfur Cluster Binding Domain	Signal Peptide Containing Protein, Adrenodoxin Family Iron-Sulfur Binding Protein, and Cytochrome C Family Heme Binding Protein	HMM Motifs BLOCKS PRINTS Pfam
133	113	S93 T89 Y9		M1-G30 Signal Peptide, V28-L74 PF00646 F-Box Domain	Signal Peptide Containing Protein, PF00646 F-Box Protein	SPScan Motifs Pfam
134	160	T46 T55 S65 S124 T125 T46		M1-A27 Signal Peptide	Signal Peptide Containing Protein, F45G2.10 and Yhr122wp Homology	SPScan Motifs BLAST

TABLE 3

Nucleotide SEQ ID NO:	Tissue Expression (Fraction of Total)	Disease/Condition-Specific Expression (Total of Fraction)	Vector
135	Hematopoietic/Immune (1.000)	Inflammation (1.000)	pBLUESCRIPT
136	Hematopoietic/Immune (0.750) Cardiovascular (0.250)	Inflammation (0.750) Cancer (0.250)	pSPORT1
137	Nervous (1.000)	Trauma (1.000)	pSPORT1
138	Musculoskeletal (1.000)	Inflammation (1.000)	pSPORT1
139	Gastrointestinal (0.714) Cardiovascular (0.143) Reproductive (0.143)	Cancer (0.714) Trauma (0.143)	pSPORT1
140	Nervous (1.000)	Neurological (0.500) Trauma (0.500)	pSPORT1
141	Reproductive (0.293) Gastrointestinal (0.146) Hematopoietic/Immune (0.146)	Cancer (0.524) Inflammation (0.256) Fetal (0.146)	pSPORT1
142	Reproductive (0.266) Gastrointestinal (0.170) Nervous (0.138)	Cancer (0.479) Inflammation (0.277) Fetal (0.181)	pINCY
143	Reproductive (0.417) Nervous (0.292) Developmental (0.125)	Cancer (0.417) Inflammation (0.250) Fetal (0.167)	pINCY
144	Reproductive (0.321) Cardiovascular (0.143) Developmental (0.143)	Cancer (0.464) Fetal (0.214) Inflammation (0.143)	pINCY
145	Reproductive (0.600) Gastrointestinal (0.400)	Cancer (0.400) Trauma (0.400) Inflammation (0.200)	pINCY
146	Cardiovascular (0.400) Dermatologic (0.200) Nervous (0.200)	Cancer (0.600) Fetal (0.600)	pINCY
147	Developmental (0.667) Gastrointestinal (0.333)	Fetal (0.667) Cancer (0.333)	pINCY
148	Reproductive (0.256) Nervous (0.248) Cardiovascular (0.137)	Cancer (0.479) Inflammation (0.214) Fetal (0.145)	pINCY
149	Reproductive (0.244) Nervous (0.178) Hematopoietic/Immune (0.167)	Cancer (0.433) Inflammation (0.322) Fetal (0.156)	pINCY

TABLE 3 (cont.)

Nucleotide SEQ ID NO:	Tissue Expression (Fraction of Total)	Disease/Condition-Specific Expression (Total of Fraction)	Vector
150	Cardiovascular (0.923) Developmental (0.077)	Cancer (0.692) Fetal (0.154) Inflammation (0.154)	pINCY
151	Reproductive (0.215) Nervous (0.190) Gastrointestinal (0.177)	Cancer (0.494) Inflammation (0.278) Trauma (0.152)	pINCY
152	Reproductive (0.200) Nervous (0.171) Hematopoietic/Immune (0.143)	Inflammation (0.371) Cancer (0.229) Fetal (0.200)	pINCY
153	Reproductive (0.333) Nervous (0.157) Hematopoietic/Immune (0.137)	Cancer (0.549) Inflammation (0.176) Fetal (0.137)	pINCY
154	Gastrointestinal (0.500) Urologic (0.167)	Inflammation (0.667) Cancer (0.167) Trauma (0.167)	pINCY
155	Gastrointestinal (0.429) Reproductive (0.286) Nervous (0.143)	Inflammation (0.429) Cancer (0.286) Trauma (0.143)	pINCY
156	Reproductive (1.000)	Cancer (0.500) Inflammation (0.500)	pINCY
157	Hematopoietic/Immune (0.346) Reproductive (0.154) Gastrointestinal (0.115)	Cancer (0.404) Inflammation (0.404) Fetal (0.212)	pINCY
158	Reproductive (0.236) Hematopoietic/Immune (0.217) Gastrointestinal (0.132)	Cancer (0.415) Inflammation (0.358) Fetal (0.142)	pINCY
159	Gastrointestinal (1.000)	Cancer (1.000)	pSPORT1
160	Developmental (0.500) Hematopoietic/Immune (0.250) Nervous (0.250)	Fetal (0.500) Inflammation (0.250) Trauma (0.250)	pINCY
161	Hematopoietic/Immune (0.250) Reproductive (0.250) Nervous (0.208)	Cancer (0.583) Fetal (0.292) Inflammation (0.250)	pINCY
162	Gastrointestinal (0.412) Reproductive (0.412) Cardiovascular (0.088)	Cancer (0.735) Inflammation (0.176) Fetal (0.029)	pINCY

TABLE 3 (cont.)

Nucleotide SEQ ID NO:	Tissue Expression (Fraction of Total)	Disease/Condition-Specific Expression (Total of Fraction)	Vector
163	Reproductive (0.298) Cardiovascular (0.170) Nervous (0.149)	Cancer (0.532) Inflammation (0.213) Fetal (0.191)	pINCY
164	Gastrointestinal (0.333) Hematopoietic/Immune (0.333) Reproductive (0.333)	Cancer (0.667) Inflammation (0.333)	pINCY
165	Reproductive (0.295) Gastrointestinal (0.159) Nervous (0.148)	Cancer (0.534) Inflammation (0.284) Fetal (0.091)	pINCY
166	Hematopoietic/Immune (0.538) Cardiovascular (0.077) Reproductive (0.077)	Inflammation (0.731) Cancer (0.154) Fetal (0.154)	pINCY
167	Reproductive (0.483) Gastrointestinal (0.121) Nervous (0.103)	Cancer (0.672) Inflammation (0.155)	pINCY
168	Gastrointestinal (0.222) Hematopoietic/Immune (0.222) Nervous (0.148)	Cancer (0.519) Inflammation (0.370) Fetal (0.259)	pINCY
169	Urologic (1.000)	Cancer (0.333) Fetal (0.333) Inflammation (0.333)	pINCY
170	Reproductive (0.214) Gastrointestinal (0.179) Nervous (0.143)	Cancer (0.643) Inflammation (0.143) Fetal (0.107)	pINCY
171	Reproductive (0.261) Developmental (0.174) Nervous (0.174)	Cancer (0.391) Fetal (0.304) Inflammation (0.217)	pINCY
172	Reproductive (0.357) Gastrointestinal (0.321) Cardiovascular (0.071)	Cancer (0.571) Inflammation (0.286) Fetal (0.107)	pINCY
173	Reproductive (0.306) Nervous (0.161) Cardiovascular (0.129)	Cancer (0.387) Inflammation (0.323) Fetal (0.226)	pINCY
174	Reproductive (0.229) Nervous (0.188) Cardiovascular (0.167)	Cancer (0.521) Inflammation (0.312) Trauma (0.146)	pSPORT1

TABLE 3 (cont.)

Nucleotide SEQ ID NO:	Tissue Expression (Fraction of Total)	Disease/Condition-Specific Expression (Total of Fraction)	Vector
175	Reproductive (0.444) Developmental (0.167) Cardiovascular (0.111)	Cancer (0.556) Fetal (0.278) Trauma (0.111)	pSPORT1
176	Reproductive (0.294) Gastrointestinal (0.176) Cardiovascular (0.118)	Cancer (0.765) Fetal (0.118) Inflammation (0.118)	pSPORT1
177	Gastrointestinal (1.000)	Cancer (0.667) Inflammation (0.333)	pINCY
178	Reproductive (0.385) Nervous (0.231) Gastrointestinal (0.154)	Cancer (0.385) Inflammation (0.385)	pINCY
179	Reproductive (0.500) Cardiovascular (0.167) Gastrointestinal (0.167)	Cancer (0.667) Fetal (0.167) Inflammation (0.167)	pBLUESCRIPT
180	Cardiovascular (0.231) Reproductive (0.231) Gastrointestinal (0.154)	Cancer (0.615) Inflammation (0.308) Fetal (0.154)	pINCY
181	Reproductive (0.324) Gastrointestinal (0.176) Cardiovascular (0.130)	Cancer (0.519) Inflammation (0.222) Fetal (0.157)	pINCY
182	Reproductive (0.320) Nervous (0.180) Gastrointestinal (0.120)	Cancer (0.580) Inflammation (0.160) Fetal (0.100)	pINCY
183	Gastrointestinal (0.667) Reproductive (0.333)	Cancer (1.000)	pINCY
184	Urologic (0.667) Dermatologic (0.333)	Cancer (0.667) Fetal (0.333)	pSPORT1
185	Cardiovascular (0.500) Reproductive (0.500)	Cancer (1.000)	pINCY
186	Reproductive (0.393) Developmental (0.107) Urologic (0.107)	Cancer (0.607) Fetal (0.179) Inflammation (0.107)	pINCY
187	Cardiovascular (0.400) Reproductive (0.333) Gastrointestinal (0.133)	Inflammation (0.467) Cancer (0.267) Fetal (0.267)	pSPORT1
188	Nervous (0.318) Reproductive (0.227) Urologic (0.136)	Cancer (0.636) Inflammation (0.136) Trauma (0.091)	pINCY

TABLE 3 (cont.)

Nucleotide SEQ ID NO:	Tissue Expression (Fraction of Total)	Disease/Condition-Specific Expression (Total of Fraction)	Vector
189	Cardiovascular (0.500) Reproductive (0.500)	Cancer (1.000)	pINCY
190	Reproductive (0.318) Nervous (0.227) Hematopoietic/Immune (0.136)	Cancer (0.500) Fetal (0.227) Inflammation (0.227)	pINCY
191	Reproductive (0.253) Cardiovascular (0.158) Gastrointestinal (0.147)	Cancer (0.463) Inflammation (0.232) Fetal (0.200)	pINCY
192	Reproductive (0.333) Gastrointestinal (0.286) Cardiovascular (0.095)	Cancer (0.571) Inflammation (0.333) Fetal (0.095)	pINCY
193	Reproductive (0.304) Cardiovascular (0.217) Gastrointestinal (0.130)	Cancer (0.435) Inflammation (0.391) Fetal (0.174)	pINCY
194	Reproductive (0.312) Nervous (0.188) Cardiovascular (0.125)	Cancer (0.438) Inflammation (0.250) Fetal (0.188)	pINCY
195	Developmental (1.000)	Fetal (1.000)	pINCY
196	Reproductive (0.233) Cardiovascular (0.209) Nervous (0.140)	Cancer (0.605) Fetal (0.186) Inflammation (0.116)	pINCY
197	Reproductive (0.182) Gastrointestinal (0.136) Hematopoietic/Immune (0.136)	Cancer (0.477) Inflammation (0.341) Fetal (0.182)	pINCY
198	Gastrointestinal (0.205) Reproductive (0.205) Cardiovascular (0.114)	Inflammation (0.341) Cancer (0.250) Fetal (0.227)	pINCY
199	Cardiovascular (0.520) Reproductive (0.280) Developmental (0.160)	Cancer (0.720) Fetal (0.200) Inflammation (0.080)	pINCY
200	Lung (0.958) Developmental (0.25) Musculoskeletal (0.042)	Cancer (0.583) Fetal or Proliferating (0.292) Inflammation (0.167)	pBLUESCRIPT
201	Reproductive (0.571) Musculoskeletal (0.143) Nervous (0.143) Urologic (0.143)	Cancer (0.429) Inflammation (0.571)	pSPORT1

TABLE 3 (cont.)

Nucleotide SEQ ID NO:	Tissue Expression (Fraction of Total)	Disease/Condition-Specific Expression (Total of Fraction)	Vector
202	Endocrine (0.250) Nervous (0.250) Cardiovascular (0.125) Developmental (0.125) Gastrointestinal (0.125) Reproductive (0.125)	Cancer (0.375) Inflammation (0.625) Fetal or Proliferating (0.125)	pSPORT1
203	Lung (1.000)	Fetal or Proliferating (1.000)	pINCY
204	Lung (0.500) Penis (0.500)	Cancer (0.500)	pINCY
205	Cardiovascular (0.231) Dermatologic (0.231) Reproductive (0.231)	Fetal or Proliferating (0.385) Cancer (0.308)	pINCY
206	Nervous (0.596) Reproductive (0.154) Gastrointestinal (0.077)	Cancer (0.442) Neurological (0.192) Inflammation (0.231)	pINCY
207	Gastrointestinal (1.000)	Inflammation (1.000)	pINCY
208	Reproductive (0.300) Hematopoietic/Immune (0.200) Nervous (0.150)	Cancer (0.450) Inflammation (0.400) Fetal or Proliferating (0.250)	pSPORT1
209	Heart (0.500) Brain (0.500)	Neurological (0.500) Inflammation (0.500)	pINCY
210	Nervous (0.625) Reproductive (0.250) Musculoskeletal (0.125)	Cancer (0.750) Fetal or Proliferating (0.250) Neurological (0.125)	pINCY
211	Nervous (0.261) Reproductive (0.304) Gastrointestinal (0.174)	Cancer (0.522) Fetal or Proliferating (0.174) Inflammation (0.130)	pSPORT1
212	Testis (1.000)	Inflammation (1.000)	pBLUESCRIPT
213	Nervous (0.400) Reproductive (0.400) Gastrointestinal (0.200)	Cancer (0.400) Inflammation (0.400) Neurological (0.200)	pBLUESCRIPT
214	Reproductive (0.476) Gastrointestinal (0.286) Cardiovascular (0.095)	Cancer (0.714) Inflammation (0.286) Neurological (0.048)	pSPORT1

TABLE 3 (cont.)

Nucleotide SEQ ID NO:	Tissue Expression (Fraction of Total)	Disease/Condition-Specific Expression (Total of Fraction)	Vector
215	Reproductive (0.284) Gastrointestinal (0.216) Nervous (0.176) Hematopoietic/Immune (0.108) Cardiovascular (0.108)	Cancer (0.486) Inflammation (0.351) Fetal or Proliferating (0.122)	pSPORT1
216	Uterus (0.500) Prostate (0.500)	Cancer (0.500) Inflammation (0.500)	pINCY
217	Nervous (0.429) Cardiovascular (0.143) Gastrointestinal (0.143) Hematopoietic/Immune (0.143) Reproductive (0.143)	Cancer (0.571) Inflammation (0.429) Fetal or Proliferating (0.285)	pSPORT1
218	Reproductive (0.450) Hematopoietic/Immune (0.200) Nervous (0.100) Gastrointestinal (0.100)	Cancer (0.650) Inflammation (0.200) Fetal or Proliferating (0.050)	pINCY
219	Reproductive (0.364) Cardiovascular (0.182) Nervous (0.182)	Cancer (0.636) Fetal or Proliferating (0.182) Inflammation (0.273)	pINCY
220	Prostate (1.000)	Inflammation (1.000)	pSPORT1
221	Developmental (0.333) Nervous (0.333) Reproductive (0.333)	Cancer (0.667) Fetal or Proliferating (0.667)	pSPORT1
222	Reproductive (0.393) Hematopoietic/Immune (0.180) Nervous (0.098) Cardiovascular (0.098)	Cancer (0.508) Inflammation (0.344) Fetal or Proliferating (0.066)	pSPORT1
223	Endocrine (0.333) Gastrointestinal (0.333) Reproductive (0.333)	Cancer (1.000)	pINCY
224	Cardiovascular (0.200) Developmental (0.200) Gastrointestinal (0.200) Reproductive (0.200) Urologic (0.200)	Cancer (0.800) Fetal or Proliferating (0.200)	pINCY
225	Lung (1.000)	Cancer (1.000)	pINCY
226	Reproductive (0.302) Hematopoietic/Immune (0.254) Cardiovascular (0.111)	Cancer (0.381) Inflammation (0.381) Fetal or Proliferating (0.286)	pSPORT1

TABLE 3 (cont.)

Nucleotide SEQ ID NO:	Tissue Expression (Fraction of Total)	Disease/Condition-Specific Expression (Total of Fraction)	Vector
227	Lymphocytes (1.000)	Inflammation (1.000)	pINCY
228	Cardiovascular (0.531) Reproductive (0.250) Urologic (0.094)	Cancer (0.656) Inflammation (0.250) Fetal or Proliferating (0.094)	pINCY
229	Reproductive (0.333) Cardiovascular (0.167) Gastrointestinal (0.167) Endocrine (0.167) Hematopoietic/Immune (0.167)	Cancer (0.500) Fetal or Proliferating (0.167) Inflammation (0.333)	pINCY
230	Hematopoietic/Immune (0.500) Reproductive (0.500)	Cell Proliferation (0.500) Inflammation (0.500)	pBLUESCRIPT
231	Cardiovascular (0.333) Nervous (0.333) Developmental (0.167)	Cancer (0.500) Cell Proliferation (0.333) Inflammation (0.167)	pINCY
232	Gastrointestinal (0.938) Reproductive (0.062)	Cancer (0.500) Inflammation (0.500)	pINCY
233	Nervous (0.324) Reproductive (0.235) Hematopoietic/Immune (0.118)	Cancer (0.456) Inflammation (0.235) Trauma (0.147)	pINCY
234	Nervous (0.255) Reproductive (0.255) Musculoskeletal (0.182)	Cancer (0.545) Inflammation (0.255) Trauma (0.109)	pINCY
235	Musculoskeletal (0.308) Reproductive (0.231) Gastrointestinal (0.154)	Cancer (0.538) Inflammation (0.231) Trauma (0.154)	pINCY
236	Nervous (1.000)	Cancer (1.000)	pINCY
237	Gastrointestinal (0.429) Hematopoietic/Immune (0.143) Nervous (0.143)	Cancer (0.571) Cell Proliferation (0.143) Trauma (0.143)	pINCY
238	Reproductive (0.254) Gastrointestinal (0.160) Nervous (0.128)	Cancer (0.453) Inflammation (0.241) Cell Proliferation (0.175)	pINCY
239	Nervous (0.333) Dermatologic (0.167) Endocrine (0.167)	Trauma (0.333) Cancer (0.167) Cell Proliferation (0.167)	pINCY

TABLE 3 (cont.)

Nucleotide SEQ ID NO:	Tissue Expression (Fraction of Total)	Disease/Condition-Specific Expression (Total of Fraction)	Vector
240	Nervous (0.273) Reproductive (0.227) Endocrine (0.136)	Cancer (0.545) Cell Proliferation (0.182) Inflammation (0.182)	pINCY
241	Reproductive (0.273) Hematopoietic/Immune (0.182) Urologic (0.182)	Cancer (0.455) Cell Proliferation (0.273) Inflammation (0.273)	pINCY
242	Endocrine (1.000)	Trauma (1.000)	pSPORT1
243	Reproductive (1.000)	Cancer (1.000)	pINCY
244	Hematopoietic/Immune (0.545) Musculoskeletal (0.182) Cardiovascular (0.091)	Inflammation (0.636) Trauma (0.182) Cancer (0.091)	pINCY
245	Hematopoietic/Immune (0.400) Musculoskeletal (0.300) Cardiovascular (0.150)	Inflammation (0.650) Cancer (0.300)	pINCY
246	Urologic (1.000)	Cancer (0.500) Cell Proliferation (0.500)	pINCY
247	Nervous (0.292) Reproductive (0.222) Musculoskeletal (0.125)	Cell Proliferation (0.625) Inflammation/Trauma (0.181)	pSPORT1
248	Reproductive (0.211) Developmental (0.132) Nervous (0.132)	Cell Proliferation (0.658) Inflammation/Trauma (0.184)	pSPORT1
249	Nervous (0.500) Gastrointestinal (0.300) Hematopoietic/Immune (0.100)	Cell Proliferation (0.900) Inflammation/Trauma (0.300)	pSPORT1
250	Cardiovascular (0.209) Gastrointestinal (0.140) Hematopoietic/Immune (0.140)	Cell Proliferation (0.605) Inflammation/Trauma (0.256)	pINCY
251	Nervous (0.308) Cardiovascular (0.154) Gastrointestinal (0.154)	Cell Proliferation (0.616) Inflammation/Trauma (0.269)	pINCY
252	Reproductive (1.000)	Cell Proliferation (1.000)	pSPORT1

TABLE 3 (cont.)

Nucleotide SEQ ID NO:	Tissue Expression (Fraction of Total)	Disease/Condition-Specific Expression (Total of Fraction)	Vector
253	Reproductive (0.324) Nervous (0.162) Gastrointestinal (0.113)	Cell Proliferation (0.641) Inflammation/Trauma (0.197)	pSPORT1
254	Reproductive (0.315) Nervous (0.296) Developmental (0.093)	Cell Proliferation (0.630) Inflammation/Trauma (0.278)	pSPORT1
255	Nervous (0.211) Reproductive (0.211) Gastrointestinal (0.158)	Cell Proliferation (0.579) Inflammation/Trauma (0.298)	pINCY
256	Reproductive (0.250) Gastrointestinal (0.148) Hematopoietic/Immune (0.148)	Cell Proliferation (0.705) Inflammation/Trauma (0.193)	pINCY
257	Hematopoietic/Immune (1.000)	Cell Proliferation (0.400) Inflammation/Trauma (0.600)	pINCY
258	Cardiovascular (0.333) Reproductive (0.333) Developmental (0.167)	Cell Proliferation (0.833) Inflammation/Trauma (0.333)	pBLUESCRIPT
259	Cardiovascular (0.333) Reproductive (0.250) Developmental (0.167)	Cell Proliferation (0.625) Inflammation/Trauma (0.208)	pINCY
260	Endocrine (0.500) Cardiovascular (0.250) Nervous (0.250)	Cell Proliferation (0.750) Inflammation/Trauma (0.500)	pINCY
261	Reproductive (0.252) Cardiovascular (0.155) Hematopoietic/Immune (0.136)	Cell Proliferation (0.728) Inflammation/Trauma (0.194)	pINCY
262	Reproductive (0.274) Cardiovascular (0.177) Nervous (0.145)	Cell Proliferation (0.742) Inflammation/Trauma (0.210)	pINCY
263	Reproductive (0.267) Cardiovascular (0.160) Hematopoietic/Immune (0.127)	Cell Proliferation (0.654) Inflammation/Trauma (0.193)	pINCY
264	Nervous (0.229) Hematopoietic/Immune (0.200) Reproductive (0.200)	Cell Proliferation (0.743) Inflammation/Trauma (0.286)	pINCY
265	Hematopoietic/Immune (0.333) Gastrointestinal (0.167) Nervous (0.133)	Cell Proliferation (0.600) Inflammation/Trauma (0.333)	pINCY

TABLE 3 (cont.)

Nucleotide SEQ ID NO:	Tissue Expression (Fraction of Total)	Disease/Condition-Specific Expression (Total of Fraction)	Vector
266	Nervous (0.290) Reproductive (0.258) Cardiovascular (0.129)	Cell Proliferation (0.677) Inflammation/Trauma (0.194)	pINCY
267	Reproductive (0.261) Hematopoietic/Immune (0.217) Cardiovascular (0.087)	Cell Proliferation (0.652) Inflammation/Trauma (0.391)	pINCY
268	Gastrointestinal (0.227) Reproductive (0.193) Hematopoietic/Immune (0.168)	Cell Proliferation (0.731) Inflammation/Trauma (0.227)	pSPORT1

TABLE 4

Polynucleotide SEQ ID NO:	Clone ID	Library	Library Description
135	443531	MPHGNOT03	The library was constructed using RNA isolated from plastic adherent mononuclear cells isolated from buffy coat units obtained from unrelated male and female donors.
136	632860	NEUTGMT01	The library was constructed using RNA isolated from peripheral blood granulocytes collected by density gradient centrifugation through Ficoll-Hypaque. The cells were isolated from buffy coat units obtained from 20 unrelated male and female donors. Cells were cultured in 10 nM GM-CSF for 1 hour before washing and harvesting for RNA preparation.
137	670010	CRBLNOT01	The library was constructed using RNA isolated from the cerebellum tissue of a 69-year-old Caucasian male who died from chronic obstructive pulmonary disease. Patient history included myocardial infarction, hypertension, and osteoarthritis.
138	726498	SYNOOAT01	The library was constructed using RNA isolated from the knee synovial membrane tissue of an 82-year-old female with osteoarthritis.
139	795064	OVARNOT03	The library was constructed using RNA isolated from ovarian tissue removed from a 43-year-old Caucasian female during removal of the fallopian tubes and ovaries. Pathology for the associated tumor tissue indicated grade 2 mucinous cystadenocarcinoma. Patient history included mitral valve disorder, pneumonia, and viral hepatitis. Family history included atherosclerotic coronary artery disease, pancreatic cancer, cerebrovascular disease, breast cancer, and uterine cancer.
140	924925	BRAINOT04	The library was constructed using RNA isolated from the brain tissue of a 44-year-old Caucasian male with a cerebral hemorrhage. The tissue, which contained coagulated blood, came from the choroid plexus of the right anterior temporal lobe. Family history included coronary artery disease and myocardial infarction.

TABLE 4 (cont.)

Polynucleotide SEQ ID NO:	Clone ID	Library	Library Description
141	962390	BRSTTUT03	The library was constructed using RNA isolated from breast tumor tissue removed from a 58-year-old Caucasian female during a unilateral extended simple mastectomy. Pathology indicated multicentric invasive grade 4 lobular carcinoma. The mass was identified in the upper outer quadrant, and three separate nodules were found in the lower outer quadrant of the left breast. Patient history included skin cancer, rheumatic heart disease, osteoarthritis, and tuberculosis. Family history included cerebrovascular disease, coronary artery aneurysm, breast cancer, prostate cancer, atherosclerotic coronary artery disease, and type I diabetes.
142	1259405	MENITUT03	The library was constructed using RNA isolated from brain meningioma tissue removed from a 35-year-old Caucasian female during excision of a cerebral meningeal lesion. Pathology indicated a benign neoplasm in the right cerebellopontine angle of the brain. Patient history included hypothyroidism. Family history included myocardial infarction and breast cancer.
143	1297384	BRSTNOT07	The library was constructed using RNA isolated from diseased breast tissue removed from a 43-year-old Caucasian female during a unilateral extended simple mastectomy. Pathology indicated mildly proliferative fibrocystic changes with epithelial hyperplasia, papillomatosis, and duct ectasia. Pathology for the associated tumor tissue indicated invasive grade 4, nuclear grade 3 mammary adenocarcinoma with extensive comedo necrosis. Family history included epilepsy, atherosclerotic coronary artery disease, and type II diabetes.
144	1299627	BRSTNOT07	The library was constructed using RNA isolated from diseased breast tissue removed from a 43-year-old Caucasian female during a unilateral extended simple mastectomy. Pathology indicated mildly proliferative fibrocystic changes with epithelial hyperplasia, papillomatosis, and duct ectasia. Pathology for the associated tumor tissue indicated invasive grade 4, nuclear grade 3 mammary adenocarcinoma with extensive comedo necrosis. Family history included epilepsy, atherosclerotic coronary artery disease, and type II diabetes.
145	1306026	PLACNOT02	The library was constructed using RNA isolated from the placental tissue of a Hispanic female fetus, who was prematurely delivered at 21 weeks' gestation. Serologies of the mother's blood were positive for CMV (cytomegalovirus).

TABLE 4 (cont.)

Polynucleotide SEQ ID NO:	Clone ID	Library	Library Description
146	1316219	BLADTUT02	The library was constructed using RNA isolated from bladder tumor tissue removed from an 80-year-old Caucasian female during a radical cystectomy and lymph node excision. Pathology indicated grade 3 invasive transitional cell carcinoma. Family history included osteoarthritis and atherosclerosis.
147	1329031	PANCNOT07	The library was constructed using RNA isolated from the pancreatic tissue of a Caucasian male fetus, who died at 23 weeks' gestation.
148	1483050	CORPNOT02	The library was constructed using RNA isolated from diseased corpus callosum tissue removed from the brain of a 74-year-old Caucasian male who died from Alzheimer's disease.
149	1514160	PANCTUT01	The library was constructed using RNA isolated from pancreatic tumor tissue removed from a 65-year-old Caucasian female during radical subtotal pancreatectomy. Pathology indicated an invasive grade 2 adenocarcinoma. Patient history included type II diabetes, osteoarthritis, cardiovascular disease, benign neoplasm in the large bowel, and a cataract. Family history included cardiovascular disease, type II diabetes, and stomach cancer.
150	1603403	LUNGNOT15	The library was constructed using RNA isolated from lung tissue removed from a 69-year-old Caucasian male during a segmental lung resection. Pathology for the associated tumor tissue indicated residual grade 3 invasive squamous cell carcinoma. Patient history included acute myocardial infarction, prostatic hyperplasia, and malignant skin neoplasm. Family history included cerebrovascular disease, type I diabetes, acute myocardial infarction, and arteriosclerotic coronary disease.
151	1652303	PROSTUT08	The library was constructed using RNA isolated from prostate tumor tissue removed from a 60-year-old Caucasian male during radical prostatectomy and regional lymph node excision. Pathology indicated an adenocarcinoma (Gleason grade 3+4). Adenofibromatous hyperplasia was also present. The patient presented with elevated prostate specific antigen (PSA). Patient history included a kidney cyst. Family history included tuberculosis, cerebrovascular disease, and arteriosclerotic coronary artery disease.

TABLE 4 (cont.)

Polynucleotide SEQ ID NO:	Clone ID	Library	Library Description
152	1693358	COLNNOT23	The library was constructed using RNA isolated from diseased colon tissue removed from a 16-year-old Caucasian male during a total colectomy with abdominal/perineal resection. Pathology indicated gastritis and pancolonitis consistent with the acute phase of ulcerative colitis.There was only mild involvement of the ascending and sigmoid colon, and no significant involvement of the cecum, rectum, or terminal ileum. Family history included irritable bowel syndrome.
153	1707711	DUODNOT02	The library was constructed using RNA isolated from duodenal tissue of a 8-year-old Caucasian female, who died from head trauma. Serology was positive for cytomegalovirus (CMV).
154	1738735	COLNNOT22	The library was constructed using RNA isolated from colon tissue removed from a 56-year-old Caucasian female with Crohn's disease during a partial resection of the small intestine. Pathology indicated Crohn's disease of the ileum and ileal-colonic anastomosis, causing a fistula at the anastomotic site that extended into pericolonic fat. The ileal mucosa showed linear and puncture ulcers with intervening normal tissue. Previous surgeries included a partial ileal resection and permanent ileostomy. Family history included irritable bowel syndrome.
155	1749147	STOMTUT02	The library was constructed using RNA isolated from stomach tumor tissue obtained from a 68-year-old Caucasian female during a partial gastrectomy. Pathology indicated a malignant lymphoma of diffuse large-cell type. Patient history included thalassemia. Family history included acute leukemia, malignant neoplasm of the esophagus, malignant stomach neoplasm, and atherosclerotic coronary artery disease.
156	1817722	PROSNOT20	The library was constructed using RNA isolated from diseased prostate tissue removed from a 65-year-old Caucasian male during a radical prostatectomy. Pathology indicated adenofibromatous hyperplasia. Pathology for the associated tumor tissue indicated an adenocarcinoma.
157	1831290	THP1AZT01	The library was constructed using 1 microgram of polyA RNA isolated from THP-1 promonocyte cells treated for three days with 0.8 micromolar 5-aza-2'-deoxycytidine. THP-1 (ATCC TIB 202) is a human promonocyte line derived from peripheral blood of a 1-year-old Caucasian male with acute monocytic leukemia.

TABLE 4 (cont.)

Polynucleotide SEQ ID NO:	Clone ID	Library	Library Description
158	1831477	THP1AZT01	The library was constructed using 1 microgram of polyA RNA isolated from THP-1 promonocyte cells treated for three days with 0.8 micromolar 5-aza-2'-deoxycytidine. THP-1 (ATCC TIB 202) is a human promonocyte line derived from peripheral blood of a 1-year-old Caucasian male with acute monocytic leukemia.
159	1841607	COLNNOT07	The library was constructed using RNA isolated from colon tissue removed from a 60-year-old Caucasian male during a left hemicolectomy.
160	1852391	LUNGFET03	The library was constructed using RNA isolated from lung tissue removed from a Caucasian female fetus, who died at 20 weeks' gestation.
161	1854555	HNT3AZT01	Library was constructed using RNA isolated from the hNT2 cell line (derived from a human teratocarcinoma that exhibited properties characteristic of a committed neuronal precursor). Cells were treated for three days with 0.35 micromolar 5-aza-2'-deoxycytidine (AZT).
162	1855755	PROSNOT18	The library was constructed using RNA isolated from diseased prostate tissue removed from a 58-year-old Caucasian male during a radical cystectomy, radical prostatectomy, and gastrostomy. Pathology indicated adenofibromatous hyperplasia. This tissue was associated with a grade 3 transitional cell carcinoma. Patient history included angina and emphysema. Family history included acute myocardial infarction, atherosclerotic coronary artery disease, and type II diabetes.
163	1861434	PROSNOT19	The library was constructed using RNA isolated from diseased prostate tissue removed from a 59-year-old Caucasian male during a radical prostatectomy with regional lymph node excision. Pathology indicated adenofibromatous hyperplasia. Pathology for the associated tumor tissue indicated an adenocarcinoma (Gleason grade 3+3). The patient presented with elevated prostate-specific antigen (PSA). Patient history included colon diverticuli and thrombophlebitis. Family history included benign hypertension, multiple myeloma, hyperlipidemia and rheumatoid arthritis.
164	1872334	LEUKNOT02	The library was constructed using RNA isolated from white blood cells of a 45-year-old female with blood type O+. The donor tested positive for cytomegalovirus (CMV).
165	1877230	LEUKNOT03	The library was constructed using RNA isolated from white blood cells of a 27-year-old female with blood type A+. The donor tested negative for cytomegalovirus (CMV).

TABLE 4 (cont.)

Polynucleotide SEQ ID NO:	Clone ID	Library	Library Description
166	1877885	LEUKNOT03	The library was constructed using RNA isolated from white blood cells of a 27-year-old female with blood type A+. The donor tested negative for cytomegalovirus (CMV).
167	1889269	BLADTUT07	The library was constructed using RNA isolated from bladder tumor tissue removed from the anterior bladder wall of a 58-year-old Caucasian male during a radical cystectomy, radical prostatectomy, and gastrostomy. Pathology indicated a grade 3 transitional cell carcinoma in the left lateral bladder. Patient history included angina and emphysema. Family history included acute myocardial infarction, atherosclerotic coronary artery disease, and type II diabetes.
168	1890243	BLADTUT07	The library was constructed using RNA isolated from bladder tumor tissue removed from the anterior bladder wall of a 58-year-old Caucasian male during a radical cystectomy, radical prostatectomy, and gastrostomy. Pathology indicated a grade 3 transitional cell carcinoma in the left lateral bladder. Patient history included angina and emphysema. Family history included acute myocardial infarction, atherosclerotic coronary artery disease, and type II diabetes.
169	1900433	BLADTUT06	The library was constructed using RNA isolated from bladder tumor tissue removed from the posterior bladder wall of a 58-year-old Caucasian male during a radical cystectomy, radical prostatectomy, and gastrostomy. Pathology indicated grade 3 transitional cell carcinoma in the left lateral bladder wall. Patient history included angina and emphysema. Family history included acute myocardial infarction, atherosclerotic coronary artery disease, and type II diabetes.
170	1909441	CONNTUT01	The library was constructed using RNA isolated from a soft tissue tumor removed from the clival area of the skull of a 30-year-old Caucasian female. Pathology indicated chondroid chordoma with neoplastic cells reactive for keratin.
171	1932226	COLNNOT16	The library was constructed using RNA isolated from sigmoid colon tissue removed from a 62-year-old Caucasian male during a sigmoidectomy and permanent colostomy.
172	1932647	COLNNOT16	The library was constructed using RNA isolated from sigmoid colon tissue removed from a 62-year-old Caucasian male during a sigmoidectomy and permanent colostomy.

TABLE 4 (cont.)

Polynucleotide SEQ ID NO:	Clone ID	Library	Library Description
173	2124245	BRSTNOT07	The library was constructed using RNA isolated from diseased breast tissue removed from a 43-year-old Caucasian female during a unilateral extended simple mastectomy. Pathology indicated mildly proliferative fibrocystic changes with epithelial hyperplasia, papillomatosis, and duct ectasia. Pathology for the associated tumor tissue indicated invasive grade 4, nuclear grade 3 mammary adenocarcinoma with extensive comedo necrosis. Family history included epilepsy, atherosclerotic coronary artery disease, and type II diabetes.
174	2132626	OVARNOT03	The library was constructed using RNA isolated from ovarian tissue removed from a 43-year-old Caucasian female during removal of the fallopian tubes and ovaries. Pathology for the associated tumor tissue indicated grade 2 mucinous cystadenocarcinoma. Patient history included mitral valve disorder, pneumonia, and viral hepatitis. Family history included atherosclerotic coronary artery disease, pancreatic cancer, cerebrovascular disease, breast cancer, and uterine cancer.
175	2280639	PROSNON01	The library was constructed and normalized from 4.4 million independent clones from the PROSNOT11 library. Starting RNA was made from prostate tissue removed from a 28-year-old Caucasian male who died from a gunshot wound. The normalization and hybridization conditions were adapted from Soares, M.B. et al. (1994) Proc. Natl. Acad. Sci. USA 91:9228-9232, using a longer (19 hour) reannealing hybridization period.
176	2292356	BRAINON01	The library was constructed and normalized from 4.88 million independent clones from the BRAINOT03 library. Starting RNA was made from brain tissue removed from a 26-year-old Caucasian male during cranioplasty and excision of a cerebral meningeal lesion. Pathology for the associated tumor tissue indicated a grade 4 oligoastrocytoma in the right fronto-parietal part of the brain.
177	2349310	COLSUCT01	The library was constructed using RNA isolated from diseased sigmoid colon tissue obtained from a 70-year-old Caucasian male during colectomy with permanent ileostomy. Pathology indicated chronic ulcerative colitis. Patient history included benign neoplasm of the colon. Family history included atherosclerotic coronary artery disease and myocardial infarctions.
178	2373227	ADRENOT07	The library was constructed using RNA isolated from adrenal tissue removed from a 61-year-old female during a bilateral adrenalectomy. Patient history included an unspecified disorder of the adrenal glands.

TABLE 4 (cont.)

Polynucleotide SEQ ID NO:	Clone ID	Library	Library Description
179	2457682	ENDANOT01	The library was constructed using RNA isolated from aortic endothelial cell tissue from an explanted heart removed from a male during a heart transplant.
180	2480426	SMCANOT01	The library was constructed using RNA isolated from an aortic smooth muscle cell line derived from the explanted heart of a male during a heart transplant.
181	2503743	CONUTUT01	The library was constructed using RNA isolated from sigmoid mesentery tumor tissue obtained from a 61-year-old female during a total abdominal hysterectomy and bilateral salpingo-oophorectomy with regional lymph node excision. Pathology indicated a metastatic grade 4 malignant mixed mullerian tumor present in the sigmoid mesentery at two sites.
182	2537684	BONRTUT01	The library was constructed using RNA isolated from rib tumor tissue removed from a 16-year-old Caucasian male during a rib osteotomy and a wedge resection of the lung. Pathology indicated a metastatic grade 3 (of 4) osteosarcoma, forming a mass involving the chest wall.
183	2593853	OVARTUT02	The library was constructed using RNA isolated from ovarian tumor tissue removed from a 51-year-old Caucasian female during an exploratory laparotomy, total abdominal hysterectomy, salpingo-oophorectomy, and an incidental appendectomy. Pathology indicated mucinous cystadenoma presenting as a multiloculated neoplasm involving the entire left ovary. The right ovary contained a follicular cyst and a hemorrhagic corpus luteum. The uterus showed proliferative endometrium and a single intramural leiomyoma. The peritoneal biopsy indicated benign glandular inclusions consistent with endosalpingiosis. Family history included atherosclerotic coronary artery disease, benign hypertension, breast cancer, and uterine cancer.
184	2622354	KERANOT02	The library was constructed using RNA isolated from epidermal breast keratinocytes (NHEK). NHEK (Clontech #CC-2501) is a human breast keratinocyte cell line derived from a 30-year-old black female during breast-reduction surgery.

TABLE 4 (cont.)

Polynucleotide SEQ ID NO:	Clone ID	Library	Library Description
185	2641377	LUNGTUT08	The library was constructed using RNA isolated from lung tumor tissue removed from a 63-year-old Caucasian male during a right upper lobectomy with fiberoptic bronchoscopy. Pathology indicated a grade 3 adenocarcinoma. Patient history included atherosclerotic coronary artery disease, an acute myocardial infarction, rectal cancer, an asymptomatic abdominal aortic aneurysm, and cardiac dysrhythmia. Family history included congestive heart failure, stomach cancer, and lung cancer, type II diabetes, atherosclerotic coronary artery disease, and an acute myocardial infarction.
186	2674857	KIDNNOT19	The library was constructed using RNA isolated from kidney tissue removed a 65-year-old Caucasian male during an exploratory laparotomy and nephroureterectomy. Pathology for the associated tumor tissue indicated a grade 1 renal cell carcinoma within the upper pole of the left kidney. Patient history included malignant melanoma of the abdominal skin, benign neoplasm of colon, cerebrovascular disease, and umbilical hernia. Family history included myocardial infarction, atherosclerotic coronary artery disease, cerebrovascular disease, prostate cancer, myocardial infarction, and atherosclerotic coronary artery disease.
187	2758485	THP1AZS08	The subtracted THP-1 promonocyte cell line library was constructed using 5.76 million clones from a 5-aza-2'-deoxycytidine (AZT) treated THP-1 cell library. Starting RNA was made from THP-1 promonocyte cells treated for three days with 0.8 micromolar AZT. The library was oligo(dT)-primed, and cDNAs were cloned directionally into the pSPORT1 vectoring system using SalI (5') and NotI (3'). The hybridization probe for subtraction was derived from a similarly constructed library, made from 1 microgram of polyA RNA isolated from untreated THP-1 cells. 5.76 million clones from the AZ-treated THP-1 cell library were then subjected to two rounds of subtractive hybridization with 5 million clones from the untreated THP-1 cell library. Subtractive hybridization conditions were based on the methodologies of Swaroop et al. (Nucl. Acids Res. (1991) 19:1954) and Bonaldo et al. (Genome Res (1996) 6: 791-806).
188	2763296	BRSTNOT12	The library was constructed using RNA isolated from diseased breast tissue removed from a 32-year-old Caucasian female during a bilateral reduction mammoplasty. Pathology indicated nonproliferative fibrocystic disease. Family history included benign hypertension and atherosclerotic coronary artery disease.

TABLE 4 (cont.)

Polynucleotide SEQ ID NO:	Clone ID	Library	Library Description
189	2779436	OVARTUT03	The library was constructed using RNA isolated from ovarian tumor tissue removed from the left ovary of a 52-year-old mixed ethnicity female during a total abdominal hysterectomy, bilateral salpingo-oophorectomy, peritoneal and lymphatic structure biopsy, regional lymph node excision, and peritoneal tissue destruction. Pathology indicated an invasive grade 3 (of 4) seroanaplastic carcinoma forming a mass in the left ovary. The endometrium was atrophic. Multiple (2) leiomyomata were identified, one subserosal and 1 intramural. Pathology also indicated a metastatic grade 3 seroanaplastic carcinoma involving the omentum, cul-de-sac peritoneum, left broad ligament peritoneum, and mesentery colon. Patient history included breast cancer, chronic peptic ulcer, and joint pain. Family history included colon cancer, cerebrovascular disease, breast cancer, type II diabetes, esophagus cancer, and depressive disorder.
190	2808528	BLADTUT08	The library was constructed using RNA isolated from bladder tumor tissue removed from a 72-year-old Caucasian male during a radical cystectomy and prostatectomy. Pathology indicated an invasive grade 3 (of 3) transitional cell carcinoma in the right bladder base. Family history included myocardial infarction, cerebrovascular disease, brain cancer, and myocardial infarction.
191	2809230	BLADTUT08	The library was constructed using RNA isolated from bladder tumor tissue removed from a 72-year-old Caucasian male during a radical cystectomy and prostatectomy. Pathology indicated an invasive grade 3 (of 3) transitional cell carcinoma in the right bladder base. Patient history included pure hypercholesterolemia and tobacco abuse. Family history included myocardial infarction, cerebrovascular disease, brain cancer, and myocardial infarction.
192	2816821	BRSTNOT14	The library was constructed using RNA isolated from breast tissue removed from a 62-year-old Caucasian female during a unilateral extended simple mastectomy. Pathology for the associated tumor tissue indicated an invasive grade 3 (of 4), nuclear grade 3 (of 3) adenocarcinoma, ductal type. Ductal carcinoma in situ, comedo type, comprised 60% of the tumor mass. Metastatic adenocarcinoma was identified in one (of 14) axillary lymph nodes with no perinodal extension. The tumor cells were strongly positive for estrogen receptors and weakly positive for progesterone receptors. Patient history included a benign colon neoplasm, hyperlipidemia, and cardiac dysrhythmia. Family history included atherosclerotic coronary artery disease, myocardial infarction, colon cancer, ovarian cancer, lung cancer, and cerebrovascular disease.

TABLE 4 (cont.)

Polynucleotide SEQ ID NO:	Clone ID	Library	Library Description
193	2817268	BRSTNOT14	The library was constructed using RNA isolated from breast tissue removed from a 62-year-old Caucasian female during a unilateral extended simple mastectomy. Pathology for the associated tumor tissue indicated an invasive grade 3 (of 4), nuclear grade 3 (of 3) adenocarcinoma, ductal type. Ductal carcinoma in situ, comedo type, comprised 60% of the tumor mass. Metastatic adenocarcinoma was identified in one (of 14) axillary lymph nodes with no perinodal extension. The tumor cells were strongly positive for estrogen receptors and weakly positive for progesterone receptors. Patient history included a benign colon neoplasm, hyperlipidemia, and cardiac dysrhythmia. Family history included atherosclerotic coronary artery disease, myocardial infarction, colon cancer, ovarian cancer, lung cancer, and cerebrovascular disease.
194	2923165	SININOT04	The library was constructed using RNA isolated from diseased ileum tissue obtained from a 26-year-old Caucasian male during a partial colectomy, permanent colostomy, and an incidental appendectomy. Pathology indicated moderately to severely active Crohn's disease. Family history included enteritis of the small intestine.
195	2949822	KIDNFET01	The library was constructed using RNA isolated from kidney tissue removed from a Caucasian female fetus, who died at 17 weeks' gestation from anencephalus.
196	2992192	KIDNFET02	The library was constructed using RNA isolated from kidney tissue removed from a Caucasian male fetus, who was stillborn with a hypoplastic left heart and died at 23 weeks' gestation.
197	2992458	KIDNFET02	The library was constructed using RNA isolated from kidney tissue removed from a Caucasian male fetus, who was stillborn with a hypoplastic left heart and died at 23 weeks' gestation.
198	3044710	HEAANOT01	The library was constructed using RNA isolated from right coronary and right circumflex coronary artery tissue removed from the explanted heart of a 46-year-old Caucasian male during a heart transplantation. Patient history included myocardial infarction from total occlusion of the left anterior descending coronary artery, atherosclerotic coronary artery disease, hyperlipidemia, myocardial ischemia, dilated cardiomyopathy, and left ventricular dysfunction. Previous surgeries included cardiac catheterization. Family history included atherosclerotic coronary artery disease.

TABLE 4 (cont.)

Polynucleotide SEQ ID NO:	Clone ID	Library	Library Description
199	3120415	LUNGTUT13	The library was constructed using RNA isolated from tumorous lung tissue removed from the right upper lobe of a 47-year-old Caucasian male during a segmental lung resection. Pathology indicated invasive grade 3 (of 4) adenocarcinoma. Family history included atherosclerotic coronary artery disease, and type II diabetes.
200	126758	LUNGNOT01	The library was constructed at Stratagene using RNA isolated from the lung tissue of a 72-year-old male.
201	674760	CRBLNOT01	The library was constructed using RNA isolated from the cerebellum tissue of a 69-year-old Caucasian male who died from chronic obstructive pulmonary disease. Patient history included myocardial infarction, hypertension, and osteoarthritis.
202	1229438	BRAITUT01	The library was constructed using RNA isolated from brain tumor tissue removed from a 50-year-old Caucasian female during a frontal lobectomy. Pathology indicated recurrent grade 3 oligoastrocytoma with focal necrosis and extensive calcification. Patient history included a speech disturbance and epilepsy. The patient's brain had also been irradiated with a total dose of 5,082 cyg (Fraction 8). Family history included a brain tumor.
203	1236935	LUNGFET03	The library was constructed using RNA isolated from lung tissue removed from a Caucasian female fetus who died at 20 weeks' gestation.
204	1359283	LUNGNOT12	The library was constructed using RNA isolated from lung tissue removed from a 78-year-old Caucasian male during a segmental lung resection and regional lymph node resection. Pathology indicated fibrosis pleura was puckered, but not invaded. Pathology for the associated tumor tissue indicated an invasive pulmonary grade 3 adenocarcinoma. Patient history included cerebrovascular disease, arteriosclerotic coronary artery disease, thrombophlebitis, chronic obstructive pulmonary disease, and asthma. Family history included intracranial hematoma, cerebrovascular disease, arteriosclerotic coronary artery disease, and type I diabetes.

TABLE 4 (cont.)

Polynucleotide SEQ ID NO:	Clone ID	Library	Library Description
205	1450703	PENITUT01	The library was constructed using RNA isolated from tumor tissue removed from the penis of a 64-year-old Caucasian male during penile amputation. Pathology indicated a fungating invasive grade 4 squamous cell carcinoma involving the inner wall of the foreskin and extending onto the glans penis. Patient history included benign neoplasm of the large bowel, atherosclerotic coronary artery disease, angina pectoris, gout, and obesity. Family history included malignant pharyngeal neoplasm, chronic lymphocytic leukemia, and chronic liver disease.
206	1910668	CONNTUT01	The library was constructed using RNA isolated from a soft tissue tumor removed from the clival area of the skull of a 30-year-old Caucasian female. Pathology indicated chondroid chordoma with neoplastic cells reactive for keratin.
207	1955143	CONNNOT01	The library was constructed using RNA isolated from mesentery fat tissue obtained from a 71-year-old Caucasian male during a partial colectomy and permanent colostomy. Family history included atherosclerotic coronary artery disease, myocardial infarction, and extrinsic asthma.
208	1961637	BRSTNOT04	The library was constructed using RNA isolated from breast tissue removed from a 62-year-old East Indian female during a unilateral extended simple mastectomy. Pathology for the associated tumor tissue indicated an invasive grade 3 ductal carcinoma. Patient history included benign hypertension, hyperlipidemia, and hematuria. Family history included cerebrovascular and cardiovascular disease, hyperlipidemia, and liver cancer.
209	1990762	CORPNOT02	The library was constructed using RNA isolated from diseased corpus callosum tissue removed from the brain of a 74-year-old Caucasian male who died from Alzheimer's disease.
210	1994131	CORPNOT02	The library was constructed using RNA isolated from diseased corpus callosum tissue removed from the brain of a 74-year-old Caucasian male who died from Alzheimer's disease.

TABLE 4 (cont.)

Polynucleotide SEQ ID NO:	Clone ID	Library	Library Description
211	1997745	BRSTTUT03	The library was constructed using RNA isolated from breast tumor tissue removed from a 58-year-old Caucasian female during a unilateral extended simple mastectomy. Pathology indicated multicentric invasive grade 4 lobular carcinoma. The mass was identified in the upper outer quadrant, and three separate nodules were found in the lower outer quadrant of the left breast. Patient history included skin cancer, rheumatic heart disease, osteoarthritis, and tuberculosis. Family history included cerebrovascular disease, coronary artery aneurysm, breast cancer, prostate cancer, atherosclerotic coronary artery disease, and type I diabetes.
212	2009035	TESTNOT03	The library was constructed using polyA RNA isolated from testicular tissue removed from a 37-year-old Caucasian male who died from liver disease. Patient history included cirrhosis, jaundice, and liver failure.
213	2009152	TESTNOT03	The library was constructed using polyA RNA isolated from testicular tissue removed from a 37-year-old Caucasian male who died from liver disease. Patient history included cirrhosis, jaundice, and liver failure.
214	2061752	OVARNOT03	The library was constructed using RNA isolated from ovarian tissue removed from a 43-year-old Caucasian female during removal of the fallopian tubes and ovaries. Pathology for the associated tumor tissue indicated grade 2 mucinous cystadenocarcinoma. Patient history included mitral valve disorder, pneumonia, and viral hepatitis. Family history included atherosclerotic coronary artery disease, pancreatic cancer, stress reaction, cerebrovascular disease, breast cancer, and uterine cancer.
215	2061933	OVARNOT03	The library was constructed using RNA isolated from ovarian tissue removed from a 43-year-old Caucasian female during removal of the fallopian tubes and ovaries. Pathology for the associated tumor tissue indicated grade 2 mucinous cystadenocarcinoma. Patient history included mitral valve disorder, pneumonia, and viral hepatitis. Family history included atherosclerotic coronary artery disease, pancreatic cancer, stress reaction, cerebrovascular disease, breast cancer, and uterine cancer.

TABLE 4 (cont.)

Polynucleotide SEQ ID NO:	Clone ID	Library	Library Description
216	2081422	UTRSNOT08	The library was constructed using RNA isolated from uterine tissue removed from a 35-year-old Caucasian female during a vaginal hysterectomy with dilation and curettage. Pathology indicated that the endometrium was secretory phase with a benign endometrial polyp 1 cm in diameter. The cervix showed mild chronic cervicitis. Family history included atherosclerotic coronary artery disease and type II diabetes.
217	2101278	BRAITUT02	The library was constructed using RNA isolated from brain tumor tissue removed from the frontal lobe of a 58-year-old Caucasian male during excision of a cerebral meningeal lesion. Pathology indicated a grade 2 metastatic hypernephroma. Patient history included a grade 2 renal cell carcinoma, insomnia, and chronic airway obstruction. Family history included a malignant neoplasm of the kidney.
218	2121353	BRSTNOT07	The library was constructed using RNA isolated from diseased breast tissue removed from a 43-year-old Caucasian female during a unilateral extended simple mastectomy. Pathology indicated mildly proliferative fibrocystic changes with epithelial hyperplasia, papillomatosis, and duct ectasia. Pathology for the associated tumor tissue indicated invasive grade 4, nuclear grade 3 mammary adenocarcinoma with extensive comedo necrosis. Family history included epilepsy, cardiovascular disease, and type II diabetes.
219	2241736	PANCTUT02	The library was constructed using RNA isolated from pancreatic tumor tissue removed from a 45-year-old Caucasian female during radical pancreaticoduodenectomy. Pathology indicated a grade 4 anaplastic carcinoma. Family history included benign hypertension, hyperlipidemia and atherosclerotic coronary artery disease.
220	2271935	PROSNON01	This normalized prostate library was constructed from 4.4 M independent clones from the PROSNOT11 library. Starting RNA was made from prostate tissue removed from a 28-year-old Caucasian male who died from a self-inflicted gunshot wound. The normalization and hybridization conditions were adapted from Soares, M.B. et al. (1994) Proc. Natl. Acad. Sci. USA 91:9228-9232, using a longer (19 hour) reannealing hybridization period.

TABLE 4 (cont.)

Polynucleotide SEQ ID NO:	Clone ID	Library	Library Description
221	2295344	BRSTNOT05	The library was constructed using RNA isolated from breast tissue removed from a 58-year-old Caucasian female during a unilateral extended simple mastectomy. Pathology for the associated tumor tissue indicated multicentric invasive grade 4 lobular carcinoma. Patient history included skin cancer, rheumatic heart disease, osteoarthritis, and tuberculosis. Family history included cerebrovascular and cardiovascular disease, breast and prostate cancer, and type I diabetes.
222	2303994	BRSTNOT05	The library was constructed using RNA isolated from breast tissue removed from a 58-year-old Caucasian female during a unilateral extended simple mastectomy. Pathology for the associated tumor tissue indicated multicentric invasive grade 4 lobular carcinoma. Patient history included skin cancer, rheumatic heart disease, osteoarthritis, and tuberculosis. Family history included cerebrovascular and cardiovascular disease, breast and prostate cancer, and type I diabetes.
223	2497805	ADRETUT05	The library was constructed RNA isolated from adrenal tumor tissue removed from a 52-year-old Caucasian female during a unilateral adrenalectomy. Pathology indicated a pheochromocytoma.
224	2646362	LUNGTUT11	The library was constructed using RNA isolated from lung tumor tissue removed from the right lower lobe a 57-year-old Caucasian male during a segmental lung resection. Pathology indicated an infiltrating grade 4 squamous cell carcinoma. Multiple intrapulmonary peribronchial lymph nodes showed metastatic squamous cell carcinoma. Patient history included a benign brain neoplasm and tobacco abuse. Family history included spinal cord cancer, type II diabetes, cerebrovascular disease, and malignant prostate neoplasm.
225	2657146	LUNGTUT09	The library was constructed using RNA isolated from lung tumor tissue removed from a 68-year-old Caucasian male during segmental lung resection. Pathology indicated invasive grade 3 squamous cell carcinoma and a metastatic tumor. Patient history included type II diabetes, thyroid disorder, depressive disorder, hyperlipidemia, esophageal ulcer, and tobacco use.

TABLE 4 (cont.)

Polynucleotide SEQ ID NO:	Clone ID	Library	Library Description
226	2755786	THP1AZS08	This subtracted THP-1 promonocyte cell line library was constructed using 5.76 million clones from a 5-aza-2'-deoxycytidine (AZ) treated THP-1 cell library. Starting RNA was made from THP-1 promonocyte cells treated for three days with 0.8 micromolar AZ. The hybridization probe for subtraction was derived from a similarly constructed library, made from RNA isolated from untreated THP-1 cells. 5.76 million clones from the AZ-treated THP-1 cell library were then subjected to two rounds of subtractive hybridization with 5 million clones from the untreated THP-1 cell library. Subtractive hybridization conditions were based on the methodologies of Swaroop et al., NAR (1991) 19:1954, and Bonaldo et al., Genome Research (1996) 6:791. THP-1 (ATCC TIB 202) is a human promonocyte line derived from peripheral blood of a 1-year-old Caucasian male with acute monocytic leukemia.
227	2831245	TLYMNOT03	The library was constructed using RNA isolated from nonactivated Th1 cells. These cells were differentiated from umbilical cord CD4 T cells with IL-12 and B7-transfected COS cells.
228	3116250	LUNGTUT13	The library was constructed using RNA isolated from tumorous lung tissue removed from the right upper lobe of a 47-year-old Caucasian male during a segmental lung resection. Pathology indicated invasive grade 3 (of 4) adenocarcinoma. Family history included atherosclerotic coronary artery disease, and type II diabetes.
229	3129630	LUNGTUT12	The library was constructed using RNA isolated from tumorous lung tissue removed from a 70-year-old Caucasian female during a lung lobectomy of the left upper lobe. Pathology indicated grade 3 (of 4) adenocarcinoma and vascular invasion. Patient history included tobacco abuse, depressive disorder, anxiety state, and skin cancer. Family history included cerebrovascular disease, congestive heart failure, colon cancer, depressive disorder, and primary liver.
230	007632	HMC1NOT01	The library was constructed using RNA isolated from the HMC-1 human mast cell line derived from a 52-year-old female. Patient history included mast cell leukemia.
231	1236968	LUNGFET03	The library was constructed using RNA isolated from lung tissue removed from a Caucasian female fetus who died at 20 weeks' gestation.
232	1334153	COLNNOT13	The library was constructed using RNA isolated from ascending colon tissue of a 28-year-old Caucasian male with moderate chronic ulcerative colitis.

TABLE 4 (cont.)

Polynucleotide SEQ ID NO:	Clone ID	Library	Library Description
233	1396975	BRAITUT08	The library was constructed using RNA isolated from brain tumor tissue removed from the left frontal lobe of a 47-year-old Caucasian male during excision of cerebral meningeal tissue. Pathology indicated grade 4 fibrillary astrocytoma with focal tumoral radionecrosis. Patient history included cerebrovascular disease, deficiency anemia, hyperlipidemia, epilepsy, and tobacco use. Family history included cerebrovascular disease and malignant prostate neoplasm.
234	1501749	SINTBST01	The library was constructed using RNA isolated from ileum tissue removed from an 18-year-old Caucasian female during bowel anastomosis. Pathology indicated Crohn's disease of the ileum. Family history included cerebrovascular disease and atherosclerotic coronary artery disease.
235	1575240	LNODNOT03	The library was constructed using RNA isolated from lymph node tissue removed from a 67-year-old Caucasian male during a segmental lung resection and bronchoscopy. This tissue was extensively necrotic with 10% viable tumor. Pathology for the associated tumor tissue indicated invasive grade 3-4 squamous cell carcinoma. Patient history included hemangioma. Family history included atherosclerotic coronary artery disease, benign hypertension, and congestive heart failure.
236	1647884	PROSTUT09	The library was constructed using RNA isolated from prostate tumor tissue removed from a 66-year-old Caucasian male during a radical prostatectomy, radical cystectomy, and urinary diversion. Pathology indicated grade 3 transitional cell carcinoma. Patient history included lung neoplasm, and benign hypertension. Family history included malignant breast neoplasm, tuberculosis, cerebrovascular disease, atherosclerotic coronary artery disease, and lung cancer.
237	1661144	BRSTNOT09	The library was constructed using RNA isolated from breast tissue removed from a 45-year-old Caucasian female during unilateral extended simple mastectomy. Pathology for the associated tumor tissue indicated invasive nuclear grade 2-3 adenocarcinoma. Patient history included valvuloplasty of mitral valve and rheumatic heart disease. Family history included cardiovascular disease and type II diabetes.

TABLE 4 (cont.)

Polynucleotide SEQ ID NO:	Clone ID	Library	Library Description
238	1685409	PROSNOT15	The library was constructed using RNA isolated from diseased prostate tissue removed from a 66-year-old Caucasian male during radical prostatectomy and regional lymph node excision. Pathology indicated adenofibromatous hyperplasia. Pathology for the associated tumor tissue indicated adenocarcinoma (Gleason grade 2+3). The patient presented with elevated prostate specific antigen (PSA). Family history included prostate cancer, secondary bone cancer, and benign hypertension.
239	1731419	BRSTTUT08	The library was constructed using RNA isolated from breast tumor tissue removed from a 45-year-old Caucasian female during unilateral extended simple mastectomy. Pathology indicated invasive nuclear grade 2-3 adenocarcinoma. Patient history included valvuloplasty of mitral valve and rheumatic heart disease. Family history included cardiovascular disease and type II diabetes.
240	2650265	BRSTNOT14	The library was constructed using RNA isolated from breast tissue removed from a 62-year-old Caucasian female during a unilateral extended simple mastectomy. Pathology for the associated tumor tissue indicated an invasive grade 3 (of 4), nuclear grade 3 (of 3) adenocarcinoma. Patient history included a benign colon neoplasm, hyperlipidemia, cardiac dysrhythmia, and obesity. Family history included cardiovascular and cerebrovascular disease and colon, ovary and lung cancer.
241	2677129	KIDNNOT19	The library was constructed using RNA isolated from kidney tissue removed a 65-year-old Caucasian male during an exploratory laparotomy and nephroureterectomy. Pathology for the associated tumor tissue indicated grade 1 renal cell carcinoma within the upper pole of the left kidney. Patient history included malignant melanoma of the abdominal skin, benign neoplasm of colon, cerebrovascular disease, and umbilical hernia. Family history included myocardial infarction, atherosclerotic coronary artery disease, cerebrovascular disease, and prostate cancer.
242	3151073	ADRENON04	The normalized adrenal gland library was constructed from 1.36 x 1e6 independent clones from an adrenal tissue library. Starting RNA was made from adrenal gland tissue removed from a 20-year-old Caucasian male who died from head trauma. The library was normalized in two rounds using conditions adapted from Soares et al. (PNAS (1994) 91:9228-9232) and Bonaldo et al. (Genome Res (1996) 6: 791-806) using a significantly longer (48-hours/round) reannealing hybridization period.

TABLE 4 (cont.)

Polynucleotide SEQ ID NO:	Clone ID	Library	Library Description
243	3170095	BRSTNOT18	The library was constructed using RNA isolated from diseased breast tissue removed from a 57-year-old Caucasian female during a unilateral simple extended mastectomy. Pathology indicated mildly proliferative breast disease. Patient history included breast cancer and osteoarthritis. Family history included type II diabetes, gallbladder and breast cancer, and chronic lymphocytic leukemia.
244	3475168	LUNGNOT27	The library was constructed using RNA isolated from lung tissue removed from a 17-year-old Hispanic female.
245	3836893	DENDTNT01	The library was constructed using RNA isolated from treated dendritic cells from peripheral blood.
246	4072159	KIDNNOT26	The library was constructed using RNA isolated from left kidney medulla and cortex tissue removed from a 53-year-old Caucasian female during a nephroureterectomy. Pathology for the associated tumor tissue indicated grade 2 renal cell carcinoma involving the lower pole of the kidney. Patient history included hyperlipidemia, cardiac dysrhythmia, menorrhagia, cerebrovascular disease, atherosclerotic coronary artery disease, and tobacco abuse. Family history included cerebrovascular disease and atherosclerotic coronary artery disease.
247	1003916	BRSTNOT03	The library was constructed using RNA isolated from diseased breast tissue removed from a 54-year-old Caucasian female during a bilateral radical mastectomy. Pathology for the associated tumor tissue indicated residual invasive grade 3 mammary ductal adenocarcinoma. Patient history included kidney infection and condyloma acuminatum. Family history included benign hypertension, hyperlipidemia and a malignant neoplasm of the colon.
248	2093492	PANCNOT04	The library was constructed using RNA isolated from the pancreatic tissue of a 5-year-old Caucasian male who died in a motor vehicle accident.
249	2108789	BRAITUT03	The library was constructed using RNA isolated from brain tumor tissue removed from the left frontal lobe a 17-year-old Caucasian female during excision of a cerebral meningeal lesion. Pathology indicated a grade 4 fibrillary giant and small-cell astrocytoma. Family history included benign hypertension and cerebrovascular disease.
250	2171401	ENDCNOT03	The library was constructed using RNA isolated from dermal microvascular endothelial cells removed from a neonatal Caucasian male.

TABLE 4 (cont.)

Polynucleotide SEQ ID NO:	Clone ID	Library	Library Description
251	2212530	SINTFET03	The library was constructed using RNA isolated from small intestine tissue removed from a Caucasian female fetus, who died at 20 weeks' gestation.
252	2253036	OVARTUT01	The library was constructed using RNA isolated from ovarian tumor tissue removed from a 43-year-old Caucasian female during removal of the fallopian tubes and ovaries. Pathology indicated grade 2 mucinous cystadenocarcinoma involving the entire left ovary. Patient history included mitral valve disorder, pneumonia, and viral hepatitis. Family history included atherosclerotic coronary artery disease, pancreatic cancer, stress reaction, cerebrovascular disease, breast cancer, and uterine cancer.
253	2280161	PROSNON01	The normalized prostate library was constructed from 4.4 M independent clones from the PROSNOT11 library. Starting RNA was made from prostate tissue removed from a 28-year-old Caucasian male who died from a self-inflicted gunshot wound. The normalization and hybridization conditions were adapted from Soares, M.B. et al. (1994) Proc. Natl. Acad. Sci. USA 91:9228-9232, using a longer (19 hour) reannealing hybridization period.
254	2287485	BRAINON01	The library was constructed and normalized from 4.88 million independent clones from the BRAINOT03 library. RNA was made from brain tissue removed from a 26-year-old Caucasian male during cranioplasty and excision of a cerebral meningeal lesion. Pathology for the associated tumor tissue indicated a grade 4 oligoastrocytoma in the right fronto-parietal part of the brain.
255	2380344	ISLTNOT01	The library was constructed using RNA isolated from a pooled collection of pancreatic islet cells.
256	2383171	ISLTNOT01	The library was constructed using RNA isolated from a pooled collection of pancreatic islet cells.
257	2396046	THP1AZT01	The library was constructed using RNA isolated from THP-1 promonocyte cells treated for three days with 0.8 micromolar 5-aza-2'-deoxycytidine. THP-1 (ATCC TIB 202)is a human promonocyte line derived from peripheral blood of a 1-year-old Caucasian male with acute monocytic leukemia.
258	2456587	ENDANOT01	The library was constructed using RNA isolated from aortic endothelial cell tissue from an explanted heart removed from a male during a heart transplant.

TABLE 4 (cont.)

Polynucleotide SEQ ID NO:	Clone ID	Library	Library Description
259	2484813	BONRTUT01	The library was constructed using RNA isolated from rib tumor tissue removed from a 16-year-old Caucasian male during a rib osteotomy and a wedge resection of the lung. Pathology indicated a metastatic grade 3 (of 4) osteosarcoma, forming a mass involving the chest wall.
260	2493851	ADRETUT05	The library was constructed RNA isolated from adrenal tumor tissue removed from a 52-year-old Caucasian female during a unilateral adrenalectomy. Pathology indicated a pheochromocytoma.
261	2495719	ADRETUT05	The library was constructed RNA isolated from adrenal tumor tissue removed from a 52-year-old Caucasian female during a unilateral adrenalectomy. Pathology indicated a pheochromocytoma.
262	2614153	GBLANOT01	The library was constructed using RNA isolated from diseased gallbladder tissue removed from a 53-year-old Caucasian female during a cholecystectomy. Pathology indicated mild chronic cholecystitis and cholelithiasis with approximately 150 mixed gallstones. Family history included benign hypertension.
263	2655184	THYMNOT04	The library was constructed using RNA isolated from thymus tissue removed from a 3-year-old Caucasian male, who died from anoxia. Serologies were negative. The patient was not taking any medications.
264	2848362	BRSTTUT13	The library was constructed using RNA isolated from breast tumor tissue removed from the right breast of a 46-year-old Caucasian female during a unilateral extended simple mastectomy with breast reconstruction. Pathology indicated an invasive grade 3 adenocarcinoma, ductal type with apocrine features and greater than 50% intraductal component. Patient history included breast cancer.
265	2849906	BRSTTUT13	The library was constructed using RNA isolated from breast tumor tissue removed from the right breast of a 46-year-old Caucasian female during a unilateral extended simple mastectomy with breast reconstruction. Pathology indicated an invasive grade 3 adenocarcinoma, ductal type with apocrine features and greater than 50% intraductal component. Patient history included breast cancer.

TABLE 4 (cont.)

Polynucleotide SEQ ID NO:	Clone ID	Library	Library Description
266	2899137	DRGCNOT01	The library was constructed using RNA isolated from dorsal root ganglion tissue removed from the cervical spine of a 32-year-old Caucasian male who died from acute pulmonary edema and bronchopneumonia, bilateral pleural and pericardial effusions, and malignant lymphoma (natural killer cell type). Patient history included probable cytomegalovirus, infection, hepatic congestion and steatosis, splenomegaly, hemorrhagic cystitis, thyroid hemorrhage, and Bell's palsy. Surgeries included colonoscopy, large intestine biopsy, adenotonsillectomy, and nasopharyngeal endoscopy and biopsy; treatment included radiation therapy.
267	2986229	CARGDIT01	The library was constructed using RNA isolated from diseased cartilage tissue. Patient history included osteoarthritis.
268	3222081	COLNNON03	The normalized colon library was constructed from $2.84x10^6$ independent clones from the COLNNOT07 library. Starting RNA was made from colon tissue removed from a 60-year-old Caucasian male during a left hemicolectomy. The normalization and hybridization conditions were adapted from Soares et al. (PNAS (1994) 91:9228-9232), Swaroop et al. (Nucl. Acids Res. (1991) 19:1954) and Bonaldo et al. (Genome Res (1996) 6: 791-806), using a significantly longer (48 hour) reannealing hybridization period.

TABLE 6

Nucleotide SEQ ID NO:	Clone ID	Fragment of SEQ ID NO	Starting Nucleotide of Fragment	Ending Nucleotide of Fragment
135	443531	443531H1	1	253
		1406807F6	152	336
		443531T6	847	355
		SBBA00451F1	396	856
		SBBA00676F1	546	865
136	632860	632860H1	13	253
		784715R3	17	666
		509590H1	455	706
137	670010	670010H1	1	263
		669971R1	1	633
138	726498	726498H1	13	263
		726498R6	13	489
		866599R3	7	660
139	795064	795064H1	86	323
		4339458H1	4	284
		937605R3	86	505
		2381151F6	592	1057
		1466346F6	857	1241
140	924925	924925H1	111	412
		3268330H1	2	239
		759120R3	111	629
141	962390	1907958F6	1	478
		023569F1	1122	470
		167282F1	1216	543
		1309211F1	911	1224

Table 5

Program	Description	Reference	Parameter Threshold
ABI FACTURA	A program that removes vector sequences and masks ambiguous bases in nucleic acid sequences.	Perkin-Elmer Applied Biosystems, Foster City, CA.	
ABI/PARACEL FDF	A Fast Data Finder useful in comparing and annotating amino acid or nucleic acid sequences.	Perkin-Elmer Applied Biosystems, Foster City, CA; Paracel Inc., Pasadena, CA.	Mismatch <50%
ABI AutoAssembler	A program that assembles nucleic acid sequences.	Perkin-Elmer Applied Biosystems, Foster City, CA.	
BLAST	A Basic Local Alignment Search Tool useful in sequence similarity search for amino acid and nucleic acid sequences. BLAST includes five functions: blastp, blastn, blastx, tblastn, and tblastx.	Altschul, S.F. et al. (1990) J. Mol. Biol. 215:403-410; Altschul, S.F. et al. (1997) Nucleic Acids Res. 25: 3389-3402.	*ESTs:* Probability value= 1.0E-8 or less *Full Length sequences*: Probability value= 1.0E-10 or less
FASTA	A Pearson and Lipman algorithm that searches for similarity between a query sequence and a group of sequences of the same type. FASTA comprises as least five functions: fasta, tfasta, fastx, tfastx, and ssearch.	Pearson, W.R. and D.J. Lipman (1988) Proc. Natl. Acad Sci. 85:2444-2448; Pearson, W.R. (1990) Methods Enzymol. 183: 63-98; and Smith, T.F. and M. S. Waterman (1981) Adv. Appl. Math. 2:482-489.	*ESTs:* fasta E value=1.06E-6 *Assembled ESTs*: fasta Identity= 95% or greater and Match length=200 bases or greater; fastx E value=1.0E-8 or less *Full Length sequences:* fastx score=100 or greater
BLIMPS	A BLocks IMProved Searcher that matches a sequence against those in BLOCKS, PRINTS, DOMO, PRODOM, and PFAM databases to search for gene families, sequence homology, and structural fingerprint regions.	Henikoff, S and J.G. Henikoff, Nucl. Acid Res., 19:6565-72, 1991. J.G. Henikoff and S. Henikoff (1996) Methods Enzymol. 266:88-105; and Attwood, T.K. et al. (1997) J. Chem. Inf. Comput. Sci. 37: 417-424.	Score=1000 or greater; Ratio of Score/Strength = 0.75 or larger; and, if applicable, Probability value= 1.0E-3 or less
PFAM	An algorithm for searching a query sequence against hidden Markov model (HMM)-based databases of protein family consensus sequences, such as PFAM.	Krogh, A. et al. (1994) J. Mol. Biol., 235:1501-1531; Sonnhammer, E.L.L. et al. (1988) Nucleic Acids Res. 26:320-322.	Score=10-50 bits for PFAM hits, depending on individual protein families

Table 5 (cont.)

Program	Description	Reference	Parameter Threshold
ProfileScan	An algorithm that searches for structural and sequence motifs in protein sequences that match sequence patterns defined in Prosite.	Gribskov, M. et al. (1988) CABIOS 4:61-66; Gribskov, et al. (1989) Methods Enzymol. 183:146-159; Bairoch, A. et al. (1997) Nucleic Acids Res. 25: 217-221.	Score=4.0 or greater
Phred	A base-calling algorithm that examines automated sequencer traces with high sensitivity and probability.	Ewing, B. et al. (1998) Genome Res. 8:175-185; Ewing, B. and P. Green (1998) Genome Res. 8:186-194.	
Phrap	A Phils Revised Assembly Program including SWAT and CrossMatch, programs based on efficient implementation of the Smith-Waterman algorithm, useful in searching sequence homology and assembling DNA sequences.	Smith, T.F. and M. S. Waterman (1981) Adv. Appl. Math. 2:482-489; Smith, T.F. and M. S. Waterman (1981) J. Mol. Biol. 147:195-197; and Green, P., University of Washington, Seattle, WA.	Score= 120 or greater; Match length= 56 or greater
Consed	A graphical tool for viewing and editing Phrap assemblies	Gordon, D. et al. (1998) Genome Res. 8:195-202.	
SPScan	A weight matrix analysis program that scans protein sequences for the presence of secretory signal peptides.	Nielson, H. et al. (1997) Protein Engineering 10:1-6; Claverie, J.M. and S. Audic (1997) CABIOS 12: 431-439.	Score=5 or greater
Motifs	A program that searches amino acid sequences for patterns that matched those defined in Prosite.	Bairoch et al. supra; Wisconsin Package Program Manual, version 9, page M51-59, Genetics Computer Group, Madison, WI.	

TABLE 6 (cont.)

Nucleotide SEQ ID NO:	Clone ID	Fragment of SEQ ID NO	Starting Nucleotide of Fragment	Ending Nucleotide of Fragment
142	1259405	1259405H1	46	277
		2472425H1	331	354
		774303R1	190	743
		1520779F1	418	1001
		1693833F6	914	1467
		1831858T6.comp	1336	1742
		1527737T6.comp	1386	1829
143	1297384	1297384H1	402	641
		1269310F6	1	492
		1457367F1	792	1380
		415587R1	1358	1712
		SANA02967F1	1143	614
144	1299627	1299627H1	1	250
		1359140F6	1004	1573
		1349224F1	1330	1731
		SBAA01431F1	46	397
		SBAA02909F1	868	262
		SBAA01156F1	901	1266
145	1306026	1306026H1	1	223
		1464088R6	302	829
		SBAA02496F1	92	568
		SBAA04305F1	366	883
146	1316219	1316219H1	246	491
		2458603F6	1	402
		2504756T6	980	380
147	1329031	1329031H1	1	264
		1329031T6	505	1
		1329031F6	1	523

TABLE 6 (cont.)

Nucleotide SEQ ID NO:	Clone ID	Fragment of SEQ ID NO	Starting Nucleotide of Fragment	Ending Nucleotide of Fragment
148	1483050	1483050H1	722	931
		855049H1	1	267
		077017F1	1069	679
		1483050F6	722	1215
		1480024T6	2063	1315
		1483050T6	2068	1535
		759486R1	1762	2089
149	1514160	1514160H1	1640	1838
		1866765T7	2383	2210
		782676R1	1652	1875
		008055X4	1090	1804
		008055X5	1316	1952
		1866765F6	2209	2391
		SAOA03127F1	2129	1703
150	1603403	1603403H1	7	224
		372910F1	420	44
		733299R7	219	420
151	1652303	1652303H1	4	256
		1671806H1	1	224
		1341743T1	2069	1900
		3803812H1	389	697
		1878546F6	747	1344
		1428640F1	1081	1664
		2058609R6	1715	2098
		1331621F1	1780	2096
		1306331T1	1897	2098

TABLE 6 (cont.)

Nucleotide SEQ ID NO:	Clone ID	Fragment of SEQ ID NO	Starting Nucleotide of Fragment	Ending Nucleotide of Fragment
152	1693358	1693358H1	41	125
		2498265H1	1	252
		1867125F6	205	373
		1693358T6	1094	416
		2245848R6	737	1103
153	1707711	1707711H1	408	626
		1484609T1	2165	1855
		1707711F6	408	987
		1267959F1	1721	2182
		1484609F1	1855	2178
		SAJA00930F1	544	1132
		SAJA01300R1	1675	1212
		SAJA00999R1	1675	1142
154	1738735	1738735H1	7	236
		SAJA00944R1	393	5
		SAJA00137F1	913	685
		SAJA03629F1	435	42
155	1749147	1749147H1	1	276
155		1749147F6	47	457
155		1749147T6	479	1
156	1817722	1817722H1	1	268
		2011085H1	344	545
157	1831290	1831290H1	10	257
		3473958H1	70	242
		1972268F6	163	617
		1301277F1	413	852
		1521574F1	1024	1602
		1561690T6	1729	1058
		891461R1	1261	1738

TABLE 6 (cont.)

Nucleotide SEQ ID NO:	Clone ID	Fragment of SEQ ID NO	Starting Nucleotide of Fragment	Ending Nucleotide of Fragment
158	1831477	1831477H1	59	337
		1582867H1	1	199
		1336769T1	1986	1639
		1933092H1	525	789
		1519909F1	841	1296
		1220946H1	1061	1318
		809556T1	1983	1687
		1217559T1	2002	1445
		1309225F1	1747	2001
159	1841607	1841607H1	13	192
		SBHA03588F1	13	172
160	1852391	1852391H1	98	367
		734140H1	1	225
		1852391F6	98	542
161	1854555	1854555H1	1	265
		2511711H1	37	58
		782453R1	223	712
		1854555F6	1	346
		1840675T6	1046	860
		2109736H1	938	1054
162	1855755	1855755H1	17	224
		3040236H1	1	179
		1283207F1	306	816
		833763T1	1148	835
		1920926R6	854	1161
163	1861434	1861434H1	13	253
		1861434T6	872	261
		SARA01525F1	426	808
		SARA02548F1	587	889

TABLE 6 (cont.)

Nucleotide SEQ ID NO:	Clone ID	Fragment of SEQ ID NO	Starting Nucleotide of Fragment	Ending Nucleotide of Fragment
164	1872334	1872334H1	1	229
		1872334F6	1	424
		SBGA03684F1	358	425
165	1877230	1877230H1	1405	1677
		2519841H1	1	251
		1877230T6	1903	1405
		1254693F1	335	716
		077020R1	682	1414
		1232336F1	906	1507
		1004952R6	1451	1904
		SARA01879F1	1545	1921
		SARA02654F1	1545	1923
166	1877885	1877885H1	68	323
		508020F1	499	51
		2751126R6	219	516
		SARA02571F1	407	499
167	1889269	1889269H1	757	1020
		1915551H1	1	191
		629493X12	481	865
		1441289F1	693	865
		1215274X34F1	1106	1631
		1818447F6	1307	1540
		1208463R1	1372	1493
168	1890243	1890243H1	9	268
		SARA01884F1	521	168
		SATA00046F1	1057	851
		SARA03294F1	1329	910
		SARA02790F1	1138	1535

TABLE 6 (cont.)

Nucleotide SEQ ID NO:	Clone ID	Fragment of SEQ ID NO	Starting Nucleotide of Fragment	Ending Nucleotide of Fragment
169	1900433	1900433H1	1	242
		SATA00396F1	409	124
		SATA02742F1	1	294
170	1909441	1909441H1	786	1048
		1398811F1	1	550
		3039939H1	607	876
		3324740H1	685	944
		1442131F6	787	1232
		2254056H1	1423	1522
		2199453T6	1955	1351
		1698531H1	1968	1796
171	1932226	1932226H1	294	510
		2320569H1	1	266
		1932226F6	294	685
		2469455T6	1475	1071
		2469455F6	1034	1492
		1907140F6	1158	1482
		SATA02592F1	857	518
172	1932647	1932647H1	17	246
		1492745T1	1582	1418
		1492745H1	1418	1599
		SASA02355F1	386	19
		SASA00117F1	250	569
		SASA00192F1	515	816
173	2124245	2124245H1	45	190
		1235393F1	495	895
		1402264F6	323	925
		1303990F1	682	1240
		1402264T6	1613	950

TABLE 6 (cont.)

Nucleotide SEQ ID NO:	Clone ID	Fragment of SEQ ID NO	Starting Nucleotide of Fragment	Ending Nucleotide of Fragment
174	2132626	2132626H1	406	651
		1723432T6	1299	746
		2132626R6	406	904
		1736723T6	1292	857
		1504738F1	868	1320
175	2280639	2280639H1	28	303
		1377560F6	261	777
176	2292356	2292356H1	717	968
		4086827H1	1	275
		1754442F6	232	577
		3571126H1	497	808
		1601305F6	808	1464
177	2349310	2349310H1	1	236
		2349310T6	682	2
178	2373227	2373227H1	298	524
		3316444H1	801	1053
		302685R6	1141	1496
		SASA02181F1	577	1
		SASA01923F1	963	466
		SASA03516F1	1102	1249
179	2457682	2457682H1	1	226
		2457682F6	1	554
180	2480426	2480426H1	1	213
		2480426F6	1	501

TABLE 6 (cont.)

Nucleotide SEQ ID NO:	Clone ID	Fragment of SEQ ID NO	Starting Nucleotide of Fragment	Ending Nucleotide of Fragment
181	2503743	2503743H1	6	222
		1853909H1	1	272
		1517619F1	172	830
		1467896F6	540	1112
		490031F1	1647	1068
		1208654R1	1382	1633
		880544R1	1450	1648
182	2537684	2537684H1	434	682
		2005493H1	1	194
		730969H1	307	547
		916487H1	723	989
		996135R1	997	1598
		1920738R6	1306	1692
		1957710F6	1472	1692
183	2593853	2593853H1	1	252
		807497H1	2	217
		914020R6	284	740
		889992R1	416	729
184	2622354	2622354H1	3	266
		2623992H1	1	246
		1556510F6	81	258
185	2641377	2641377H1	126	369
		4341415H2	10	345
		SBCA07049F3	126	599

TABLE 6 (cont.)

Nucleotide SEQ ID NO:	Clone ID	Fragment of SEQ ID NO	Starting Nucleotide of Fragment	Ending Nucleotide of Fragment
186	2674857	2674857H1	139	393
		1872373H1	1	270
		470512R6	1486	1502
		1728547H1	1285	1508
		3013651F6	1423	1987
		SBCA01366F1	819	385
		SBCA00694F1	973	1198
187	2758485	2758485H1	20	267
		3097533H1	1	158
		1578959F6	291	771
188	2763296	2763296H1	63	301
		3486025F6	1	130
		SBDA07002F3	63	687
189	2779436	2779436H1	1	233
		2779436F6	1	577
		SBDA07009F3	1	608
190	2808528	2808528H1	25	335
		2611513F6	2	489
		SBDA07021T3	1058	443
191	2809230	2809230H1	409	630
		2213849H1	1	133
		711706R6	396	691
		958323R1	407	800
		030732F1	1366	623
192	2816821	2816821H1	210	501
		3746964H1	1	307
		2816821F6	210	682
		948722T6	959	527

TABLE 6 (cont.)

Nucleotide SEQ ID NO:	Clone ID	Fragment of SEQ ID NO	Starting Nucleotide of Fragment	Ending Nucleotide of Fragment
193	2817268	2817268H1	42	282
		3591308H1	13	264
		419522R1	179	808
		2073028F6	446	924
		1308781F6	869	1112
194	2923165	2923165H1	8	295
		2011630H1	18	238
		1457250F1	268	856
		754668R1	327	878
		1406510F6	558	901
195	2949822	2949822H1	1	280
		SBDA07078F3	1	606
196	2992192	2992192H1	25	321
		2534324H2	1	240
		2815255T6	690	219
		1551107T6	893	471
		1551107R6	471	690
197	2992458	2992458H1	48	362
		2618951H1	1	247
		1479252F1	163	610
		1879054H1	563	840
		1879054F6	563	1096
		2215240H1	951	1202
		1535968T1	1729	1173

TABLE 6 (cont.)

Nucleotide SEQ ID NO:	Clone ID	Fragment of SEQ ID NO	Starting Nucleotide of Fragment	Ending Nucleotide of Fragment
198	3044710	3044710H1	652	952
		3741773H1	1	283
		859906X42C1	94	192
		1534347F1	90	268
		1421122F1	830	1392
		1303865F1	1033	1487
		1704452F6	1432	1934
		1251642F1	2006	1544
		1781694R6	1894	2017
199	3120415	3120415H1	72	363
		1360123T1	523	141
		1375015H1	380	526